論文 / 著書情報
Article / Book Information

題目(和文)	
Title(English)	Study on the synthesis and physicochemical properties of CHA-type aluminosilicate zeolites with Al atom distribution in the zeolite framework controlled
著者(和文)	西鳥羽俊貴
Author(English)	Toshiki Nishitoba
出典(和文)	学位:博士(工学), 学位授与機関:東京工業大学, 報告番号:甲第10985号, 授与年月日:2018年9月20日, 学位の種別:課程博士, 審査員:吉田 尚弘,野村 淳子,鎌田 慶吾,本倉 健,横井 俊之
Citation(English)	Degree:Doctor (Engineering), Conferring organization: Tokyo Institute of Technology, Report number:甲第10985号, Conferred date:2018/9/20, Degree Type:Course doctor, Examiner:,,,,
学位種別(和文)	博士論文
Type(English)	Doctoral Thesis

学位論文

Study on the synthesis and physicochemical properties of CHA-type aluminosilicate zeolites with Al atom distribution in the zeolite framework controlled

(骨格内 Al 原子分布を制御した CHA 型アルミノシリケートゼオライトの合成と物理化学的特性に関する研究)

東京工業大学　大学院総合理工学研究科

化学環境学専攻

西鳥羽　俊貴

Toshiki Nishitoba

2018

Contents

Chapter I General Introduction

1.1 Zeolite and its application in catalysis 3

1.1.1 Synthesis of light olefins from methanol 3

1.1.2 Utilization of zeolite as automobile exhaust gas catalyst 5

1.2 Structure and acid properties of zeolite 6

1.2.1 Zeolite structure 6

1.2.2 Acid property expression mechanism of zeolite 7

1.2.3 Shape selectivity of zeolites 9

1.3 Al distribution in aluminosilicate zeolties 10

1.3.1 Control of Al distribution 10

1.3.2 Evaluation of Al distribution 14

1.4 CHA-type zeolite

1.4.1 Structure of **CHA** 17

1.4.2 Synthesis of **CHA**-type aluminosilicate 17

1.4.3 Synthesis of **CHA** using **FAU**-type zeolite 18

1.4.4 Synthesis of **CHA** without OSDAs 19

1.5 Objects and outline of this thesis 20

1.6 Outline of this study 21

Chapter II Al Distribution and Catalytic Performance of CHA-type Zeolite Synthesized with Various Organic Structure Directing Agents

2.1 Introduction 32

2.2 Experimental 33

2.2.1. Synthesis of **CHA**-type zeolites 33

2.2.2. Characterization 34
2.2.3. Hydrothermal treatment 35
2.2.4. MTO reaction 35

2.3. Results and Discussion 36
2.3.1. Physicochemical properties 36
2.3.2. Estimated of Al distribution 37
2.3.3. Hydrothermal stability 38
2.3.4. MTO performance 39

2.4 Conclusions 40

References 40

Chapter III Effect of Starting Materials on the Al Distribution and Catalytic Performance of CHA-type aluminosilicate Zeolites

3.1 Introduction 54

3.2 Experimental 55
3.2.1. Preparation of **CHA**-type zeolites 55
3.2.2. Characterization 56
3.2.3 Hydrothermal treatment 57
3.2.4 MTO reaction 57

3.3 Results and Discussion 58
3.3.1. Synthesis and Physicochemical properties 58
3.3.2. Estimation of Al distribution 59
3.3.3. Hydrothermal stability 61
3.3.4. Catalytic performance in the MTO reaction 62

3.4. Conclusion 64

Reference 65

Chapter IV Effect of Starting Material on the Al Distribution and Catalytic Performance of CHA-type Zeolite Synthesized without Organic Structure Directing Agents

4.1. Introduction 85

4.2. Experimental 86
4.2.1. Synthesis of **CHA**-type zeolite 86
4.2.2. Characterization 86
4.2.3. Hydrothermal treatment 87
4.2.4. MTO reaction 87

4.3. Results and discussion 88
4.3.1. Synthesis of **CHA**-type zeolite from amorphous aluminosilicate gel without OSDA 88
4.3.2. Synthesis of **CHA**-type zeolite from **FAU** without OSDA 88
4.3.3. Effect of starting material on Al atom distribution 90
4.3.4. Hydrothermal stability and MTO performance 91

4.4 Conclusion 92

Reference 93

Chapter V General Conclusion 106

Chapter I

General Introduction

Chemical products are indispensable for human life. Examples of the oil crisis of the 1970s were remarkable, the petroleum co-products as plastics and papers was threatened. In recent industries, catalysts have greatly contributed to the production of chemical products. A representative example of an industrial process using a catalyst is ammonia synthesis. An iron catalyst that synthesizes ammonia from nitrogen and hydrogen was discovered in 1905. In 1912, the ammonia synthesis began operation at the chemical plant. And a large amount of nitrogen fertilizer was produced using ammonia as a raw material. As a result, the production volume of agricultural crops increased dramatically, making a contribution to the solution of food problems accompanying the sharp increase in world population. Table 1.1 shows an example in which a catalyst is used as an industrial process, but in the modern chemical industry most processes are carried out using catalysts. [1]

Table 1.1 Industrial applications of catalysts

Process	**catalyst**
Synthesis of ammonia	$Fe\text{-}Al_2O_3\text{-}K_2O$
Synthesis of Methanol	$Cu\text{-}ZnO\text{-}Al_2O_3$
Hydro desulfurization	Sulfurization $Co\text{-}Mo\text{-}Al_2O_3$
Methane steam reforming	$Ni\text{-}Al_2O_3$
Carbon monoxide shift reaction	Cu-ZnO
Sulfuric acid production	$V_2O_5\text{-}K_2O\text{-}Al_2O_3$
Ethylene oxide	$Ag\text{-}Al_2O_3$
Methanol oxidation	Unsupported Ag
Propylene hydration	Ion exchange resin

1.1 Zeolite and its application in catalysis

Cracking of petroleum is mentioned as a famous industrial process using zeolite catalyst. This process, operating in 1936, coupled with the discovery of the huge oil field in 1938 brought about the development of energy supply and chemical industry. Zeolite is widely used industrially as a catalyst and adsorbent. A list of applications of zeolite is shown in Table 1.2. [2] Zeolite is utilized that takes makes use of the shape selectivity (1.2.2.) and ion exchange capacity (1.2.3.). The reactions applied industrially of zeolite are roughly classified as follows: Fluid catalytic cracking, methanol to olefin propylene as acid catalyst, synthesis of cyclohexanone oxime, propylene oxide as an oxidation catalyst. Furthermore, NH_3-SCR and synthesis of propylene oxide utilizes the ion exchange capacity of zeolite. Applications as catalysts are represented by acid reactions and oxidation reactions in chemical synthesis, but zeolite catalysts are also utilized in a wide range of fields, such as the use as an environmental catalyst for the purpose of decomposing automobile exhaust gas.

Table 1.2 Industrial application of zeolite and Zeolite structure

Process	catalyst
Fluid catalytic cracking	Pt / USY
Methanol to olefin, propylene	Al-MFI, SAPO-34
Transalkylation in the cymene method	MCM-22
Synthesis of cyclohexanone oxime	TS-1+H_2O_2
Synthesis of propylene oxide	TS-1+H_2O_2
Synthesis of methylamine	Modified mordenite
Synthesis of ethanolamine	La-MFI
NH_3-SCR	Cu-β
Hydration of cyclohexene	Al-MFI
Hydration of cyclopentene	mordenite
Beckmann rearrangement	Silicalite

1.1.1 Synthesis of light olefins from methanol

The synthesis of light olefins from methanol is mainly used as a catalyst for MTP (Methanol-To-Propylene) and MTO (Methanol-To-Olefin). These reactions attracted attention as a result of the two oil crises of the 1970s, and many research and development were done. As representative catalysts, ZSM-5 developed by Mobil and SAPO - 34 developed by UOP are famous and many review articles have been discussed. [3,4] Characteristically, it is a fluidized bed process when **CHA**-type zeolite is used as a catalyst. Although **CHA**-type zeolite is easy to produce light olefins because its own small pores, and catalyst deactivation is fast. Therefore, it is a requiring regeneration. The reaction mechanisms are discussed in various reviews, it is said that the reaction proceeds via an intermediate such as $(:CH_2)_n$ on the solid catalyst. [5-9] As an olefin generation mechanism in MTO reaction, oxonium ylide mechanism, carbene mechanism, carbocation mechanism, free radical mechanism and "hydrocarbon-pool" mechanism has been proposed. Current mainstream is the "dual-cycle mechanism" in which the "hydrocarbon-pool" mechanism has been modified. [10] The "hydrocarbon-pool" mechanism increases the adsorption species of $(CH_2)_n$ continuously and increases olefins. Figure 1.1 shows the reaction scheme of "dual-cycle mechanism" of MTO reaction. After that, "aromatics-based cycle" was found in which aromatics such as benzene and toluene play an important role in propylene production. [11] Progress was then made by a "dual-cycle mechanism" was proposed in which aromatics-based cycle and propylene intermediates react simultaneously. [12]

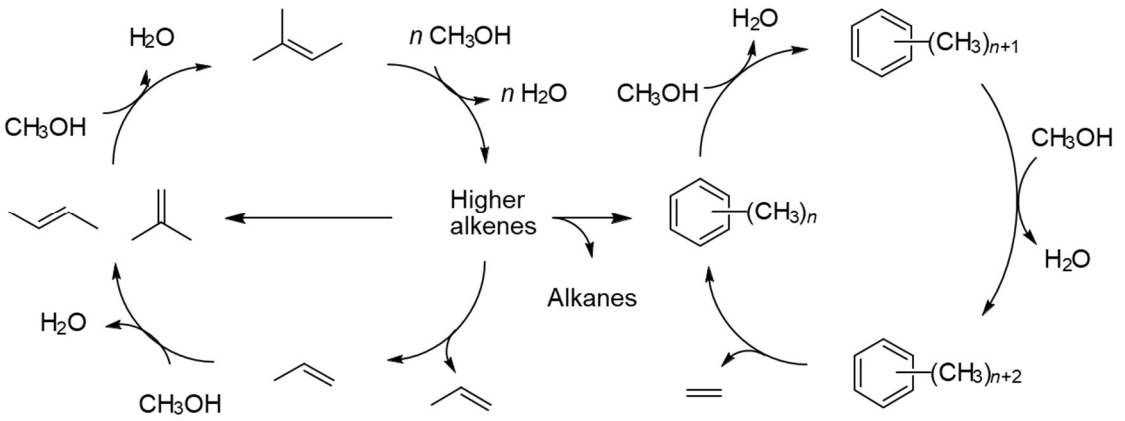

Figure **1.1.** The reaction model of dual-cycle mechanism.

1.1.2 Utilization of zeolite as automobile exhaust gas catalyst

Studies related to zeolite in the selective NOx reduction method by NH_3 and hydrocarbons expected as a practical process of automobile exhaust gas purification catalyst were first reported by Iwamoto et al. [13], Held et al. [14] on Cu exchange zeolite. In NH_3-SCR, urea water is used as a reducing agent, and NO_X is decomposed using NH_3 generated by thermal decomposition of urea as a reducing agent. When sulfur content in diesel fuel is high, vanadium-containing catalyst is used. But when it is less, Fe zeolite and Cu zeolite are used. Fe zeolite showed a remarkable rise in purification rate as the ratio of NO_2 in NO_X increased and the purification rate is high in the high temperature range. as compared with Cu zeolite. As zeolite, β-zeolite is used for Fe-SCR and CHA-type zeolite is used for Cu-SCR. In 2009 Bull et al. [15] reported that Cu-exchanged SSZ-13 had comparable NOxSCR conversion and greater hydrothermal stability and resistance to hydrocarbon poisoning than medium-pore zeolites. Fickel et al.[16] reported that Cu-SAPO-34 had catalytic performance and hydrothermal aging resistance similar to Cu-SSZ-13. These features enabled the first on road commercial applications of SCR to appear in the US in 2010, and today it is not uncommon to find diesel emission fluid

(DEF), as aqueous solution of urea, advertised on highway billboards. The pace of this commercialization has been remarkable.

1.2. Structure and acid properties of zeolite

1.2.1 Zeolite structure

The pore size of zeolite is a factor that shows specific activity and attracts attention in many catalytic reactions. [17,18] The pore size of zeolite is roughly divided into large pores, medium pores and small pores and It is formed that A number of T-atom (T= Si) was 8, 10, 12 respectively so called “n membered ring” (n = 8,10,12). The relation between the pore diameter of each zeolite and the number of member rings is shown in Table 1.3. [19], and famous zeolite structure showed Figure 1.2. Each number of member rings is different by about 1 Å, and 12-menber ring zeolite is suited reaction of large molecule as sugar. The 10-membered ring zeolite can selectively separate aromatics such as xylene and toluene and 8-membered ring zeolite, small molecules as methane, NO and methanol can enter the pores. In addition, number of membered ring was same even though the pore diameter is different due to the crystal structure. In particular, small pore zeolites attracts attention that lower olefins are the product of interest can be selectively produced in MTO reaction and A can inhibit catalyst poisoning and side reactions by CH contained in automobile exhaust gas in the NH_3-SCR reaction. According to the website of IZA, there are more than 10 small pore zeolites, and various structures exist even in the small pore zeolite. The CHA structure has a wide range of generation and has merit that it can be synthesized by various methods. [20] Especially for the amount of Al in the framework it can be synthesized from Si / Al = 2 to pure silica.

Table 1.3. Membered ring number and Pore size in famous zeolite

Zeolite code	dimension	Pore size / Å	Membered ring number
BEA	3	6.6×6.7, 5.6×5.6	12-12-12
FAU	3	7.4×7.4	12-12-12
MFI	3	5.5×5.1, 5.3×5.6	10-10-10
MWW	2	5.5×4.0, 5.1×4.1	10-10
FER	2	5.4×4.2, 4.8×3.5	10-8
CHA	3	3.8×3.8	8-8-8

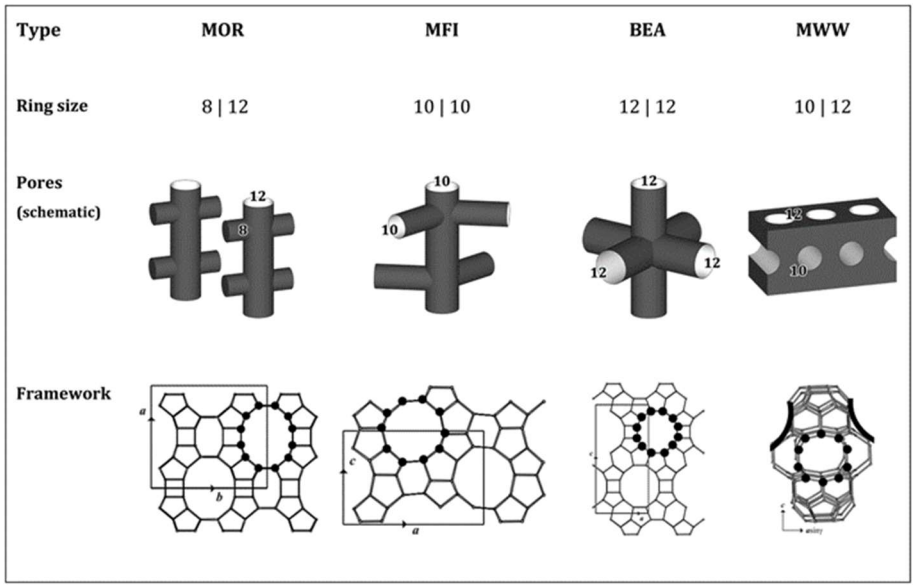

Figure 1.2 Framework structure and pore structure drawings adopted from [19].

1.2.2 Acid property expression mechanism of zeolite

The OH group showing the solid acidity is attributed to the partial structure of the zeolite framework. For example, Y type zeolite which is synthesized in the form of Na^+, NH_4-Y is obtained by ion exchanging Na^+ with NH_4^+, Further, HY is obtained by calcination over 623 K. The OH groups are present in a bridge to the ions of Al and Si. in

the dehydrated zeolite as shown in Figure 1.3. Therefore, stretching vibration of OH group is observed in the infrared absorption spectrum measured at room temperature. Absorption of this OH group disappears when pyridine is adsorbed, and absorption of pyridinium ion appears. This indicates that the OH group bridged to the ions of Al and Si is capable of imparting H^+ to pyridine which is the base molecule. Furthermore, when heating is performed at 773 K or higher, the acidic OH group is eliminated as H_2O.

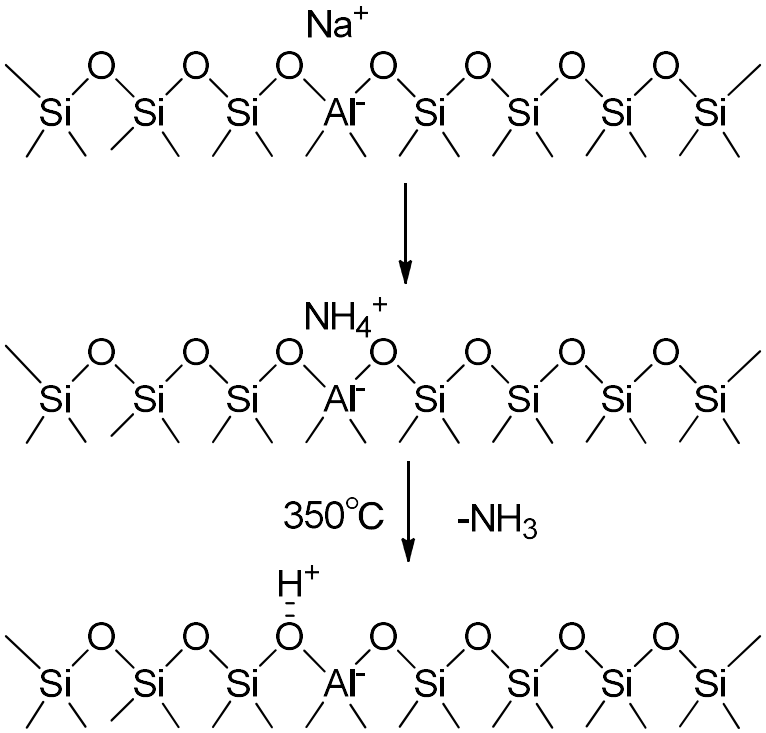

Figure.1.3 Mechanism of expressed acidic OH functional group in zeolite.

As a result, Lewis acid is expressed. It is believed that the trigonal coordinate Al is out of framework and chemical species such as $(AlO)^+$ are present in the pores. Therefore, it is reasonable to think that Lewis acid expression is due to aluminum outside the framework. The lattice defect after Al dislocation forms a silanol nest. In addition, the defect site may be repaired by supplying Si from a portion having relatively low crystallinity in the crystal

during calcination. Dealumination from acidic zeolite occurs in normal calcination process, and the process is known that the presence of extra framework aluminum thus formed also affects the action of acidic OH groups.

1.2.3 Shape selectivity of zeolites

a) Reactant regulation selectivity

The selectivity determined by the size of the reactive molecule, the reaction of the molecule which cannot enter into the zeolite pores or which is difficult to enter is regulated, and molecules which can easily enter react preferentially.

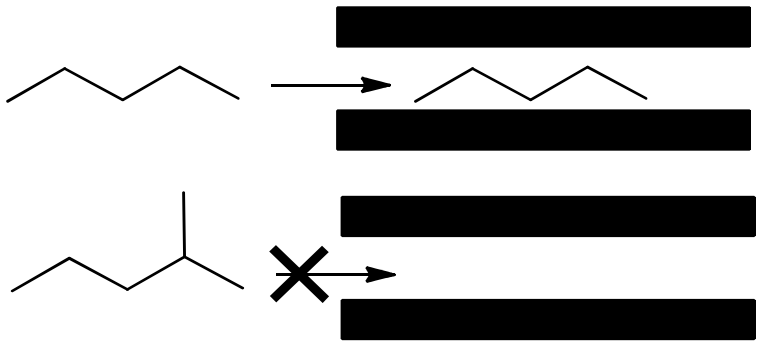

Figure 1.4 Reactant shape selectivity model.

b) Product regulatory selectivity

The molecules generated in the zeolite pores, only molecules that can sufficiently diffuse into the pores and can exit the crystal are obtained as products, and molecules that are too large come out of the crystal after converting them into small molecules. In order for a selectivity that utilizes the difference in product diffusion rate to be established, it is necessary that the secondary conversion reaction such as isomerization and decomposition of large molecules generated in the pores is sufficiently fast is there.

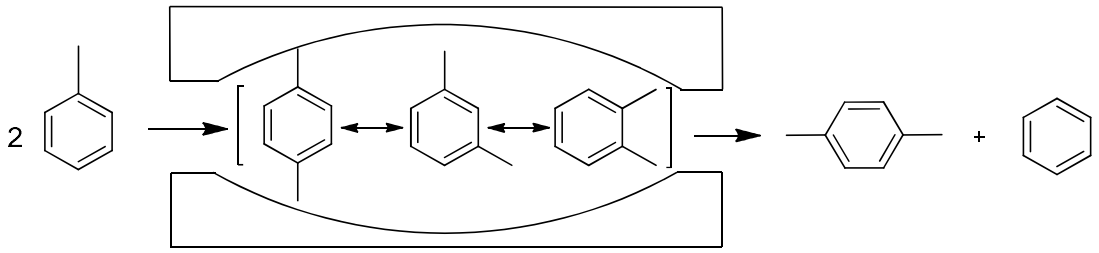

Figure 1.5 Product shape selectivity model

c) Transition state regulatory selectivity

We explain that certain reactions do not occur despite the inhomogeneous diffusion of reactants and product molecules in the pores. For example, 1,3,5-trimethylbenzene is less likely to be formed by disproportionation of m-xylene with H-mordenite. This result was explained that it is not via a bulky transition state but product regulatory selectivity due to 1,3,5-trimethylbenzene can easily enter in mordnaite.

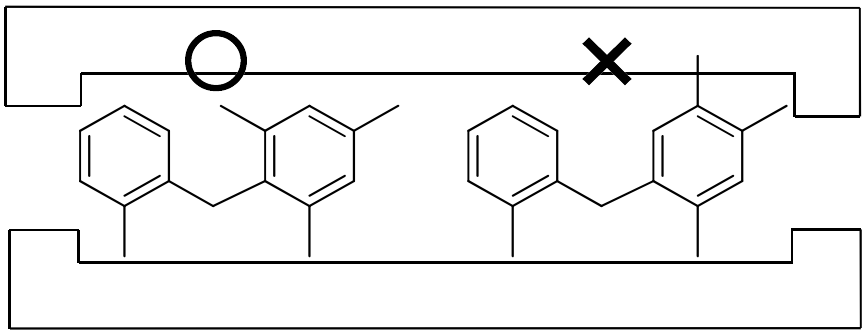

Figure 1.6 Transition-state shape selectivity model.

1.3 Al distribution in aluminosilicate zeolites

1.3.1 Control of Al distribution

It is well recognized that, to balance the charge, Al^{3+} species are located near cations including inorganic cations, for example, Na^{+}, K^{+}, or organic ones, such as quaternary ammonium ions as OSDAs. Hence, the number of the cations affects the Al content, and the location of Al atoms may be dependent on their size and type.

One type of Al arrangement describes the location of Al atoms among different pores of a given zeolite. A synthesis strategy to control the distribution of Al in the zeolite by using different OSDAs in the presence or absence of Na cation has been developed [20]. For example, the distribution of framework Al atoms in either 8-membered ring (8-MR) or 10-MR of the **FER**-type zeolite can be controlled by using mixtures of OSDAs with different sizes (Figure 1.7) [21]. Recently, our laboratory has also revealed that the Al distribution in the **RTH**-type zeolite can be controlled by using OSDAs with different sizes [22].

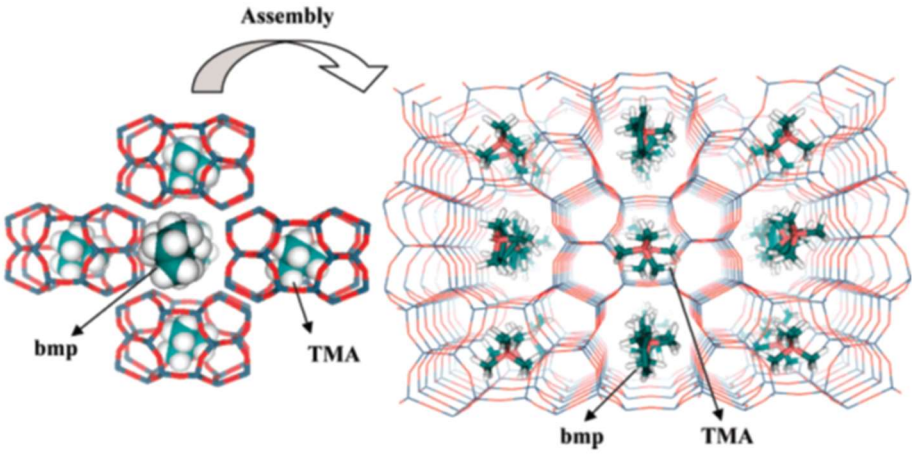

Figure 1.7 Scheme of the self-assembly of tetramethylammonium (TMA)-filled cavities around benzylmethylpyrrolidinium(bmp) molecules to give the final ferrierite structure [23].

More recently, our laboratory has reported a new class of ZSM-5 with controlled Al distribution by using tetrapropylammonium(TPA)hydroxide as OSDA in the absence or presence of Na cation [24]. It was found that the Al atoms in the ZSM-5 synthesized with only TPA in the absence of Na cation are selectively located at the intersections, and that the Al atoms in the ZSM-5 synthesized with both TPA and Na cation are located not only at the intersection but also in narrow straight and/or sinusoidal channels (Figure 1.8). In

the cracking of methylcyclohexane (MCH) and methanol to olefins (MTO) reactions, the ZSM-5 with Al atoms located at the intersections exhibited a shorter catalytic lifetime. Very recently, the regulation of framework Al siting and acid distribution in ZSM-5 was achieved by using different silicon sources during the hydrothermal synthesis [25]. The ZSM-5 with Al atoms located at the intersections gave higher selectivity to ethene and aromatics and a larger hydrogen transfer index (HTI) in MTO reaction, whereas the ZSM-5 with Al atoms in narrow straight and/or sinusoidal channels exhibited higher selectivity to propene and higher olefins.

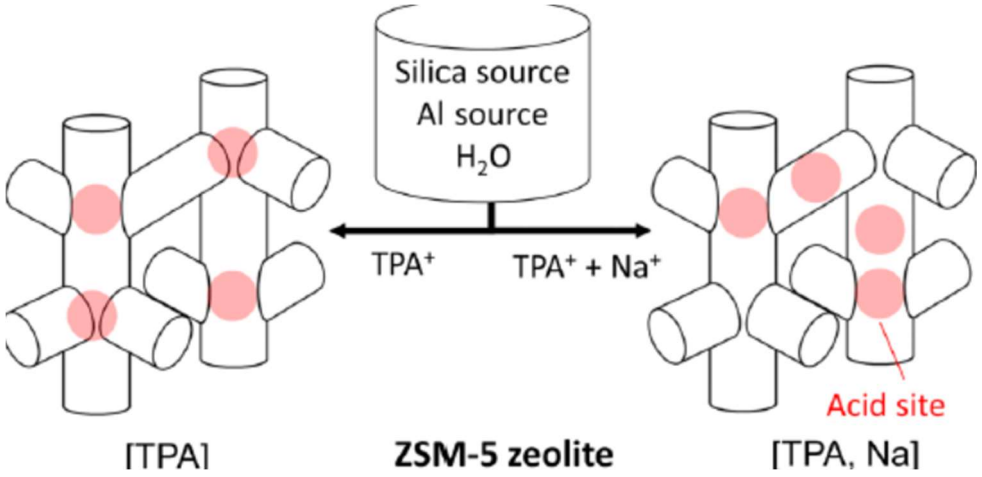

Figure 1.8 Synthesis strategy to control the distribution of Al in ZSM-5 zeolite [24].

The post-synthesis method was also employed to control the Al atom distribution in zeolite. Recently, our laboratory has synthesized the **CON**-type aluminosilicate zeolites by direct or post-synthesis methods and found that there is a significant difference in the state of tetrahedrallycoordinated Al species between the directly and post-synthesized zeolites, leading to the marked difference in the MTO reaction. Besides the direct and post-synthesis methods, dealumination is also a good choice to control the Al distribution. For example, van Bokhoven et al. reported the stepwise dealumination of zeolite Beta at specific T-sites [26]. Matias et al. suggested that acid sites in the outer cups of the MCM-

22 zeolite can be completely deactivated by dealumination through nitric acid treatment, while the acid treatment simultaneously damaged the super cage system. However, only 20% of the aluminum was extracted from the zeolite by this acid treatment [27]. Recently, our laboratory has reported that the acid treatment of the MCM-22 precursor under severe conditions (2 M HNO_3 at 423 K for 20 h in an autoclave), followed by calcination can selectively remove the Al atoms on the T2 site in the hexagonal model, which form the acid sites within the super cages. Thus dealuminated MCM-22 showed a higher propylene selectivitythanH-ZSM-5 and H-Beta zeolite catalysts with similar acid amounts in n-hexane cracking [28].

Another type of Al arrangement describes the proximity of Al atoms within the framework, ranging from the limit of Al site isolation (Al-O(-Si-O)$_x$-Al, $x \geq 3$) to higher densities of proximal or "paired" Al atoms, which are defined here as two Al atoms separated by either one or two Si atoms in a 6-MR (Al-O(-Si-O)$_x$-Al, $x = 1, 2$) (Figure 1.9). Dedecek and his co-workers reported that framework Al siting and distribution is not random or controlled by simple rules and depends on the conditions of the zeolite synthesis. Al in Al-O-(Si-O)$_2$-Al in one 6-MR and single Al atoms predominate in Si-rich zeolites and their population can be varied to a large extent [29-30].

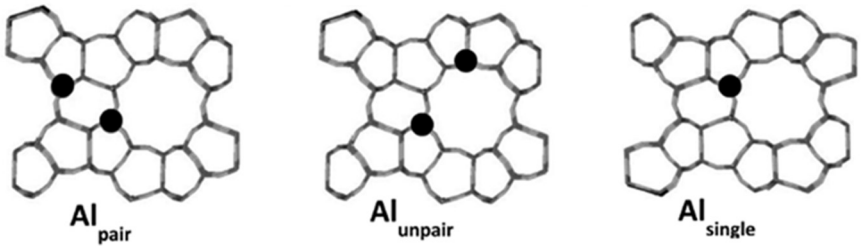

Figure 1.9 Schematic arrangement of Al atoms in Al pairs (Al pair), close Al atoms in different rings (Al unpair), and single Al atoms [31].

1.3.2 Evaluation of Al distribution

Methods for the evaluation of Al distribution have attracted a considerable interest and also been extensively investigated [32-37]. Up to now the distribution of Al atoms in the zeolite lattice could be monitored mainly by ^{29}Si MAS NMR. However, the data about the nonequivalent aluminum T sites, present in the ^{27}Al MAS NMR spectra, was obscured by second-order effects of quadrupolar interaction. By applying the five-quantum ^{27}Al MQMAS NMR method to ZSM-5 type zeolites, at least two nonequivalent aluminum T sites in the ZSM-5 can be distinguished [38]. Recently, Lercher and his co-workers have applied a combination of extended X-ray absorption fine structure (EXAFS) analysis and ^{27}Al MASNMR spectroscopy supported by DFT-based molecular dynamics simulations to estimate the Al distribution of Beta [39]. In addition, the Al atoms distribution in framework has also been directly estimated by ultra-high resolution TEM and STEM.

Among the evaluation methods of Al distribution, the combination of ^{29}Si and ^{27}AlMAS NMR spectroscopies, divalent Co(II) ion exchange capacity, and the concentration of bare Co(II) ions in dehydrated zeolites analyzed by the UV-vis. spectroscopy has been widely used to distinguish the various Al-O-(Si-O)$_n$-Al sequences. [40] It was reported that using exchanged Co^{2+} ions as probes for ‘‘Al pairs’’ to estimate the occurrence of ‘‘Al pairs’’ in the framework of ZSM-5 and their spatial distribution in

zeolites. The visible spectra of Co^{2+} ions were used as monitor the distribution of Co^{2+} ions, as well as thus ‘‘Al pairs’’. The visible spectroscopy in Co-ZSM-5 were identify three types of the ‘‘bare’’ Co^{2+} ions (α-, β- and γ-type Co^{2+} ions in Figure 1.13). Theα-type Co^{2+} ions correspond to a single bound 15100 cm-1. The β-type Co^{2+} ions correspond to four bounds at 16100, 17150, 18500 and 20800cm-1. The γ-type Co^{2+} ions are manifested by a doublet at 20100 and 22000 cm-1 [41]. As shown in Figure1.10, the α-type were belonging to the cationic site in the straight channel of ZSM-5. A cationic site of theβ-type corresponds to the deformed 6-MR of the channels intersection. The cationic site of γ-type represents six-coordinated Co^{2+} ions in a complex, boat shaped, accessible only from the sinusoidal channel [42-43].

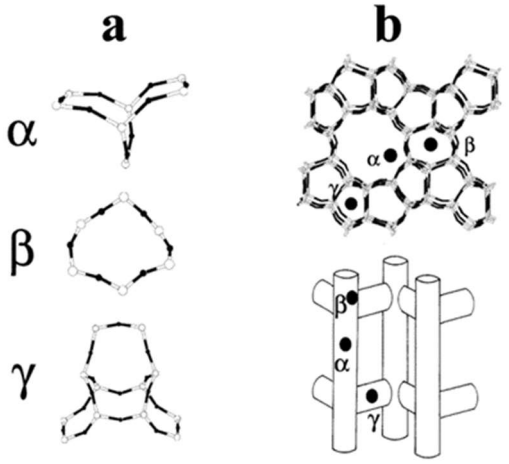

Figure 1.10 (a) Local structures of the α, β and γ cationic sites and (b) their location in the ZSM-5 channel structure [41].

Recently, our laboratory has also reported that the distribution of acid sites in the micro pore has been estimated based on the constraint index (CI). The CI is defined as the cracking rate of n-hexane to that of its isomer 3-methylpentane, and expressed as the following equation], where k_H and k_{3MP} are the rates of the cracking of n-hexane (H) and 3-methylpentane (3-MP), respectively [44].

$$CI = \frac{k_H}{k_{3MP}} = \frac{\log (1\text{- conversion of hexane})}{\log (1\text{- conversion of 3-methylpentane})}$$

The CI value was an extremely useful catalytic test for investigating the relative pore sizes and shape selective properties of acidic zeolites and that originally was developed in the Mobil laboratories [45-47]. On the basis of CI, Frillette classified materials with a CI greater than 12 as small pore, that is, having ≤ 8 - ring pores; CI less than 1 are defined as large pore, with ≥ 12 - ring pores; and materials with CI between 1 and 12 as intermediate pores, having 10 - ring pores [48].

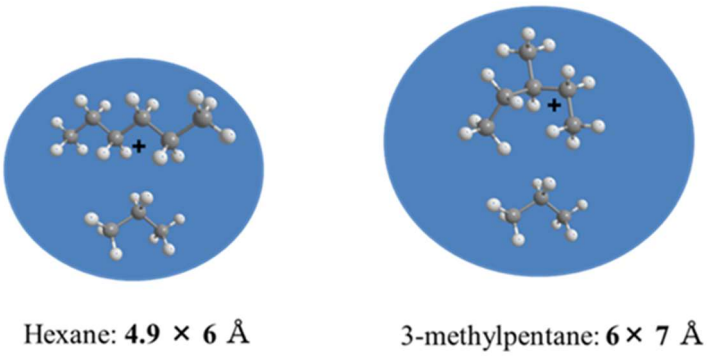

Figure 1. 11 Dimensions of transition states of C6 paraffins [51].

In general, in the cracking via the carbeniumion/β-scission mechanism, the reactivity of paraffins having a tertiary carbon atom is higher than that of n-paraffins. However, in medium pore (10-MR) zeolites, the Cl value is larger than unity and increased with a decrease in the size of void space [49-50]. This would be caused by the narrow spaces impose more severe steric constraint on the bulky transition state of 3-methylpentane than on that of n-hexane (Figure 1.14). Therefore, it is expected that the ZSM-5 zeolite with a

larger amount of acid sites located in the intersections exhibits a lower CI value.

1.4 CHA-type zeolite

1.4.1 Structure of CHA

CHA zeolites contain one unique T-site and double 6-membered ring (6-MR) building units that interconnect to form 8-MR windows (0.38 nm diam.), which limit transport into larger cages (0.82 nm diam., 18 T atoms per cage). (Figure 1.12) And it has one unique nonequivalent tetrahedral site (T site) in double 6-membered ring (D6R) building unit that connects to form a three-dimensional pore system with the large cha cages.

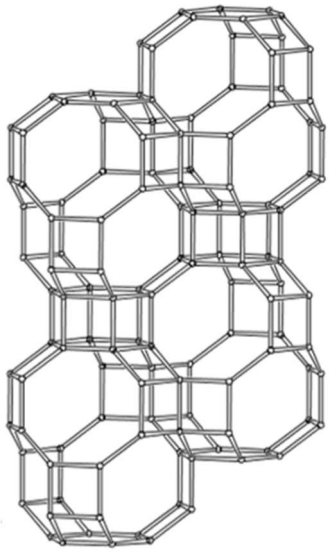

Figure 1.12 Structure of CHA-type zeolite.

1.4.2 Synthesis of CHA-type aluminosilicate

The most famous synthetic process in the synthesis of **CHA**-type aluminosilicate is SSZ-13 invented by Chevron in 1985. [52] This process dramatically improved the crystallization region of the **CHA**-type zeolite. This method can synthesize of **CHA**-type zeolite in the region of low aluminum content. It is reported that TMAdaOH which is the organic structure directing agents is suitable size for cha cage of **CHA**-type zeolite. It is

thought that it is a factor of high silicaization that it is SDA suitable for cage. Table 1.4 summarizes the synthesis method of the paper using TMAdaOH at synthesis and the composition of **CHA**-type zeolite to be produced. The **CHA**-type zeolite in the region of Si/Al ratio about 5- 60 has been synthesized in a system without seed crystals. It has been reported that the synthesis range becomes high silica to about Si / Al = 150 using seed crystals. In addition, pure silica **CHA** can be obtained by synthesizing **CHA**-type zeolite by the fluoride method. It has been successfully synthesized a high-silica **CHA**-type zeolite by various synthesis methods, and it is understood that the structure-directing agents used for zeolite synthesis and the raw material greatly influence the composition and physical properties of the zeolite to be obtained.

Table 1.4 Synthesis of SSZ-13 using various methods

Crystallization temperature (ºC)	Crystallization time (day)	Seed	Synthesis method	Si/Al	Reference
120 - 140	6	-	-	4.8 – 14	52
140	6	-	-	5-21	53
160	7	-	-	4.7 – 55	54
150	5	2wt%	-	14 – 67	55
170	4	5wt%	-	10 – 140	56
155	1d 16h	-	HF method	20 - pure silica	57

1.4.3 Synthesis of CHA using FAU-type zeolite

Table 1.5 summarizes the synthesis of **CHA**-type zeolite when **FAU**-type zeolite is used as a raw material for the **CHA**-type zeolite produced in this synthesis system. The first report on the synthesis of **CHA**-type zeolite using **FAU**-type zeolite as a raw material is a system which dissolves **FAU** by KOH solution made in 1983 and synthesizes. [58] This synthesis method is carried out without using a structure directing agent, and **CHA**-

Table 1.5 Synthesis of **CHA**-type zeolite using **FAU**-type zeolite as raw materials

Crystallization temperature (ºC)	Crystallization time (day)	Seed	Synthesis method	Si/Al	Reference
80	5	-	-	2.0 -2.7	58
135	60 h	-	-	6.5-12.5	59
125 - 170	2	2wt%	-	13 - 67	61
120	21	-	-	16.9	62
125	7-14	-	-	5.2-21	63
160	5.2-8.0	10wt%	-	5.2-8.0	64

type zeolite having a low Si / Al ratio is produced. Thereafter, from 1989 onwards, the synthesis of **CHA**-type zeolite using **PHI**-type and **FAU**-type zeolite as a raw material and TMAdaOH as a structure directing agents was reported. [59 - 60] Since this synthesis system can be synthesized by using it as a zeolite raw material having a framework structure, the time of crystallization is very short. Furthermore, in 2007, synthesis of **CHA**-type zeolite using BTMAOH which is less expensive SDA has been carried out. [62,63] It is possible to synthesize a **CHA**-type zeolite having Si / Al = about 14 - 30 by synthesizing from **FAU**-type zeolite of Si/Al = 30 -55 as a raw material. Recently, it has reported that the synthesis of **CHA**-type zeolite using **FAU**-type zeolite as a starting material and TEAOH as a structure directing agent succeeded. [64]

1.4.4. Synthesis of CHA without OSDAs

Synthesis of **CHA**-type zeolite under OSDA-Free conditions has not been reported for a long time since synthesis in KOH system using **FAU** in 1983. [58] Recently, synthesis of **CHA**-type zeolite by Seed assist method from amorphous silica source, alumina source has been reported. [68] In addition, synthesis conditions under OSDA-Free conditions are summarized in Table 1.6. For synthesis under the OSDA-Free

condition, a method using a seed crystal, a synthesis method with a fluoride, and a synthesis method using **FAU** can be mentioned. [65] In both methods, it is understood that the Si/Al ratio in the zeolite is synthesized in the region of high Al content of about 2.0 - 4.8. In the synthesis under the OSDA-Free condition, the counter cations contained in the raw material are only Na^+ and K^+, which are contained a lot when forming the cha cage. Therefore, in order to compensate the charge of the zeolite, there are many Al sources in the framework it is considered to be included. [67].

Table 1.6 Synthesis of **CHA**-type zeolite under OSDA-Free conditions

Crystallization temperature (ºC)	Crystallization time (day)	Seed	Synthesis method	Products	Si/Al	Reference
80	120 h	-	-	CHA	2.4	58
120 - 160	24 - 120 h	10	HF method	CHA	2.0 - 3.5	65
150	40 h	10	-	CHA+Am.	19	66
150 - 170	48 - 72 h	20	Seed-assist	CHA	5.2	67

1.5 Objects and outline of this thesis

Our lives have become enriched with chemical products. The raw material of this chemical product is mainly petroleum. However, the production volume of petroleum is unstable. As a breakthrough to that end, aiming at the production of chemical products using various raw materials that do not depend on fossil resources. The catalyst as a zeolite plays an indispensable role in realizing these processes. Furthermore, zeolite has a specific crystal structure, introduction and identification of an active site is easier than other catalysts. Indeed, analysis and control of Al distribution, which is the active site in zeolite, are being actively reported. In recent years among a number of zeolites, **CHA**-type zeolite of small pore zeolite is particularly attracting attention. This zeolite is

characterized by selectivity of products in MTO reaction utilizing small pores and high hydrothermal stability. Therefore, this work synthesis of **CHA**-type zeolite form various synthesis method and the control of Al distribution in product, after we evaluated hydrothermal stability and catalytic properties in products.

1.6. Outline of this study

The present dissertation deals with studies on the effect of structure directing agents, silica source, alumina source upon synthesis of **CHA**-type zeolite on Al atoms of product was clarified. We investigated the influence of **CHA**-type zeolite on Al atom distribution in the framework by using structure directing agent of various molecular sizes. In addition, **FAU**-type zeolite was used as a silica alumina source. It is thought that the partial structure of **FAU**-type zeolite influences the Al atom distribution of **CHA**-type zeolite produced.

In chapter II, the synthesis of **CHA**-type zeolite using various SDA and evaluation of hydrothermal stability and Methanol-to-olefin reaction activity. **CHA**-type zeolite was synthesized using NaOH in addition to the N,N,N-trimethyl-adamantammonium hydroxide (TMAdaOH), N-methyl-3-quinuclidinol hydroxide, benzyl trimethyl-ammonium hydroxide, tetraethylammonium hydroxide, KOH and NaOH as a structure directing agent. The products were evaluated by XRD, SEM, ICP, ^{29}Si MAS NMR, ^{27}Al MAS NMR. Depending on the variety of SDA, the region of Si / Al ratio in products is different. In each sample, the amount of defect site and particle diameter are different, so that using TMAdaOH as a structure directing agent, the hydrothermal stability and the lifetime of the MTO reaction are short in the region of high

Al content. It was suggested that the uniformity of Al atoms in the zeolite particles affect hydrothermal stability and MTO lifetime.

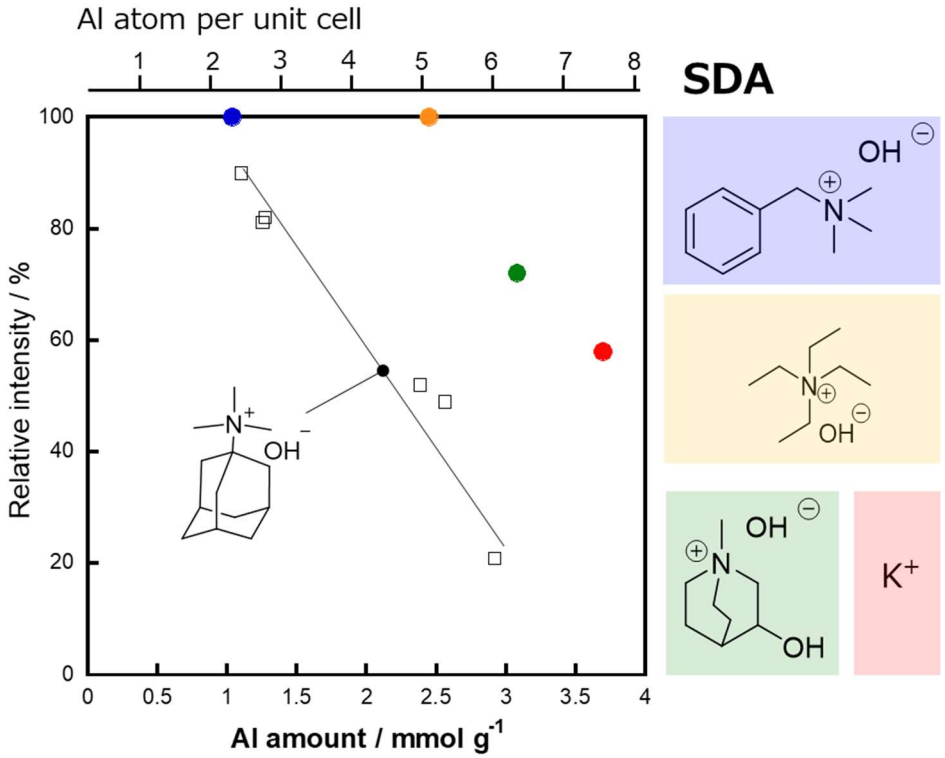

Figure 1.13 Synthesis of **CHA**-type zeolite Using **FAU** and amorphous silica alumina

In the case of using OSDA different from chapter II, the Si / Al ratio of **CHA** generated was greatly different. Further, the distribution of Al atoms in the framework was suggested to affect catalytic activity. In Chapter III, focusing on the raw silica source and alumina source, synthesis was carried out using **FAU** type zeolite which feeds nano parts in a synthetic gel as a raw material. In chapter III, I report The impact of starting materials on the Al distribution of the **CHA**-type aluminosilicate zeolites was investigated. The **CHA**-type aluminosilicate zeolites were synthesized in the presence of N,N,N-trimethyl-1-adamantammonium cation from the different starting materials including fumed silica, aluminum hydroxide, and the **FAU**-type zeolite with their proportions varied. In this work, the proportion of "Q^4(nAl)", $Si(OSi)_{4-n}(OAl)_n$, and "Q^3(nAl)", $Si(OSi)_{3-}$

$_n(OH)(OAl)_n$, in the total framework Si atoms which can be estimated by solid-state ^{29}Si MAS NMR technique, has been applied to an index for Al distribution. When the proportion of the Al source derived from the **FAU**-type zeolite was increased, the proportion of $Q^4(2Al)$ was increased. Thus, we found a facile method for controlling the Al distribution in the **CHA**-type zeolite by varying the starting materials. Finally, the impacts of the Al distribution on the hydrothermal stability and catalytic properties in the methanol to olefins (MTO) reaction were investigated. We successfully found that, under the same Al content, the zeolite with a high proportion of $Q^4(2Al)$ exhibited a low hydrothermal stability and a short catalytic life in the methanol to olefins reaction compared to that with a low proportion.

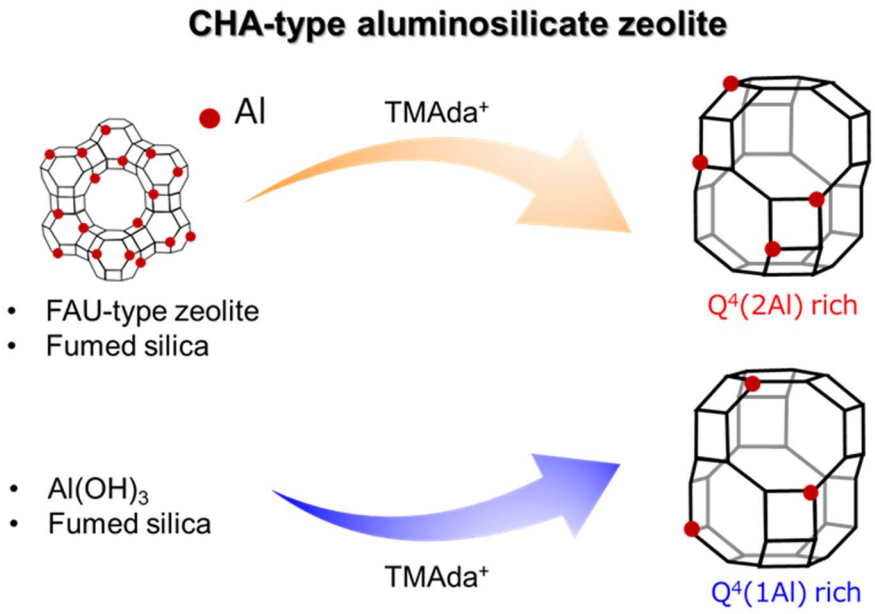

Figure 1.14 Synthesis of **CHA**-type zeolite Using **FAU** and amorphous silica alumina

We found that $Q^4(2Al)$ rich **CHA** type zeolite is produced by using $Q^4(2Al)$ rich **FAU** from Chapter III. If the starting material **FAU** affects the Al distribution of the

product, Q^4 (1Al) rich **CHA** type zeolite should be produced using Q^4 (1Al) rich **FAU**. So that, In the Chapter IV. We investigated the influence of **CHA** type zeolite produced by the starting material on Al distribution under OSDA - Free condition, which is a region with a large amount of Al. As raw materials for the synthesis, amorphous silica source, alumina source and Q^4 (1Al) rich **FAU** type zeolite were used. Estimation of Al atom distribution of the produced **CHA** type zeolite was carried out by ^{29}Si MAS NMR. As a result, when Q^4 (1Al) rich FAU (Si / Al = 15) was used as a raw material, the amount of Q^4 (1Al) was larger than when amorphous silica source and alumina source were used The obtained sample was evaluated for hydrothermal stability by hydrothermal stability test and catalytic activity by MTO reaction. Q^4 (1Al) rich **CHA** was found to have high hydrothermal stability and long catalyst life in the MTO reaction.

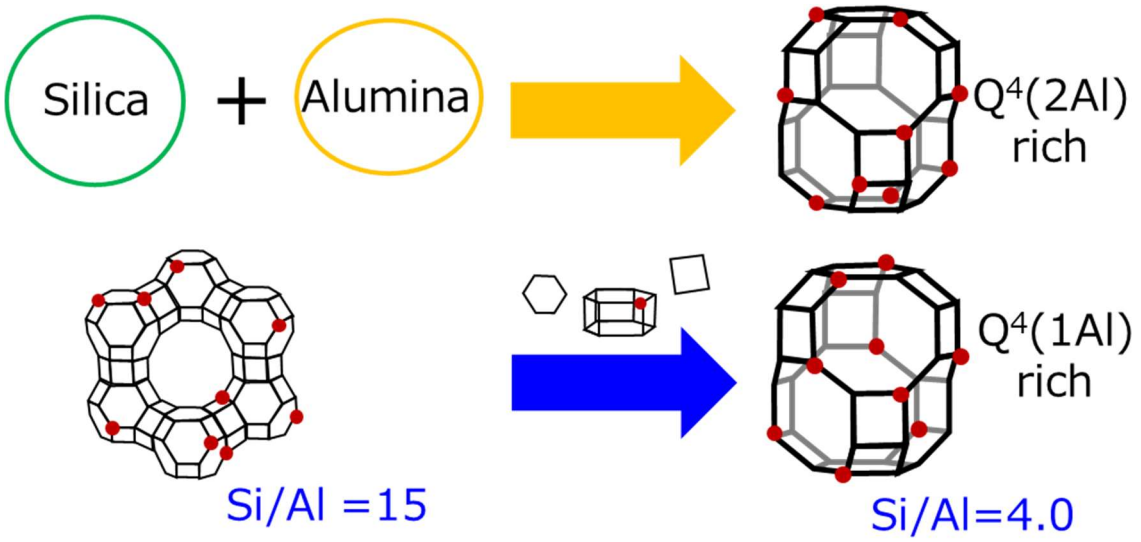

Figure 1.15 Synthesis of CHA-type zeolite Using FAU and amorphous silica alumina

References

[1] Kikuti E., Syamizu Y., Segawa K., Tada A., Hattori H., *Atarasii Syokubai Kagaku*, *(New catalyst chemistry) SANKYO-PUBLISHINHG,* **2013**

[2] Setoyama T., *Japan Zeolite Association All Rights Reserved,* **2013,** 30, 95

[3] Takagi M., *Atarashii Puropirenn Seizou purosesu*, *(New propylene production process), S&T-PUBLISHING*, **2013**

[4] Lin Z., U.S.-China Coal Conversion and Carbon Management Workshop, **2009**

[5] Chang C.D., *Catal. Rev. Sci. Eng.*, **1984**, 26, 323

[6] Chang C.D., *Stud. Surf. Sci. Catal.*, **1991**, 61, 393

[7] Stocker M., *Microporous Mesoporous Mater.*, **1999**, 29, 3

[8] Keil F.J., *Microporous Mesoporous Mater.*, **1999**, 29,49

[9] Olsbye U., Svelle S., Bjorgen M., Beato P., Janssens T. V. W., Joensen F., Bordiga S.,Lillerud K. P., *Angew. Chem. Int. Ed.*, **2012**, 51, 5810

[10] Bjorgen M., Svelle S., Joensen F., Nerlov J., Kolboe S., Bonino F., Palumbo L., Bordiga S., Olsbye U., *J.Catal.*, **2007**, 249, 195

[11] Mikkelsen O., Ronning P. O., Kolboe S., *Micropor. Mesopor. Mater.*, **2000**, 40, 95

[12] Svelle S., Joensen F., Nerlov J., Olsbye U., Lillerud K. P., Kolboe S., Bjorgen M., *J. Am. Chem. Soc.*, **2006**, 128, 14770

[13] Iwamoto M., *Syokubai* **1990**, 32, 430

[14] Held W., et al., *SAE Trans.*, **1990**, 209

[15] Bull I., Xue W. M., Burk P., Boorse R. L., Gajek R. T., Cannan T. R., Flanigen E. M., *J. Am. Chem. Soc*., **1984**, 106, 6092

[16] Fickel D. W., D'Addio E., Lauterbach J. C., Caudle M. T., Google Patents, **2015**.

[17] Davis M.E., Lobo R.F., *Chem. Mater.*, **1992**, 4, 756

[18] Cundy C. S., CoX P. A., *Chem. Rev.*, **2003**, 103, 663

[19] Baerlocher C. H., McCusker L. B., Olson D.H., Atlas of Zeolite, Framework Typs, 6th ed., Elsevier, Amsterdam, **2007**; see also : http://www.iza-structure. org/databases/

[20] Zones S. I., Patent **1985**

[20] Kamimura Y., Tanahashi S., Itabashi K., Sugawara A., Wakihara T., Shimojima A., Okubo T., *J. Phys. Chem. C,* **2011**, 115 744

[21] Janda A., Alexis B. T., *J. Am. Chem. Soc*., **2013**, 135, 19193

[22] Liu M., Yokoi T., Yoshioka M., Imai H., Kondo J. N., Tatsumi T., *Phys. Chem. Chem. Phys.*, **2014**, 16, 4155

[23] Pinar A. B., Hortiguela L. G., Pariente J. P., *Chem. Mater.*, **2007**, 19, 5617

[24] Yokoi T., Mochizuki H., Namba S., Kondo J. N., Tatsumi T., *J. Phys. Chem. C*, **2015**, 119, 15303

[25] Stein A., *Adv. Mater. No. 10*, 2003, 16, 15

[26] van Bokhoven J. A., Koningsberger D. C., Kunkeler P., van Bekkum, and Kentgens A. P. M., *J. Am. Chem. Soc.*, **2000**, 122, 12842

[27] Matias P., Lopes J.M., Ayrault P., Laforge S., Magnoux P., Guisnet M., Ribeiro F. R., App. Catal. A, **2009**, 31, 207

[28] Matias P., Lopes J.M., Laforge S., Magnoux P., Russo P.A., Ribeiro C. M.M.L., Guisnet M., Ribeiro F. R., *J. Catal*., **2008**, 259, 190

[29] Gobbi G. C., Kennedy G. J., Fyfe C. A., *Chem. Lett*., **1983**, 1551.

[30] Gonzales N. O., Chakraborty A. K., Bell A. T., *Catal. Lett.*, **1998**, 50, 135.

[31] jerk D., Kaucky D., Wichterlova B., *Micropor. Mesopor. Mater.*, **2000**, 35, 483

[32] Pinar A. B., Gó mez-Hortigüela L., Pé rez-Pariente P., *J. Mater.*, **2007**, 19 5617

[33] Pinar A. B., Pariente J. P., Hortigüela L. G., WO116 958-A1. **2008**

[34] Pinar A. B., Alvare C. M., Grande-Casa M., Parient P., *J. Catal.*, **2009**, 263, 258

[35] Alvarez C. M., Pinar A. B., García R., Casas M. G., Pariente P., *Top. Catal.*, **2009**, 52, 1281

[36] Hortigüela L. G., Pinar A. B., Cora F., Pariente P., *Chem. Commun.*, **2010**, 46, 2073

[37] Leshkov Y. R., Moliner M., Davis M. E., *J. Phys. Chem. C*, **2011**, 115, 1096

[38] Liu M., Yokoi T., Yoshioka M., Imai H., Kondo J. N., Tatsumi T., *J. Phys. Chem. Chem. Phys.*, **2014**, 16, 4155

[39] Vjunov A., Fulton J. L., Huthwelker T., Pin S., Mei D., Schenter G. K., Govind N., Camaioni D. M., Hu J. Z., Lercher J. A., *J. Am. Chem. Soc.*, **2014**, 136, 8296

[40] Jerk D., Kaucky D., Wichterlova B. Gonsiorova O., *Phys. Chem. Chem. Phys.*, **2002**, 4, 5406

[41] den Ouden C. J. D., Jackson R. A., Catlow C. R. A., Post M. F. M., *J. Phys. Chem.*, **1990**, 94, 5286.

[42] Gobbi G. C., Kennedy G. J., Fyfe C. A., *Chem. Lett.*, **1983**, 1551.

[43] Gonzales N. O., Chakraborty A. K., Bell A. T., *Catal. Lett.,* **1998**, 50, 135.

[44] den Ouden C. J. D., Jackson R. A., Catlow C. R. A., Post M. F. M., J. *Phys. Chem.*, **1990**, 94, 5286.

[44] Frilette V. J., Haag W. O., Lago R. M., *J. Catal.*, **1981**, 67, 218

[45] SASOL/Chevron slurry phase distillate, in: Proceedings 17th World Petroleum Congress, Rio de Janeiro, Brazil, September 1, **2002**, 6, 90.

[46] Schmidt F., Kohler E., Guisnet M., Gilson J. P., *Imperial College Press, London*, **2002**, 153.

[47] Kiovsky J.R., Goyette W. J., Notermann T.M., *J. Catal.*, **1978**, 52, 25.

[48] Michael S., *Micropor. Mesopor. Mater.*, **2005**, 82 257

[49] Vjunov A., Fulton J. L., Huthwelker T., Pin S., Mei D., Schenter G. K., Govind N., Camaioni D. M., Hu J. Z., Lercher J. A., *J. Am. Chem. Soc.*, **2014**, 136, 8296

[50] Frilette V. J., Haag W. O., Lago R. M., *J. Catal.*, **1981**, 67, 218

[51] Mochizuki H., Doctor thesis.

[52] Santilli, D. S., Zomes, S. I., U.S. Patent, 4,496,786

[53] Eilertsen, E. A., Nilsen M. H., Wendelbo R., Olsbye U., Lillerud K. P., *Stud. Suf. Sci. Catal.*, **2008**, 174, 265

[54] Deimund M. A., Harrison L., Lunn J. D., Liu, Y.; Malek, A.; Shayib, R.; Davis, M. E., *ACS Catal.*, **2016**, 6, 542 -550.

[55] Zhu Q., Kondo J. N., Ohnuma R., Kubota Y., Yamaguchi M., Tatsumi T., *Micropor. Mesopor. Mater.*, **2008**, 112, 153

[56] Kubota Y., *JP20169118* **2016**

[57] Eilertsen, E. A., Arstad B., Svelle S., Lillerud K. P., *Micropor. Mesopor. Mater.*, **2012**, 153, 94

[58] Bourgogne, M., Guth J. L., Wey R., U. S. Patent 4,503,024 1985

[59] Zones S. I., *J. Chem. Soc. Fraday Trans.*, **1991**, 87, 3709

[60] Zones S. I., Van Nordstand R. A., *Zeolites*, **1988**, 8, 166

[61] Takata, T.; Tsunoji, N.; Takamitsu, Y.; Sadakane, M.; Sano, T., *Micropor. Mesopor. Mater.*, **2016**, 225, 524

[61] Itakura M., Inoue T., Takahashi A., Fujitani T., Oumi Y., Sano T., *Chem. Lett.* **2008**, 37, 908

[62] Itaura M., Goto I., Takahashi A., Fujitani T., Ida Y., Sadakane M., Sano T., *Micropor. Mesopor. Mater.*, **2011**, 144, 91

[63] Martin N., Moliner M. Corma A., *Chem Commun.*, **2015**, 51, 9965

[64] Liu B., Zheng Yihong Z., Hu N., Gui T., Li Y., Zhang F., Zhou R., Chen X., Kita H., et al., *Micropor. Mesopor. Mater.*, **2014**, 196, 270

[65] Goel, A., Zones S. I., Iglesia E., *Chem. Mater*., **2015**, 27, 2056

[66] Imai H., Hayashida N., Yokoi T., Tatsumi T., *Micropor. Mesopor. Mater.*, **2014**, 196, 341

Chapter II

Al Distribution and Catalytic Performance of CHA-type Zeolites Synthesized with Various Organic Structure Direct Agents

2.1. Introduction

The synthesis of **CHA**-type aluminosilicate was firstly reported by Zones et al. in 1985. [1] **CHA**-type zeolite can be synthesized by using various organic structure directing agents (OSDAs). The most famous OSDA for synthesizing **CHA**-type aluminosilicate is trimethyladamantylammonium hydroxide (TMAdaOH). From the viewpoint of cost reduction, the cheaper OSDA such as benzyltrimethylammonium hydroxide (BTMAOH), triethylammonium hydroxide (TEAOH) , and etc. was reported. [2,3]

It was well-known that the Al distribution within framework of the zeolite is different can be influenced by the type and proportion of OSDA used during synthesis. In 2013, PérezPariente and coworker synthesized **FER**-type zeolite with various OSDAs and reported that Al atom distribution in the framework was different. [4] Recently, our laboratory has found that the distribution of Al atoms in the **MFI** frameworks can be changed by using tetrapropylammonium hydroxide (TPAOH) as OSDA with and without Na^+ cations in the synthesis of ZSM-5. The Al atoms in ZSM-5 synthesized with only TPAOH in the absence of Na cations are preferentially located at the intersections with wide space into ZSM-5. However, the Al atoms are located not only at the intersections but also in narrow straight and/or sinusoidal channels when ZSM-5 was synthesized with both TPAOH and Na cations [5] Furthermore, we found that the Al atoms in ZSM-5 synthesized with pentaerythritol (PET) as pore filling-agent in the presence of Na cations are preferentially located in narrow straight and/or sinusoidal channels. [6,7.8] Gounder and coworker also reported that Al atom distribution in the **CHA** structure was changed by changing the proportion of $TMAda^+$ and Na^+. [9] Isolated Al species existed abundantly when the synthesis was carried out using only TMAdaOH. However, there

are many Al species existing in close proximity when increasing the amount of Na in synthetic gel. In this chapter, we clarified the change of n Al atom distribution in **CHA**-type zeolite by changing the type of OSDA in the synthetic gel and the effect on the catalytic performance.

2.2 Experimental

2.2.1 Synthesis of CHA-type zeolites

The starting materials used in this study were fumed silica (Cab-O-Sil M5), aluminum hydroxide (Aldrich), the **FAU**-type zeolite (CBV-720, Si/Al = 15), NaOH (Wako, 99.8%) and KOH (Wako, 99.8%). Various organic compounds such as trimethyladamanthylammonium hydroxide (TMAdaOH), benzyltrimethylammouium hydroxide (BTMAOH) N-methyl-3-hydroxyl Quinuqurizinol cation (M3HQuiOH), and triethylammonium hydroxide (TEAOH) were used as OSDA. TMAdaOH and M3HQuiOH were obtained from purchased adamantanamine (Tokyo Chemical Industry Co., Ltd.) and 3-hydroxyl-Quinuqurizinol (Tokyo Chemical Industry Co., Ltd.) respectively, via methylation with iodomethane followed by anion exchange using ion-exchange resin. was obtained from purchased.

The molar composition of the mother gels and synthesis conditions are summarized in Table 2.1. For all the cases, 5-10 wt% (based on the weight of SiO_2) of the calcined SSZ-13 (Si/Al = 7.7) were used as seed crystals. The prepared mother gels were crystallized at 403 - 443 K in a rotating oven at 40 rpm for 2-7 days. The obtained as-synthesized Na-type product was filtered, dried at 373 K, calcined at 873 K in air. The ion-exchange was carried out with stirring at 353 K for 3 h using 2.5 M NH_4NO_3 aqueous solution twice to obtain the NH_4-type. After collecting the solid by filtration, the resultant

product was calcined in air at 873 K for 3 h to obtain the H-type zeolite. The final products were denoted by [TEA, Na], [BTMA, Na], [M3HQui, Na], [TMAda, Na_L], and [TMAda, Na_H]. Here, L and H means low and high Si/Al ratio in the synthetic gels. In addition, the SSZ-13 synthesized without using any OSDA were denoted by [Na, K].

2.2.2. Characterization

Powder X-ray diffraction (XRD) patterns were obtained on a Rint-Ultima III (Rigaku) instrument using a Cu Kα X-ray source (40 kV, 20 mA). Nitrogen adsorption measurements to determine the BET surface area (S_{BET}), external surface area (S_{EXT}), and micro pore volume (V_{micro}) were conducted at 77 K on a Belsorp-mini II (MicrotracBEL) instrument. Field-emission scanning electron microscopic (FE-SEM) images of the powder samples were obtained on an S-5200 microscope (Hitachi) operating at 1 kV. The Si/Al ratio of the samples was determined by using an inductively coupled plasma-atomic emission spectrometer (ICP-AES, Shimadzu ICPE-9000). The amounts of OSDA in the as-synthesized samples and coke formed during the reaction were determined from the weight loss from 473 to 1073 K in a thermogravimetric (TG) profile, which was performed on a thermogravimetric-differential thermal analyzer (TG-DTA, Rigaku Thermo plus EVO II). To estimate the acidic amount, ammonia desorption (NH_3-TPD) profiles were recorded on Multitrack TPD equipment (MicrotracBEL).

The high-resolution ^{27}Al MAS NMR spectra, ^{29}Si MAS NMR and ^{29}Si CP MAS NMR spectra were obtained on a JEOL ECA-600 spectrometer (14.1 T) equipped with an additional 1 kW power amplifier. The ^{27}Al and ^{29}Si chemical shifts were referenced to -0.54 at -34.12 ppm, $AlNH_4(SO_4)_2 \cdot 12H_2O$ and Polydimethylsiloxane (PDMS), respectively. The samples were spun at 15 kHz by using a 4 mm ZrO_2 rotor.

2.2.3. Hydrothermal treatment

About 300 mg of zeolite pellets (50/80 mesh) without a binder were packed into a quartz tubular flow micro reactor (6 mm inner diameter) and heated under air stream at heating rate of 5 K min^{-1} from room temperature to 973 K. Then, hydrothermal treatment was carried out at 973 K for 1h with 20 vol% H_2O (P_{H2O} = 20.3 kPa, W/F = 1.62, N_2 balance) to investigate hydrothermal stability of the zeolites. The stability was evaluated based on the relative crystallinity, which is defined as change in the sum of the intensities of the diffraction peaks assigned to the **CHA** structure [10].

2.2.4. MTO reaction

The MTO reaction over the H-type zeolites at 623 K under was carried out in a quartz tubular flow micro reactor (6 mm inner diameter) loaded with 100 mg of zeolite pellets (50/80 mesh) without a binder. The pressure of methanol was set at 5 kPa with He as a carrier gas. W/F for methanol was set at 34 g-cat h mol^{-1}. The catalyst was activated in flowing He at 773 K for 2 h prior to the reaction, and then cooled to the desired reaction temperature. The MTO reaction gives ethylene (C2=), propene (C3=), butenes (C4=), paraffins (C1-C4), over-C5 hydrocarbons, and dimethyl ether (DME) as products. The reaction products were analyzed by an online gas chromatograph (GC-2014, Shimadzu) equipped with HP-PLOT/Q capillary column and an FID detector. The selectivities of the products were calculated on the carbon number basis.

2.3. Results and Discussion

2.3.1. Physicochemical properties

Figure 2.1 showed XRD pattern of the **CHA**-type zeolite synthesized by various SDA, and in each sample was observed **CHA** structure. The intensity ratio of each peaks

were different depending on the included SDA and Crystal growth. After calcined samples of [BTMA, Na] and [TMAda, Na], the intensity of the first peak was the highest. and the highest peaks of [K, Na] was 20 and 32 º. The **CHA** were synthesized in OSDA-Free conditions are known to the peak intensity of 20, 32 ° is increased. [11] Figure 2.2 shows the SEM image of the obtained samples, the shape of each sample has a structure such that stacked. The particle size was large in the [TEA, Na]. In other cases, the particle size was the same.

It was reported that the OSDA greatly affects the physicochemical properties of zeolite. [15] The physicochemical properties of the synthesized samples are summarized in Table 2.2. The composition analysis of each sample revealed that the ratio of Si/Al in products is greatly different. [K, Na], [M3HQui, Na] was produced with a low Si/Al ratio, and [TEA, Na] was Si/Al = 6.7, [BTMA, Na] was high silica region such as Si/Al = 15. When investigating the Na/Al ratio and the SDA/Al ratio of the products, the sample was increased Si/Al ratio with increasing SDA/Al ratio in zeolite. The SDA used in zeolite synthesis, which has a high Si/Al ratio as C/N ratio in SDA increased. [12] [BTMA, Na] has a higher Si/Al ratio due to include many SDA in framework. The N_2 adsorption and desorption isotherms for all of the samples exhibited a typical patterning of microporous materials with a plateau a high relative pressures (type I, IUPAC). The BET surface area (S_{BET}) and micropore volume (Vm) of [K, Na], [M3HQui, Na] and [TMAda, Na] were smaller than those of [TEA, Na] and [BTMA, Na]. The external surface area (S_{EXT}) of [TEA, Na] was smaller than other samples, this result was supported that [TEA, Na] was large particle size.

2.3.2. Estimated of Al distribution

Recently, Okubo and coworker reported that the distribution of Al atoms in the framework can be controlled by arbitrarily selecting OSDA. [16] Here, Al atom distribution of **CHA**-type zeolite synthesized with different OSDA was estimated from NMR measurement.

Figure 2.3A shows the ^{27}Al MAS NMR spectra of all the samples. The peak derived from a tetrahedral coordinate Al species was observed at 58 ppm in any sample, and an extra framework Al species near 0 ppm was not observed. Figure 2.3B showed the ^{29}Si MAS NMR spectra of all the samples and the result of deconvolution of the spectra are summarized in Table 2.3. Assignment of the observed peak was carried out in [Ref 13,14]. [K, Na], [M3HQui, Na] and [TMAda, Na] were observed $Si(OSi)_4$, "Q^4(0Al)", $Si(OSi)_3(OAl)_1$, "Q^3(1Al)", $Si(OSi)_2(OAl)_2$, "Q^4(2Al)", $Si(OSi)_3(OH)$, "Q^3(0Al)", $Si(OSi)_1(OAl)_3$, "Q^4(3Al)". [TEA, Na] and [BTMA, Na] were observed Q^4(0Al), Q^4(1Al), and Q^4(2Al), which were not observed Q^4(3Al) due to low Al amount. The amounts of Q^4(3Al) and Q^4(2Al) in CHA were increased with increasing the amount of Al in the framework from the results of the deconvolution of each sample. [K, Na] showed that the Si/Al ratio obtained by NMR was low and the proportion of Q^4(3A1) and Q^4(2A1) was higher than other sample. In addition, [BTMA, Na] has a high Si/Al ratio and a high proportion of Q^3(0Al). The relationship between the Si/Al ratio of the obtained zeolite and the ratio of Q^4(1Al) and Q^4(2Al) is shown Figure 2.4. Comparing the [TMAda, Na_L] and [TMAda, Na_H], the amount of Q^4(1Al) was decreased with decreasing the amount of Al species. The proportion of Q^4(2Al) was hardly observed in the range of low Al amount. Comparing the Q^4(2Al) ratio and Q^4(1Al) ratio of **CHA**-type zeolite synthesized by TMAdaOH, was no significant difference. In addition, the proportion of

Q^4(2Al) was high using K^+ cation compered to using other SDA. This result was implied that pairing Al species was formed because of using small counter cation. Furthermore, in the case of [BTMA, Na], the proportion of Q^4(2Al) in the framework was small and large number of defect sites due to When using [M3HQui, Na] and [TEA, Na], the Al distribution was not changed compared to [TMAda, Na].

2.3.3. Hydrothermal stability

Figure 2.5 showed the hydrothermal stability of the different **CHA**-type zeolites. With increasing the Al amount in [TMAda, Na], the hydrothermal stability was decreased. It has been reported that Al species contained in the framework desorbs by hydrothermal treatment and samples with higher amounts of Al in the framework have lower stability under hydrothermal conditions. [17] Comparing the hydrothermal stability of **CHA**-type zeolite synthesized using each structure directing agents with the hydrothermal stability when using [TMAda, Na], [BTMA, Na] showed the same hydrothermal stability as [TMAda, Na], and [TEA, Na], [M3HQui, Na] and [K, Na] showed high hydrothermal stability. Particularly in the region with a large amount of Al, the difference in hydrothermal stability was remarkably observed. Hydrothermal stability of the zeolite is influenced by the particle diameter, Al content in framework the Al amount and defects site. In the synthesis using various SDA, the amount of Al and the particle state of the obtained **CHA** were different, which is considered to have been influenced by these.

In addition, Figure2.6 shows a model of **CHA**-type zeolite introduced a structure directing agent. When SDA having a small size is used as a structure directing agents, many counter cations can be introduced into the cha cage. One of the causes of the

difference in hydrothermal stability tends to be that cages with a large amount of Al and small cages tend to be formed in the system using TMAdaOH for SDA.

2.3.4. MTO performance

CHA-type zeolites in one catalyst that allows the synthesis of selectively light olefins from methanol. **CHA**-type zeolite does not detect high carbon number component and shows high selectivity of low carbon number such as ethylene or propylene. The MTO reaction activity is affected by the particle diameter, particle shape, Al amount, and Al distribution. [18] Therefore, MTO reaction was performed on **CHA** synthesized with various SDA, and the difference in life time and activity was examined.

The result of MTO reaction on **CHA**-type zeolite synthesized using TMAdaOH with different Si/Al ratio and **CHA** synthesized using different OSDA is shown in Figure2.7. Catalytic life time of MTO over [TMAda, Na] was shorted with increasing Al amount in framework. The zeolite with short catalyst life tend to produce coke in MTO reaction. [19] Therefore, this result suggests that the coke is easy to produce and catalytic life time is short when the Al species in **CHA**-type zeolite is large amount and dense. In the case of the **CHA**-type zeolite synthesized by various SDA, the catalytic life time was not changed in the region with a small Al amount (Al amount: 1.0 mmol g^{-1}) but [K, Na], [M3Qui, Na] produced in the region with a large amount of Al had a longer catalytic life time than [TMAda, Na]. [TEA, Na] has a shorter catalyst life than [TMAda, Na]. It is known that the sample with a large particle size has a short catalytic life time [20], and this result showed that [TEA, Na] has a short lifetime due to the large particle diameter. Based on these facts, in the case of using TMAdaOH, cages with densely packed Al atoms and few cages are present and pore blockage tends to occur in densely packed cages, so

[K, Na], [M3Qui, Na], it can be suggested that deactivation was faster.

2.4 Conclusions

We synthesized **CHA**-type zeolite using various SDA and evaluated physicochemical, hydrothermal and catalytic properties. When synthesized using BTMAOH for SDA, Formation of **CHA**-type zeolite with Si/Al = 15 was confirmed. In addition, when TEAOH, M3HQuiOH, KOH were used for SDA, it was confirmed that Si/Al = 4.0 - 6.0 was generated in the high Al content region. **CHA**-type zeolite was confirmed in a wide range in the case of using the TMAdaOH as SDA. Comparison of hydrothermal stability of **CHA**-type zeolite, there was no significant difference between [BTMA, Na] and [TMAda, Na] in the high silica region but [TEA, Na], [M3HQui, Na] and [K, Na] in the high Al region have higher hydrothermal stability than [TMAda, Na].

References

[1] Zones, S. I. Zeolite SSZ-13 and its method of preparation. Patent **1985**

[2] Itakura M., Inoue T., Takahashi A., Fujitani T., Oumi Y., Sano T., *Chem. Lett.* **2008** 37 908

[3] Martin N., Moliner M. Corma A., *Chem Commun.*, **2015**, 51, 9965

[4] Pinar A. B., Gómez-Hortigüela L., McCusker L. B., PérezPariente J., *Chem. Mater.*, **2013**, 25, 3654.

[5] Yokoi T., Mochizuki H., Namba S., Kondo J. N., Tatsumi T., *J. Phys. Chem. C,* **2015**, *119*, 15303.

[6] Yokoi T., Mochizuki H., Biligetu T., Wang Y., Tatsumi, T., *Chem. Lett.*, **2017**, 46, 798–800

[7] Biligetu, T.; Wang, Y.; Nishitoba, T.; Otomo, R.; Park, S.; Mochizuki, H.; Kondo, J.

N.; Tatsumi, T.; Yokoi, T., *J. Catal.*, **2017**, 353, 1

[8] Park, S.; Biligetu, T; Wang, Y.; Nishitoba, T.; Junko N. Kondo, Yokoi, T., *Catal. Today*, in press. https://doi.org/10.1016/j.cattod.2017.07.022.

[9] Iorio, J. R. D.; Gounder, R., *Chem. Mater.*, **2016**, 28, 2236

[10] Takata, T.; Tsunoji, N.; Takamitsu, Y.; Sadakane, M.; Sano, T., *Micropor. Mesopor. Mater.*, **2017**, 246, 89

[11] Imal, H.; Hayashida, N.; Yokoi, T.; Tatsumi, T.; *Micropor. Mesopor. Mater.,* **2014**, 15, 341

[12] Kubota Y., Helkamp M. M., Zones S. I., Davis M. E., *Micropor. Mater.* **1996**, 6, 213

[13] Lippmaa E., Satnoson M. M. A., Engelhardt G., Grimmer A. R., *J. Am. Chem. Soc.* **1980**, 102, 4889

[14] Klinowski, J., *Prog. Nucl. Magn. Reson. Spectrosc.* **1984**, 16, 237

[15] Yokoi T., Mochizuki H., Namba S., Kondo J. N., Tatsumi T., *J. Phys. Chem. C* **2015**, 119, 15303

[16] Muraoka K., Chaikittisilp, W., Yanaba Y., Yoshikawa T., Okubo T., *Angew. Chem. Int. Ed.*, **2018**, 57, 3742

[17] Masuda T., Fujikata Y., Mukai R. S., Hashimoto K., *Applied Catalysis A General*, **1998**, 172, 73

[18] Zhu Q., Kondo N. J., Ohuuma R., Kubota Y., Yamaguchi M., Tatsumi T., *Micropor. Mesopor. Mater.*, **2008**, 112, 153

[19] Muller S., Liu Y., Kirchberger F. M., Tonigold M., Sanchez M., Lercher J. A., *J. Am. Chem. Soc.*, **2016**, 138, 15994

[20] Nishiyama N., Kawaguchi M., Hirota Y., Vu V. D., Egashira Y., *Applied Catalysis A :General*, **2009**, 362, 193

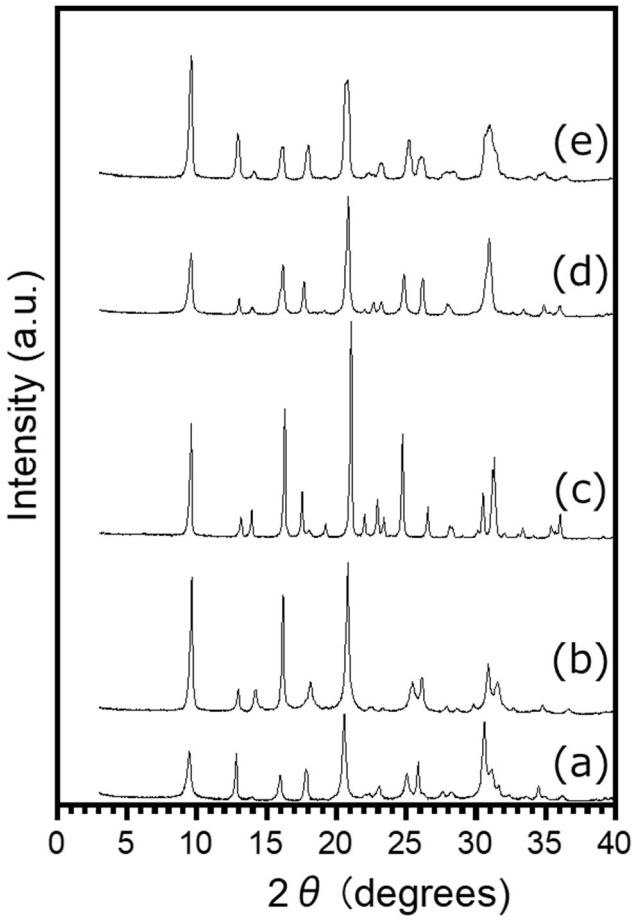

Figure 2.1 XRD patterns of [K, Na] (a), [TEA, Na] (b), [BTMA, Na] (c), [M3QuiOH, Na] (d) and [TMAda, Na] (e)

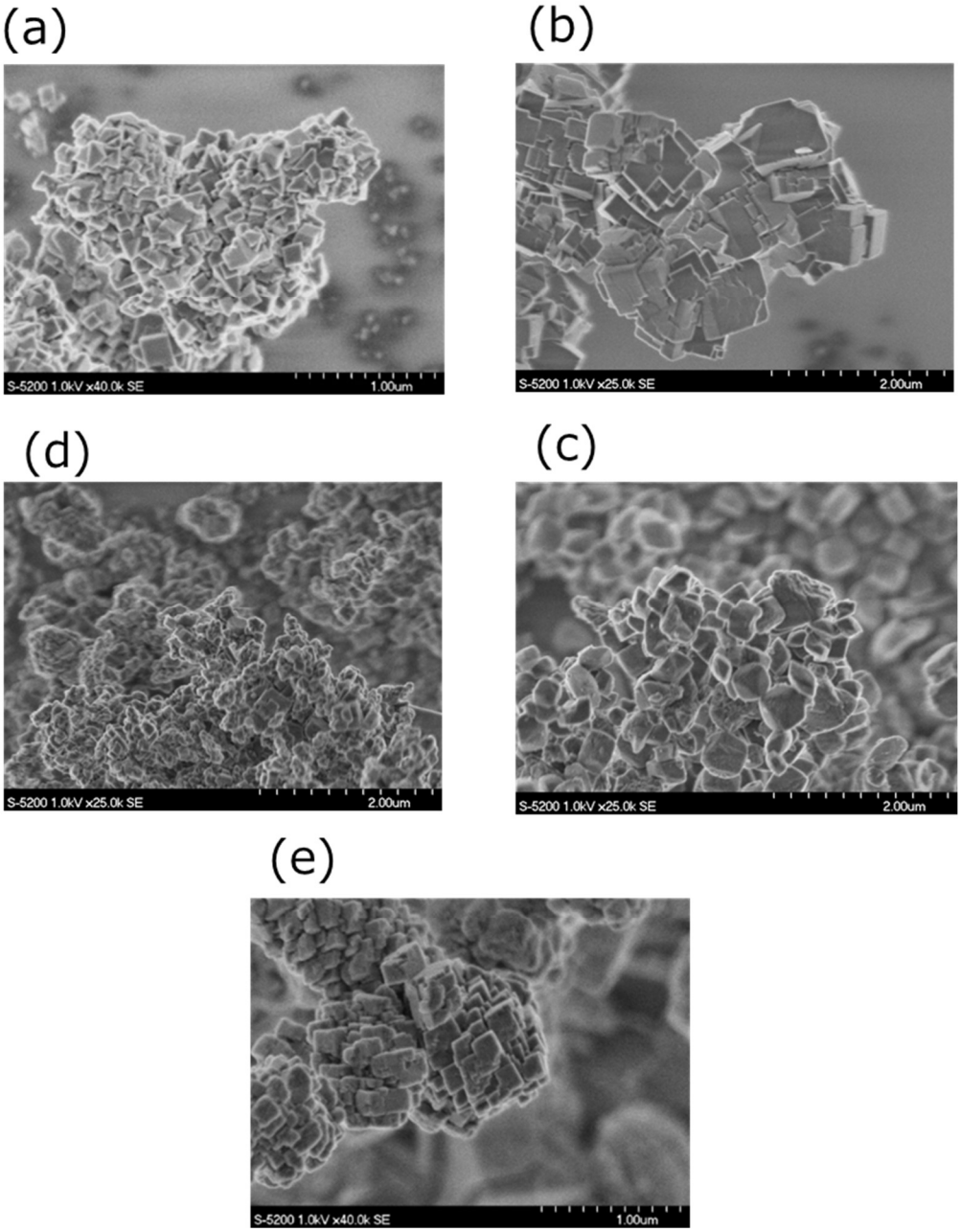

Figure 2.2 SEM images of (a) [K, Na], (b) [TEA, Na], (c) [BTMA, Na], (d) [M3HQui, Na] and (e) [TMAda, Na]

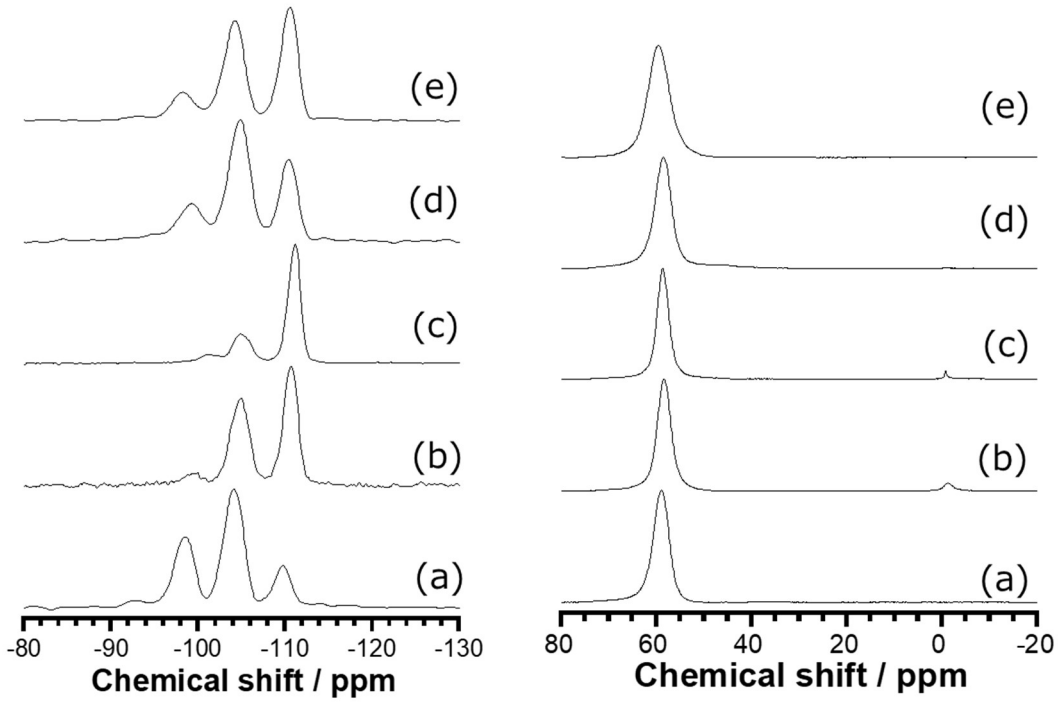

Figure 2.3 ^{29}Si MAS NMR and ^{27}Al MAS NMR spectra. (left: ^{29}Si MAS NMR, right: ^{27}Al MAS NMR) (a) [K, Na], (b) [TEA, Na], (c) [BTMA, Na], (d) [M3HQui, Na], (e) [TMAda, Na]

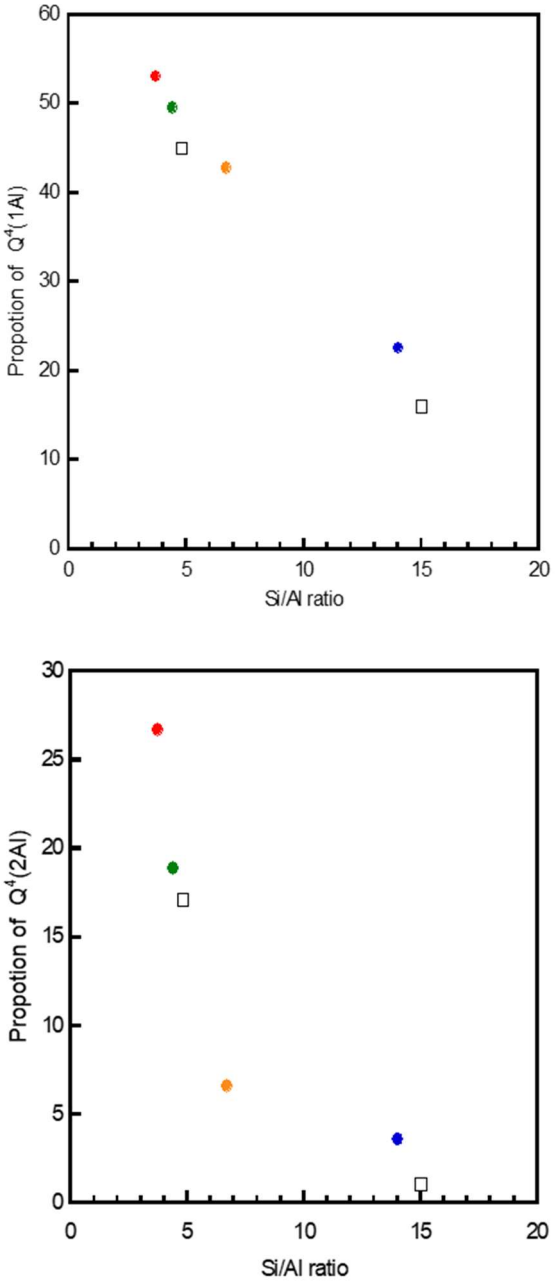

Figure 2.4 Relationship between the Si/Al ratio of the obtained zeolite and the proportion of Q^4(1Al) and Q^4(2Al), □: [TMAda, Na], ●: [M3HQui, Na], ●: [BTMA, Na], ●: [TEA, Na], ●: [K, Na]

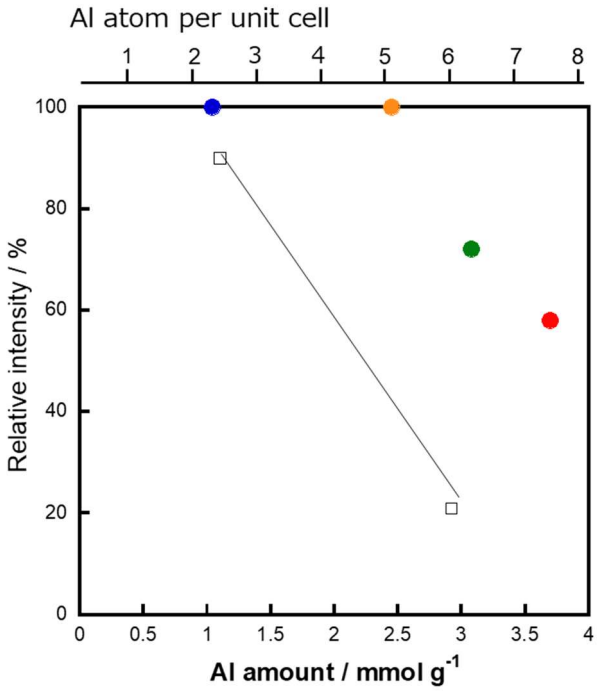

Figure 2.5 Relationship of Al amount and hydrothermal stability

□: [TMAda, Na], ●: [M3HQui, Na], ●: [BTMA, Na], ●: [TEA, Na], ●: [K, Na]

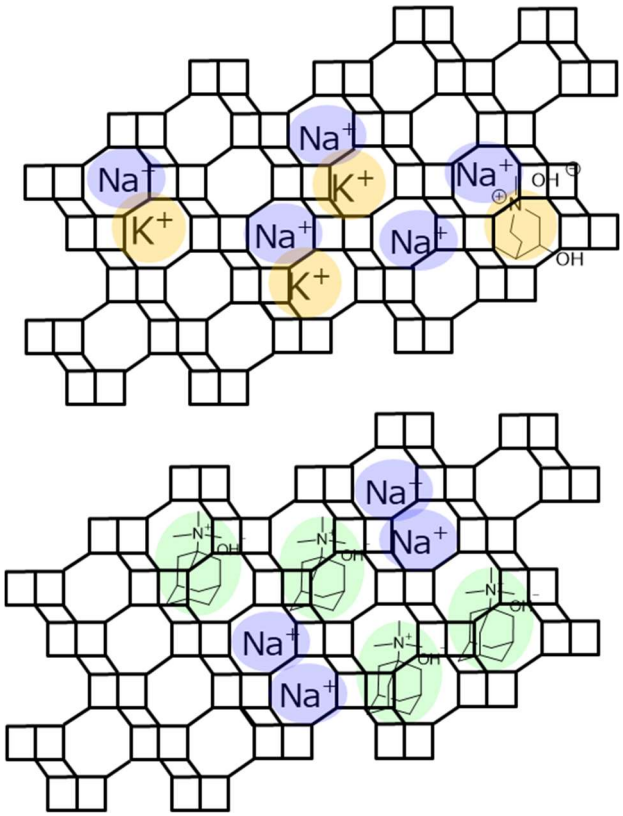

Figure 2.6 The model of **CHA**-type zeolite introduced a structure directing agent.

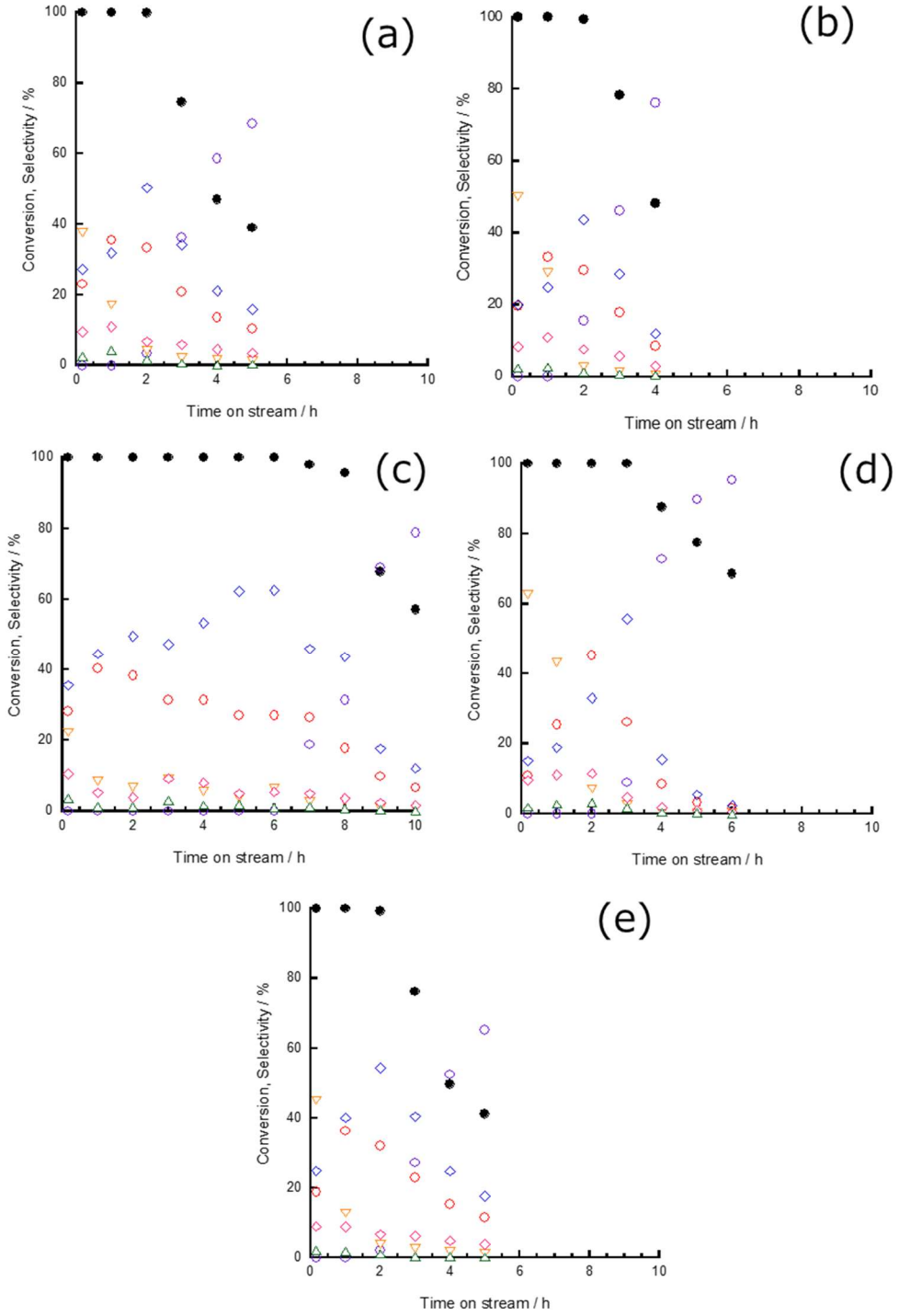

Figure 2.7 MTO reaction results of (a) [K, Na], (b) [TEA, Na], (c) [BTMA, Na], (d) [M3HQui, Na], (e) [TMAda, Na] Reaction conditions; P_{MeOH}, 5 kPa; W/F= 34 g h mol^{-1}; reaction temp., 623 K.

● ; Conversion, ◇: propene, ▽: paraffin, ○: ethane, ◇ : C4s, ○: DME, △:over C5

Table 2.1. Synthesis conditions of **CHA**-type zeolites

Sample	Molar compositions in the gels				Temp. / ºC	Time / h
	Si/Al	Na/Si	OSDA/Si	H_2O/Si		
[K, Na][a]	15	0.6	0.1[d]	100	170	40
[TEA, Na][b]	15	0.6	0.55	40	170	72
[BTMA, Na][b]	30	0.2	0.2	5	130	168
[M3HQui, Na][b]	15	0.2	0.15	40	170	120
[TMAda, Na_L][c]	5	0.2	0.2	40	170	120
[TMAda, Na_H][c]	15	0.2	0.2	40	170	120

a silica source: fumed silica, alumina source: $NaAlO_2$.

b silica source and alumina source: **FAU**-type zeolite.

c silica source: fumed silica, alumina source: $Al(OH)_3$.

d K/Si ratio.

Table 2.2 Physicochemical properties of different **CHA**-type zeolites

Sample	Si/Al[a]	Na/Al[a]	SDA/Al[a]	Acid Amount[b] /mmol g^{-1}	Textural properties[b]		
					S_{BET} / m^2 g^{-1}	S_{ext} / m^2 g^{-1}	V_{micro} / m^2 g^{-1}
[K, Na]	3.7	0.70	-	1.7	632	44	0.24
[TEA, Na]	6.7	-	0.38	-	783	11	0.31
[BTMA, Na]	15	-	0.88	-	813	32	0.40
[M3QuiOH, Na]	4.4	-	0.25	-	510	37	0.21
[TMAda, Na_L]	4.6	0.29	0.29	1.8	623	-	0.26
[TMAda, Na_H]	14.5	-	-				

a): Measured calcined Na-from or as-made sample.

b): Measured by H-form sample.

Table 2.3 Deconvolution of ^{29}Si MAS NMR spectra of **CHA**-type zeolite

Sample	Si/Al [a] (NMR)	Proportion of $Q^4(nAl)$ [b] and $Q^3(nAl)$ [c] / %				
		$Q^4(3Al)$	$Q^4(2Al)$	$Q^3(0Al)$	$Q^4(1Al)$	$Q^4(0Al)$
K, Na	4.0	2.2	23.7	≦0.1	47.3	20.5
TEA, Na	7.1	≦0.1	6.6	≦0.1	42.8	50.6
BTMA, Na	13.3	≦0.1	3.6	6.6	22.6	67.1
M3HQui, Na	4.2	1.8	19.8	≦0.1	50.7	27.7
TMAda, Na	4.6	2.1	17.8	≦0.1	44.6	35.5

a: Si/Al atomic ratio in the sample determined by ^{29}Si MAS NMR spectra.

b: $Q^4(nAl)$: $Si(OSi)_{4-n}(OAl)_n$.

c: $Q^3(nAl)$: $Si(OSi)_{3-n}(OH)(OAl)_n$.

Chapter III

*Effect of Starting Materials on the Al distribution and Catalytic performance of **CHA**-type Aluminosilicate Zeolites*

3.1 Introduction

The Al distribution in the **CHA**-type zeolite has been discussed in terms of the distance between Al atoms, so-called "isolated" or "pairing" Al spices. Actually, in addition to the Al amount, its distribution in the **CHA**-framework greatly affects the catalytic activities. Davis and his coworkers reported that the **CHA**-type zeolite with a high proportion of pairing Al spices led to the production of heavier coke in the MTO reaction compared to that with a high proportion of isolated Al spice. [1] Schneider and his coworker have investigated that the influence of the isolated and pairing Al species on the Cu-ion exchange and the NH_4 adsorption states based on by the DFT calculation. [2] Recently, Gounder and his coworker have found that the only use of N, N, N-trimethyl-1-adamantammonium cation ($TMAda^+$) as an organic-structure-directing agent (OSDA) resulted in the preferential formation of "isolated" Al species in the **CHA**-type aluminosilicate zeolite, while the use of $TMAda^+$ in combination with Na^+ of led to the formation of pairing Al spices with a high proportion. [3] Thus, the distribution of Al atoms in the **CHA**-type zeolite framework has been mostly investigated in terms of the charge balance so far.

The **CHA**-type aluminosilicate zeolites are directly synthesized from an amorphous aluminosilicate gel by using $TMAda^+$ as OSDA. It can also be synthesized from the **FAU**-type zeolite as Si and Al sources in the presence or absence of TMAdaOH. [4-6]. The influence of the starting materials, i.e., Si and Al sources, has been investigated in terms of the composition in the final **CHA** framework, while its impact on the Al distribution has not fully been investigated to date. In this work, the proportion of "Q^4(nAl)", $Si(OSi)_{4-n}(OAl)_n$, and "Q^3(nAl)", $Si(OSi)_{3-n}(OH)\ (OAl)_n$, in the total framework Si atoms, which can be estimated by solid state ^{29}Si MAS NMR technique,

has been applied to as an index for Al distribution. Previous chapter report that synthesis of **CHA**-type zeolite using various SDA. However, those synthesis methods were difficult of control of Al amount, Al distribution and particle shape.

In this chapter, in order to clarify the influence of the starting materials on the Al distribution in the **CHA**-type zeolite, the **CHA**-type aluminosilicate zeolites were synthesized in the presence of TMAdaOH from the different starting materials including fumed silica, aluminum hydroxide, and the **FAU**-type zeolite, with their proportions varied. The synthesized products were carefully characterized by various techniques, especially solid-state NMR. Finally, the impacts of the Al distribution on the hydrothermal stability and catalytic properties in the MTO reaction were investigated.

3.2 Experimental

3.2.1 Preparation of CHA-type zeolites

The raw materials used in this study were fumed silica (Cab-O-Sil M5), aluminum hydroxide (Aldrich), the **FAU**-type zeolite (JRC-Z-Y5.5, Si/Al = 2.8), NaOH (Wako, 99.8%) and TMAdaOH. TMAdaOH was obtained from purchased adamantanamine (Tokyo Chemical Industry Co., Ltd.) via methylation with iodomethane followed by anion exchange using ion-exchange resin.

The **CHA**-type aluminosilicate zeolites were synthesized according to the previous report [7]. For the purpose of investigating the effect of the starting materials, $Al(OH)_3$ and the **FAU**-type zeolite (Si/Al = 2.8) were used as Al source with their proportions varied; the proportion (x) was defined as follows.

$$\mathbf{x = Al_{FAU} / (Al_{FAU} + Al_{Al(OH)3})}$$

where Al_{FAU} and $Al_{Al(OH)3}$ are the number of the Al atoms from the **FAU**-type zeolite and $Al(OH)_3$, respectively, and x was varied ranging from 0 to 1.0. At x = 0.1–1.0,

the molar composition of the mother gel was 1 SiO_2 / 0.05 Al_2O_3 / 0.2 NaOH / 0.2 $TMAda^+$/ 10 H_2O. At x = 0, the H_2O composition was changed from 10 to 30. The molar compositions of the starting materials were listed in Table S1. After adding the calcined SSZ-13 (Si/Al = 7.7) as seed crystals (5.0 wt%), the prepared mother gel was stirred at 353K for 3h followed by crystallized at 423 K in a rotating oven at 40 rpm for 5 days. The obtained as-synthesized Na-type product was filtered, dried at 373 K, calcined at 873 K in air. The ion-exchange was carried out with stirring at 353 K for 3 h using 2.5 M NH_4NO_3 aqueous solution twice to obtain the NH_4-type. After collecting the solid by filtration, the resultant product was calcined in air at 873 K for 3 h to obtain the H-type zeolite. Thus obtained products were designated as CHA-F-x.

3.2.2 Characterization

Powder X-ray diffraction (XRD) patterns were obtained on a Rint-Ultima III (Rigaku) instrument using a Cu Kα X-ray source (40 kV, 20 mA). Nitrogen adsorption measurements to determine the BET surface area (S_{BET}), external surface area (S_{EXT}), and micropore volume (V_{micro}) were conducted at 77 K on a Belsorp-mini II (MicrotracBEL) instrument. Field-emission scanning electron microscopic (FE-SEM) images of the powder samples were obtained on an S-5200 microscope (Hitachi) operating at 1 kV. The Si/Al ratio of the samples was determined by using an inductively coupled plasma-atomic emission spectrometer (ICP-AES, Shimadzu ICPE-9000). The amounts of $TMAda^+$ in the as-synthesized samples and coke formed during the reaction were determined from the weight loss from 473 to 1073 K in a thermogravimetric (TG) profile, which was performed on a thermogravimetric-differential thermal analyzer (TG-DTA, Rigaku Thermo plus EVO II). To estimate the acidic amount, ammonia desorption (NH_3-TPD)

were recorded on Multitrack TPD equipment (MicrotracBEL).

The high-resolution ^{27}Al MAS NMR spectra, ^{29}Si MAS NMR and ^{29}Si CP MAS NMR spectra were obtained on a JEOL ECA-600 spectrometer (14.1 T) equipped with an additional 1 kW power amplifier. The ^{27}Al and ^{29}Si chemical shifts were referenced to -0.54 at -34.12 ppm, $AlNH_4(SO_4)_2 \cdot 12H_2O$ and Polydimethylsiloxane (PDMS), respectively. The samples were spun at 15 kHz by using a 4 mm ZrO_2 rotor. Fourier transform infrared (FT-IR) spectra were obtained at a resolution of 4 cm^{-1} by using a Jasco 4100 FTIR spectrometer equipped with a Triglycine sulfate (TGS) detector. A total of 64 scans were averaged for each spectrum. IR spectra of the clean disk were recorded in vacuum at 153 K to obtain background spectra. The sample was pressed into a self-supporting disk (20 mm diameter, 30−40 mg) and placed in an IR cell attached to a closed-gas circulation system. The sample was pretreated by evacuation at 773 K, followed by adsorption of 500 Pa Pyridine at 153 K. Then, the sample was evacuated at the same temperature for 30 min. The spectra were recorded at 153 K.

3.2.3 Hydrothermal treatment

About 300 mg of zeolite pellets (50/80 mesh) without a binder were packed into a quartz tubular flow microreactor (6 mm inner diameter) and heated under air stream at heating rate of 5 K min^{-1} from room temperature to 1073 K. Then, hydrothermal treatment was carried out at 1073 K for 1h with 40 vol% H_2O (P_{H2O} = 40.5 kPa, W/F =1.62, N_2 balance) to investigate hydrothermal stability of the zeolites. The stability was evaluated based on the relative crystallinity, which is defined as change in the sum of the intensities of the diffraction peaks assigned to the **CHA** structure. [8]

3.2.4 MTO reaction

The MTO reaction over the H-type zeolites at 623 K under was carried out in a quartz tubular flow microreactor (6 mm inner diameter) loaded with 100 mg of zeolite pellets (50/80 mesh) without a binder. The pressure of methanol was set at 15 kPa with He as a carrier gas. W/F for methanol was set at 34 g-cat h mol^{-1}. The catalyst was activated in flowing He at 773 K for 2 h prior to the reaction, and then cooled to the desired reaction temperature. The MTO reaction gives ethene (C2=), propene (C3=), butenes (C4=), paraffins (C1-C4), over-C5 hydrocarbons, and dimethyl ether (DME) as products. The reaction products were analyzed by an online gas chromatograph (GC-2014, Shimadzu) equipped with HP-PLOT/Q capillary column and an FID detector. The selectivities of the products were calculated on the carbon number basis.

3.3 Results and Discussion

3.3.1. Synthesis and Physicochemical Properties

The XRD patterns of the as-synthesized products are shown in Figure 3.1, indicating that the products exhibited the pure **CHA** phase irrespective of *x*. The FE-SEM images revealed that the particle shape and size of the products except for $x = 1.0$ were almost similar; they have typical cubic particles about ca. 100-300 nm in size (Figure 3.2). At $x = 1.0$, cubic particles about ca. 500 nm in size were formed.

The physicochemical properties of the synthesized Na-type products are summarized in Table 3.1 and H-type products are summarized Table 3.2. When *x* ranged from 0 to 0.5, the Si/Al ratio in the products was almost constant (ca. 10), being consistent with that in the starting materials. However, at $x > 0.75$, the Si/Al ratio was over 13. The yield of the solid product, which was based on the weight of as-synthesized product excluded from the organic content from $TMAda^+$, was decreased along with *x*. The **FAU**-

type zeolite used would be dissolved under the strongly base conditions, forming amorphous aluminosilicate species. Thus formed aluminosilicate species would be re-crystallized into the **CHA** structure in combination with $TMAda^+$. The fact that the yield and Al content were decreased along with *x* suggests that the produced Si and Al sources derived from the **FAU**-type zeolite are not effectively incorporated into the **CHA**-type framework compared to those from the amorphous sources. The total amount of Na^+ and $TMAda^+$ in the as-synthesized samples was almost one, indicating that the negative charges of Al atom were balanced by $TMAda^+$ in addition to Na^+. Based on the TG-DTA and CHN elemental analyses, the numbers of $TMAda^+$ per unit cell of the **CHA** structure were estimated at approximately 2 irrespective of *x*. Considering the size of $TMAda^+$, one $TMAda^+$ molecule should be located in the large *cha* cage with its molecular structure intact. Since one unit cell consists of two *cha* cages and two D6R, all of the *cha* cages would be fully occupied by $TMAda^+$; Na^+ would be preferentially located at D6R. From the N_2 adsorption and desorption measurement results, the adsorption isotherms of all of the samples exhibited a typical patterning of microporous materials (type I, IUPAC). The specific surface area (S_{BET}) and the micropore volume (V_{micro}) were estimated at more than 700 m^2/g and 0.28 cm^3/g, respectively.

3.3.2. Estimation of Al distribution

Figure 3.3 shows the ^{27}Al MAS NMR spectra of the Na-type products, indicating that the spectra of all the products exhibited an intense peak at ca. 55 ppm, which is assigned to tetrahedrally coordinated Al atoms in the framework. The peak at 0 ppm, which is assigned to octahedral coordinated Al atoms, was not remarkably observed in any samples, indicating that most of the Al atoms introduced into the synthesis gel were incorporated into the **CHA** framework.

The ^{29}Si MAS NMR spectra of the calcined Na-type products are shown in Figure 3.4, indicating two strong sharp peaks at -111 and -105 ppm, and one weak broad peak around -100 ppm. The peak at -111 ppm is assigned to "Q^4(0Al)", **Si**$(OSi)_4$. It has been well recognized that the substitution of one Al atom by one Si atoms in the zeolite framework leads to the downfield shift with about 5 ppm [9]. Hence, the peak at -105 ppm has been assigned to "Q^4(1Al)", **Si**$(OSi)_3(OAl)_1$. The broad peak at around -100 ppm consists of two peaks at -101 and -99 ppm. For all the products, the intensity of the peak at -99 ppm was significantly enhanced in the ^{29}Si CP/MAS NMR spectra (not shown here). Therefore, the peaks at -101 and -99 ppm could be assigned to "Q^4(2Al)", **Si**$(OSi)_2(OAl)_2$ and "Q^3(0Al)", **Si**$(OSi)_3(OH)$, respectively. The proportion of these Si species estimated based on the relative peak areas are listed in Table 3.4. The **FAU**–type zeolite (Si/Al = 2.8) used as Si and Al sources consists of Q^4(0Al), Q^4(1Al), Q^4(2Al) and Q^4(3Al) with the proportion of 13.0, 40.9, 38.8 and 7.4 %, respectively. (Table 3.4)

Although the proportion of Q^4(0Al) was almost unchanged irrespective of *x*, that of Q^3(0Al), *i.e.*, structural defect sites, was increased along with *x*. This is probably because the **FAU**-type zeolite used as the starting material hampered the crystallization, being consistent with the decreases in the yield and Al content. Interestingly, a tendency for a decrease in the proportion of Q^4(1Al) was observed along with *x*, while the proportion of Q^4(2Al) was slightly on the increase. Thus, we successfully found that the Al distribution was varied dependent on the starting materials, *i.e.*, the proportion of the **FAU**-type zeolite as Si and Al sources, with the Al content almost kept.

The ^{29}Si MAS NMR spectra also gave us the information about Si/Al ratio in the framework. [9,10] The Si/Al ratios estimated by the ^{29}Si MAS NMR measurements were almost consistent with those by the ICP measurements (Table 3.2); almost all of the Al

atoms are incorporated into the **CHA** framework, being supported by the ^{27}Al MAS NMR spectra. Figure 3.6 shows the relationship between **FAU** amount of raw material and amount of Q^4(1Al), Q^4(2Al) in **CHA**. As the amount of Al in the **FAU** increased, the amount of Q^4(1Al) in the product decreased and the amount of Q^4(2Al) increased. In addition, when the amount of Na contained in each generated sample was measured, the Na / Al ratio was about 0.17 - 0.21 in every sample. This result showed that the Na species was not affected Al distribution of **CHA** framework. Therefore, **CHA**-type zeolite was affected by **FAU** as the starting material, and it is possible to control the Al distribution using **FAU**. And Figure 3.7 showed that the pyridine adsorption IR spectra of CHA-F-0.1 and CHA-F-1.0. The spectrum of CHA-F-1.0 was observed four peaks. The peak of 1447 -1450 cm^{-1} was assigned by Luis acid site and 1540 cm^{-1} and 1590, 1625 cm^{-1} was assigned by Bronsted and Luis acid site.

3.3.3. Hydrothermal stability

The hydrothermal stability of the **CHA**-type zeolite is a quite important issue for practical application, and it would be generally related with the framework structure of zeolite, defect site, Al content and its distribution. [11-13] Here, the impact of the Al distribution on the hydrothermal stability was investigated.

The NH_4-type samples of were treated under steam conditions, 1073 K and 40 vol% steam (P_{H2O} = 40.5kPa, W/F =1.62, N_2 balance). The XRD patterns of the CHA-F-0.1 and CHA-F-0.75 samples before and after the steam treatment are representatively shown in Figure 3.8. Although the intensities were slightly decreased after the steam treatment for both samples, the **CHA**-type structure was retained. There was a slight difference in the degree in the decrease in the intensities between CHA-F-0.10 and CHA-F-0.75; CHA-F-0.1 was more stable than CHA-F-0.75. For all the samples, the Q^4(2Al)

and Q^4(1Al) peaks in the ^{29}Si MAS NMR spectra were dramatically decreased after the steam treatment due to the decrease in the framework Al atoms by the steam treatment (Figure 3.9). The Q^4(1Al) and Q^4(2Al) peaks were hardly observed for CHA-F-0.75, while, for CHA-F-0.1, the Q^4(1Al) were slightly retained.

The stability against the steam treatment was evaluated based on the relative crystallinity, which is defined as the change in the sum of the intensities of the peaks assigned to the **CHA** structure at $2\theta = 5$ - 40º. Figure 3.10 shows the relationships between the relative crystallinity and the proportions of $Q^4(n\text{Al})$ and $Q^3(n\text{Al})$ in the parent samples. The proportions of Q^3(0Al) and Q^4(1Al) had a slight impact on the hydrothermal stability under almost the same Al content; a tendency for a decrease in the relative crystallinity was observed with an increase in the proportion of Q^3(0Al), while the decrease was suppressed by increasing that of Q^4(1Al). Note that, the relative crystallinity was evidently decreased along with the proportion of Q^4(2Al) irrespective of x. These results imply that the amount of Q^4(2Al) in framework is one of the factors for affecting the hydrothermal stability. We have considered that in addition to the defect sites, the Al distribution in the framework affects the hydrothermal stability, and that the Al atoms in Q^4(2Al) would be easily dealuminated than those in Q^4(1Al). Figure 3.11 showed the model of Q^4(2Al). The Q^4(2Al) species was close to Bronsted acid site. so that the hydrophilic of around Q^4(2Al) species was increased. And the partial structure was distorted by Q^4(2Al) species.

Thus obtained findings suggest that the **CHA**-type aluminosilicate zeolite synthesized from the **FAU**-type zeolite with a high proportion is not stable against hydrothermal treatment because such obtained zeolite has higher proportions of Q^3(0Al) and Q^4(2Al) (Table 3). In addition, hydrothermal stability was performed on **CHA**

synthesized at various ratio of **FAU**. The result of ^{29}Si MAS NMR of each sample after the hydrothermal stability is shown in Figure 3.12. The peaks intensity of Q^4(1Al) and Q^4(2Al) were weak with increasing The hydrothermal stability was observed to be lower for samples with higher amounts of **FAU** used as raw materials. This result suggests that the sample of including large amount of Q^4(2Al) in the framework was unstable.

3.3.4. Catalytic performance in the MTO reaction

CHA-type aluminosilicate zeolite is well-known as an excellent catalyst for the MTO reaction; it selectively produces light olefins, in particular ethene (C2=) and propene (C3=). [14-16] The catalytic properties are strongly dependent on the acidic properties as well as particle size. Very recently, we have found that the Al distribution in the MFI framework has a great impact on the catalytic performance in the MTO reaction. Therefore, CHA-F-0.1, CHA-F-0.25, and CHA-F-0.5, which have almost the same Si/Al ratio, were representatively applied as catalyst for the MTO reaction.

Figure 3.13 shows the changes in the methanol conversion and the products' selectivities along with time on stream (TOS) at 623 K. There was no significant difference in the products distributions. However, a marked difference in the catalytic life was observed under the similar Si/Al ratio and the particle morphology. Regarding the catalytic life, the conversions of methanol at TOS = 480 min for CHA-F-0.1, CHA-F-0.25 and CHA-F-0.5 were 100, 97 and 94 %, respectively, and this order was consistent with the proportion of Q^4(2Al). It was confirmed that the deactivation was due to the coke deposits, not any structural changes. The amounts of coke after the reaction were estimated at 12.5, 14.8 and 18.2 wt% for CHA-F-0.1, CHA-F-0.25 and CHA-F-0.5, respectively. In the DTA profiles, all samples showed feast peak around 728 K, However the second peak was 798 K, 810, 817 K respectively (Figure 3.14), implying that more

heavy and incombustible coke were formed on CHA-F-0.5. The coke in the MTO reaction would be formed via aromatic compounds as coke precursors [17]. It is considered that they are formed by a successive reaction of propylene and butenes via dehydrogenation including hydride transfer, which is enhance by Lewis acid sites [18], and/or paring Al species [1]. The wide *cha* cage would be enough for such successive reactions involving bulky molecules. Thus, the CHA-F-0.5 catalyst with higher proportion of Q^4(2Al) produced much heavy coke, resulting in the short catalytic life compared to CHA-F-0.1 and CHA-F-0.25. In conclusion, the proportion of Q^4(2Al) would strongly influence the catalytic properties under the same Al content. In addition, the selectivity of MTO reaction was compared for CHA-F-0.1 and CHA-F-1.0, which showed significant differences in Q^4(1Al) amount and Q^4(2Al) amount. Figure 3.13 shows the relationship between the conversion and product distribution of each sample. In the case of low conversion region was produced the large amount of diethyl ether. In addition, the ethylene and propene selectivity was showed constant value the region of conversion over 40%. Compering the product distribution of both sample, ethylene selectivity of CHA-F-1.0 was higher than another one. Figure 3 15 showed the reaction mechanism of MTO reaction. MTO reaction in zeolite had two reaction mechanism which name is olefin based cycle and Aromatic based cycle. The first step was reacted by olefin based cycle and produced heavy hydrocarbons. After that, the Aromatics was produced by hydrogen transfer reaction. It was suggested that The Q^4(2Al) was promoted polymerization of hydrocarbons because of close to Al atoms. Therefore, this result suggests that The **CHA** including large amount of Q^4(2Al) was easy to generate of the aromatics, and promoted the producer of ethylene.

3.4 Conclusion

The **CHA**-type aluminosilicate zeolites were synthesized in the presence of TMAdaOH from the different starting materials including fumed silica, aluminum hydroxide, and the **FAU**-type zeolite, with their proportions varied. The ^{29}Si MAS NMR spectra clearly showed that thus obtained zeolites had different Al distributions depending on the proportion of the **FAU**-type zeolite as the starting material; a method for controlling Al distribution in the **CHA**-type zeolite has successfully been developed. The use of the **FAU**-type zeolite with a high proportion led to the high proportion of Q^4(2Al). We also clarified the impact of the Al distribution on the hydrothermal stability, and found that the proportion of Q^4(2Al) might be one of the factors for affecting the hydrothermal stability. The **CHA**-type aluminosilicate zeolite synthesized from the **FAU**-type zeolite with a high proportion showed a short catalytic life in the MTO reaction compared to that with a low proportion. In the metal-cation exchanged **CHA**-type zeolites, the Al distribution in the **CHA**-type framework will affect the state of metal cations, e.g., Cu^{2+}. Therefore, the fine-tuning of Al distribution is believed to enhance the catalytic performance and the hydrothermal stability. Our findings will contribute to the development of a new class of zeolite catalysts with the distribution of heteroatoms in the framework controlled, improving various functions in zeolites.

References:

[1] Deimund M. A., Harrison L., Lunn J. D., Liu Y., Malek A., Shayib R., Davis M. E., *ACS Catal.* **2016**, *6*, 542

[2] Paolucci C., Parekh A. A., Khurana I., Iorio J. R. D., Li H., Caballero J. D. A., Shih A. J., Anggara T., Delgass W. N., Miller J. T., Ribeiro F. H., Gounder R., Schneider W. F., *J. Am. Chem. Soc.* **2016**, *138*, 6028

[3] Iorio J. R. D., Gounder R., *Chem. Mater.* **2016**, *28*, 2236

[4] Bourgogne M., Guth J. L., Wey, R. U.S. Patent 4503024, **1983**.

[5] Zones S. I., *J. Chem. Soc. Faraday Trans.* **1991**, *87*, 3709

[6] Takata T., Tsunoji N., Takamitsu Y., Sadakane M., Sano T., *Micropor. Mesopor. Mater.* **2017**, *246*, 89

[7] Eilertsen E. A., Nilsen M. H., Wendelbo R., Olsbye U., Lillerud K. P., *Stud. Surf. Sci. Catal.* **2008**, *174A*, 265

[8] Takata T., Tsunoji N., Takamitsu Y., Sadakane M., Sano T., *Micropor. Mesopor. Mater.* **2016**, *225*, 524

[9] Lippmaa E., Satnoson M. M. A., Engelhardt G., Grimmer A. R., *J. Am. Chem. Soc.* **1980**, *102*, 4889

[10] Klinowski J., *Prog. Nucl. Magn. Reson. Spectrosc.* **1984**, *16*, 237

[11] Prodinger S., Derewinski M. A., Vjunov A., Burton S. D., Arslan I., Lercher J. A., *J. Am. Chem. Soc.* **2016**, *138*, 4408

[12] Maier S. M., Jentys A., Lercher J. A., *J. Phys. Chem. C* **2011**, *115*, 8005

[13] Lercher J. A., *Micropor. Mesopor. Mater.* **2012**, *164*, 9

[14] Yuen L., Zones S. I., Harris T. V., Gallegos E. J., Auroux A., *Micropor. Mater.* **1994**, *2*, 105

[15] Zhu Q., Kondo J. N., Ohnuma R., Kubota Y., Yamaguchi M., Tatsumi T., t*Micropor. Mesopor. Mater.* **2008**, *112*, 153

[16] Bleken F., Bjorgen M., Palumbo L., Bordiga S., Svelle S., Lillerud K., Olsbye U., *Topics in Catalysis* **2009**, *52*, 218

[17] Olsbye U., Svelle S., Bjorgen M., Beato P., Janssens T. V. W., Joensen F., Bordiga S., Lillerud K. P., *Angew. Chem. Int. Ed.* **2012**, *51*, 5810

[18] Mueller S., Liu Y., Kirchberger F. M., Tonigold M., Sanchez-Sanchez M., Lercher J. A., *J. Am. Chem. Soc.* **2016**, *138*, 15994

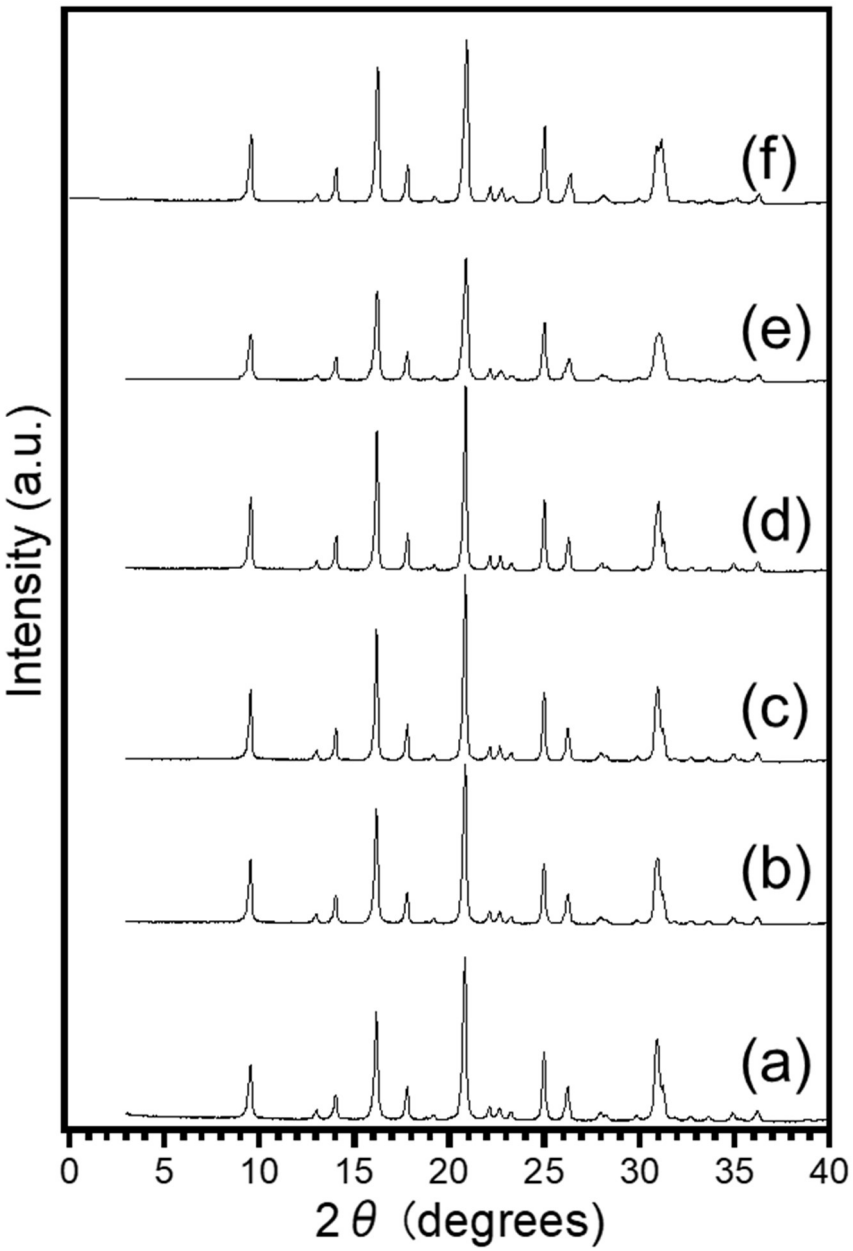

Figure 3.1 XRD patterns of (a) CHA-F-0, (b) CHA-F-0.1, (c) CHA-F-0.25, (d) CHA-F-0.5, (e) CHA-F-0.75, and (f) CHA-F-1.0.

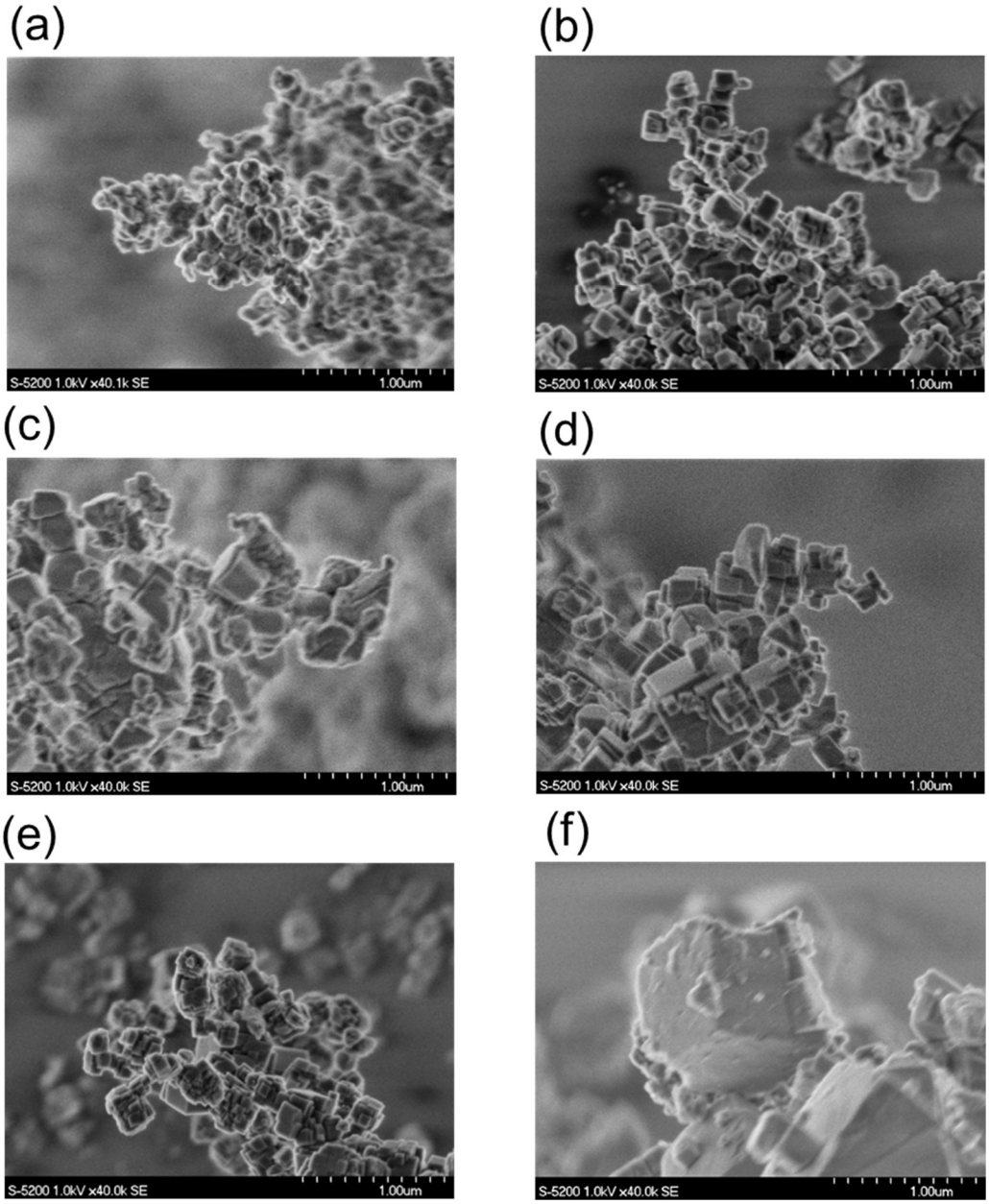

Figure 3.2 SEM images of (a) CHA-F-0, (b) CHA-F-0.1, (c) CHA-F-0.25, (d) CHA-F-0.5, (e) CHA-F-0.75, and (f) CHA-F-1.0.

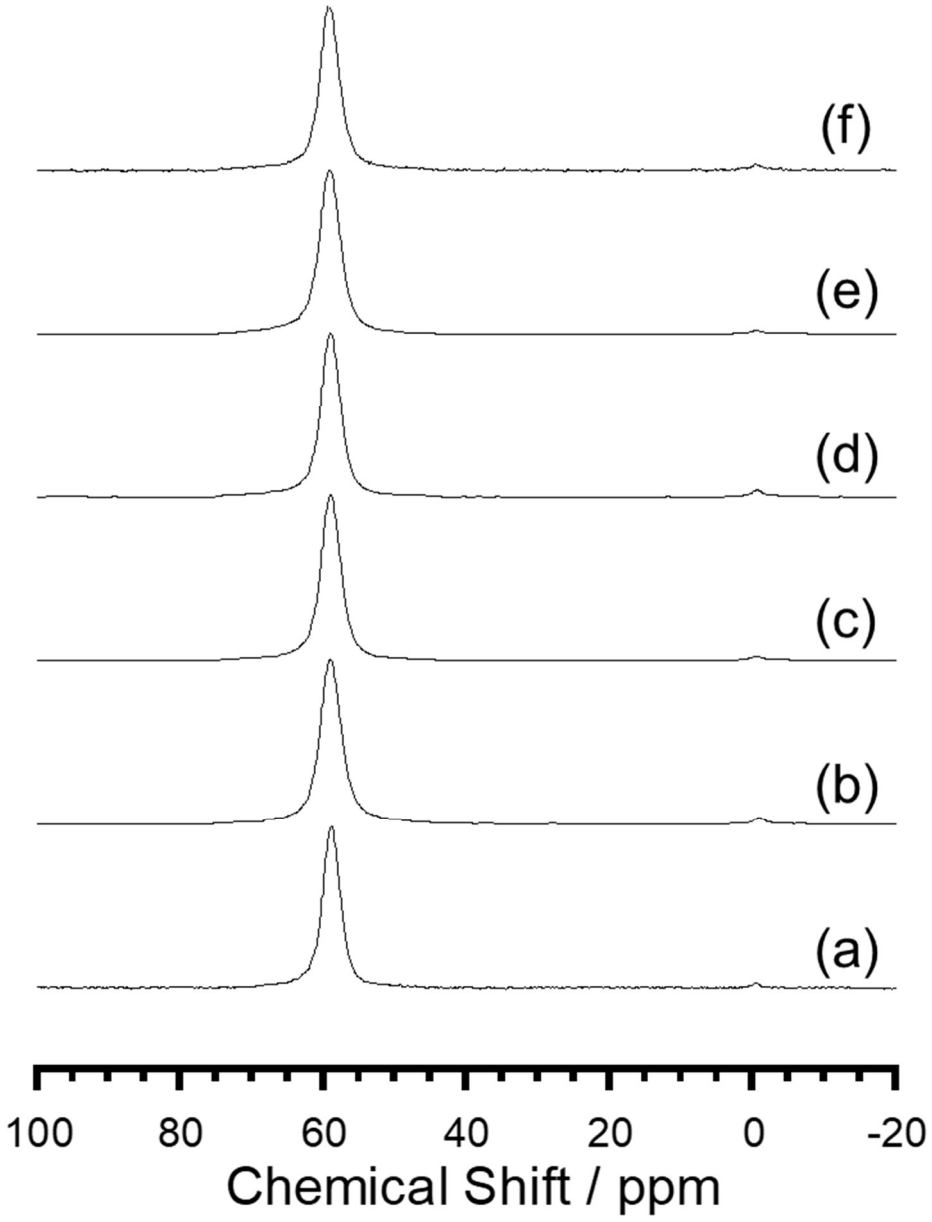

Figure 3.3 ^{27}Al MAS NMR spectra of Na-form **CHA**-type zeolite (a) CHA-F-0, (b) CHA-F-0.1, (c) CHA-F-0.25, (d) CHA-F-0.5, (e) CHA-F-0.75, and (f) CHA-F-1.0.

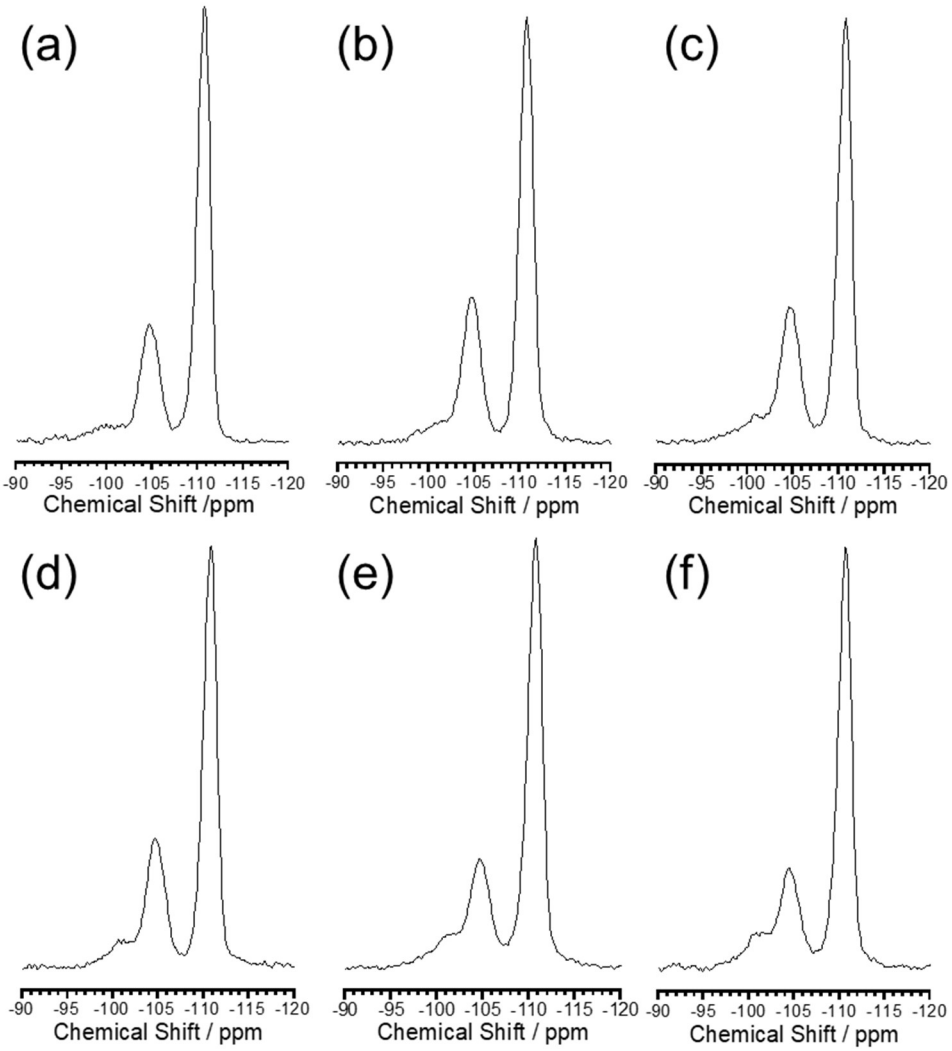

Figure 3.4 ^{29}Si MAS NMR spectra of Na-form **CHA**-type zeolite (a) CHA-F-0, (b) CHA-F-0.1, (c) CHA-F-0.25, (d) CHA-F-0.5, (e) CHA-F-0.75, and (f) CHA-F-1.0.

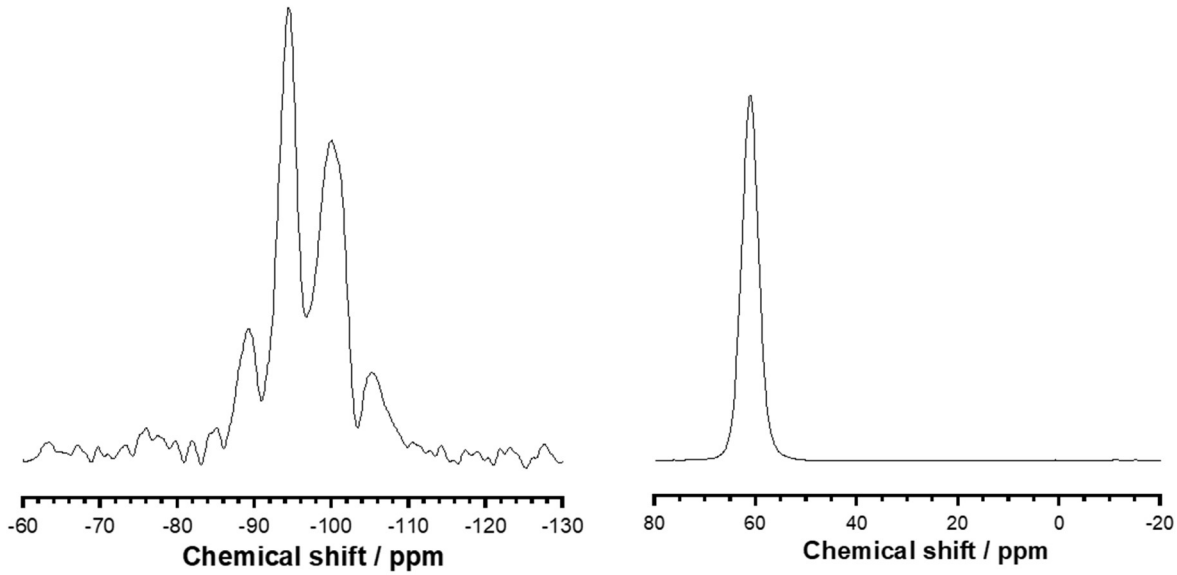

Figure 3.5 ^{29}Si MAS NMR (left) and ^{27}Al MAS NMR (right) spectra of the **FAU**-type zeolite (Si/Al = 2.8) used as an raw material.

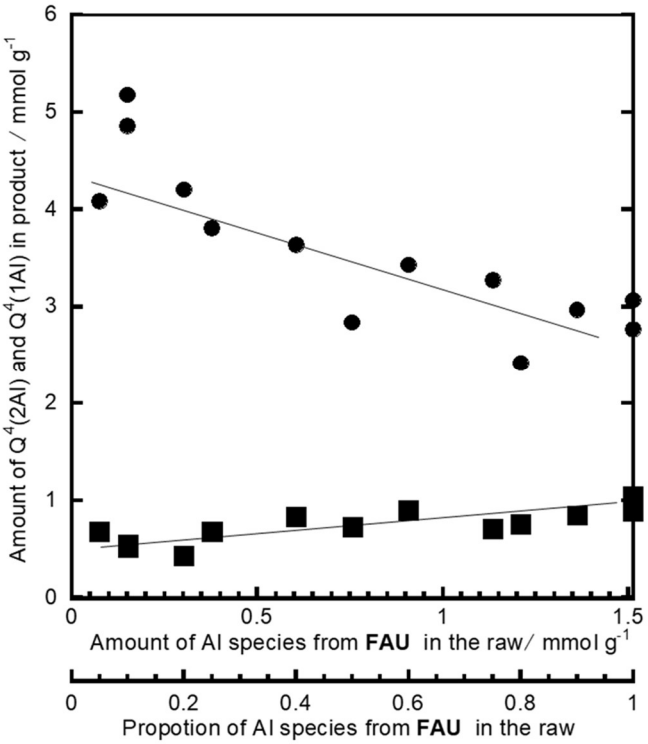

Figure 3.6 Relationship between the amount of Al species from **FAU** type zeolite in the raw materials and the amount of Q^4(1Al) and Q^4(2Al). (●: Q4(1Al), ■: Q4(2Al))

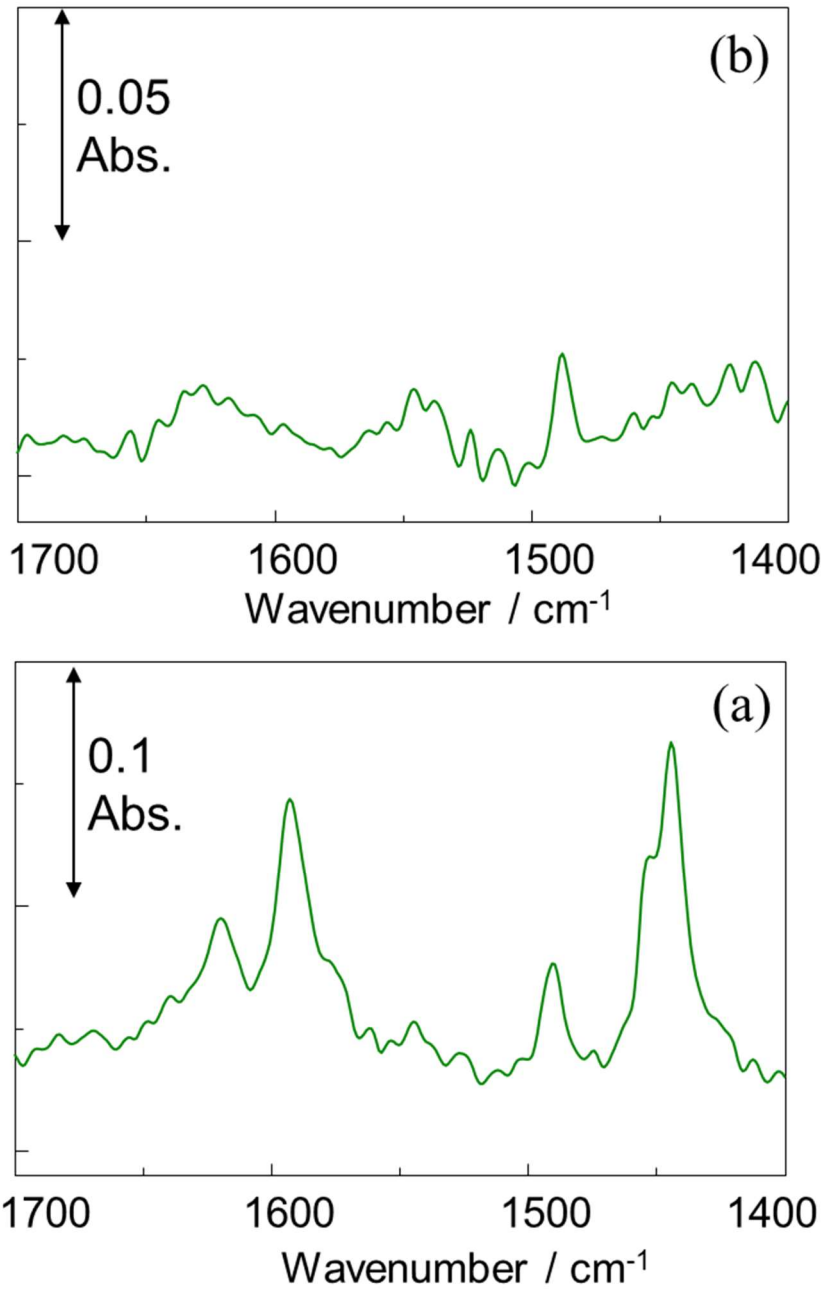

Figure 3.7 Pyridine adsorption IR spectra of H form **CHA**-type zeolite. (a) CHA-F-0.1 and (b) CHA-F-1.0

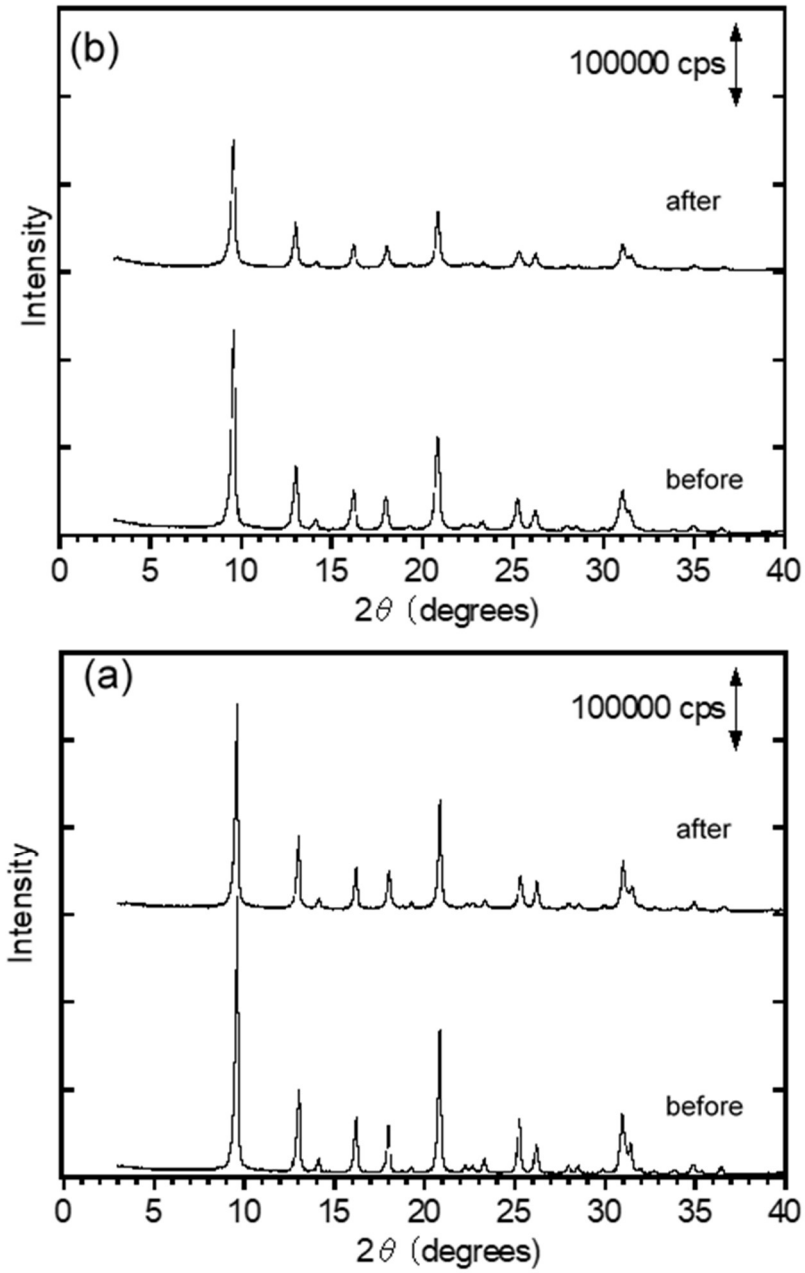

Figure 3.8 XRD patterns of (a) CHA-F-0.1 and (b) CHA-F-0.75 before and after the steam treatment.

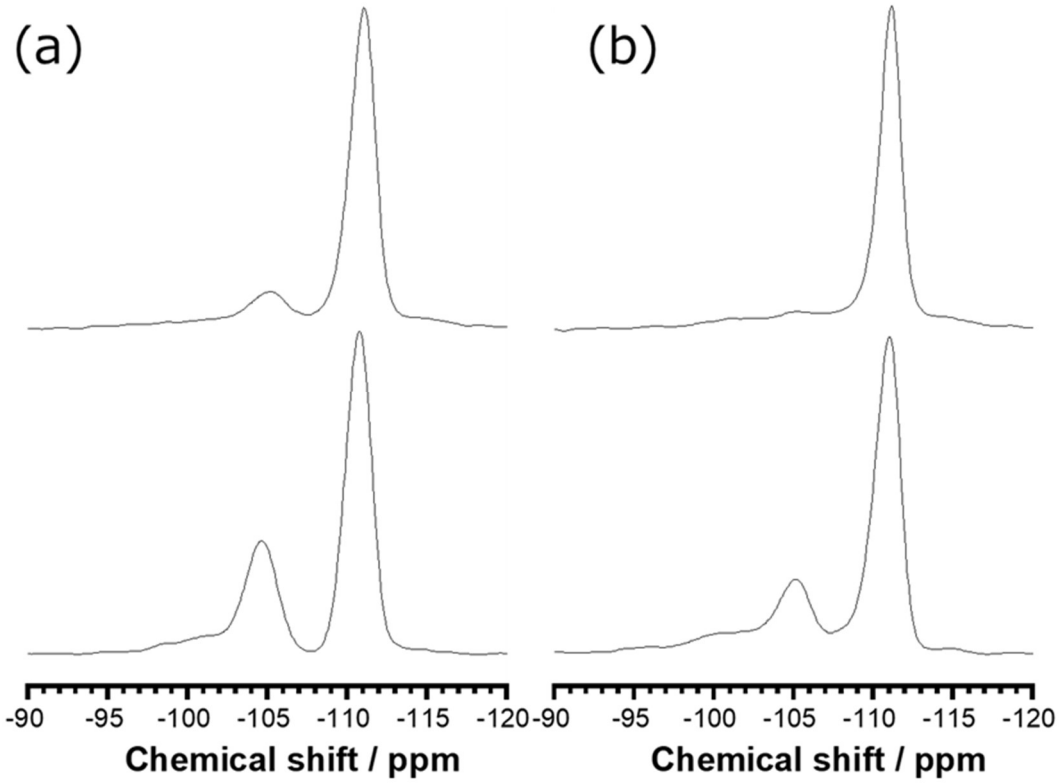

Figure 3.9 ^{29}Si MAS NMR spectra of (a) CHA-F-0.1 and (b) CHA-F-0.75 before (bottom) and after (top) the steam treatment.

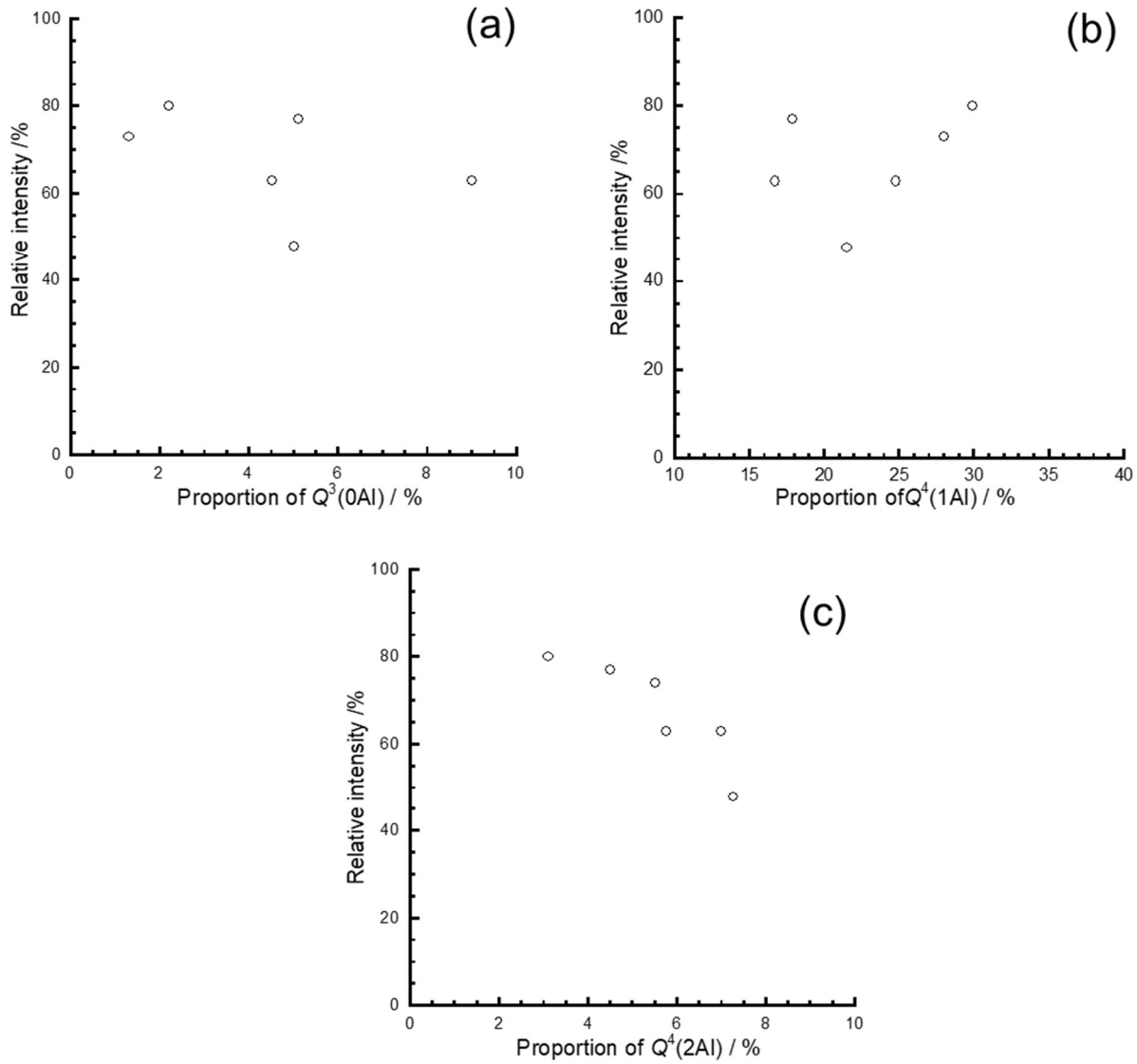

Figure 3.10 Relationships between the relative crystallinity and the proportion of (a) Q^3(0Al), (b) Q^4(1Al) and (c) Q^4(2Al).

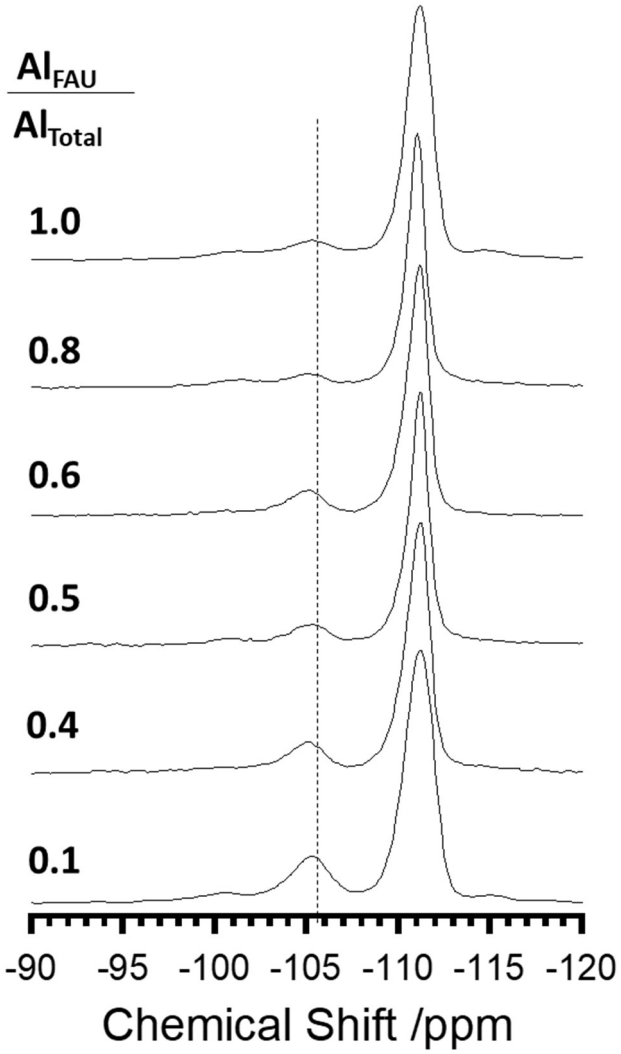

Figure 3.11 ^{29}Si MAS NMR spectra of **CHA** after steam-treatment using various proportion of **FAU** as raw material.

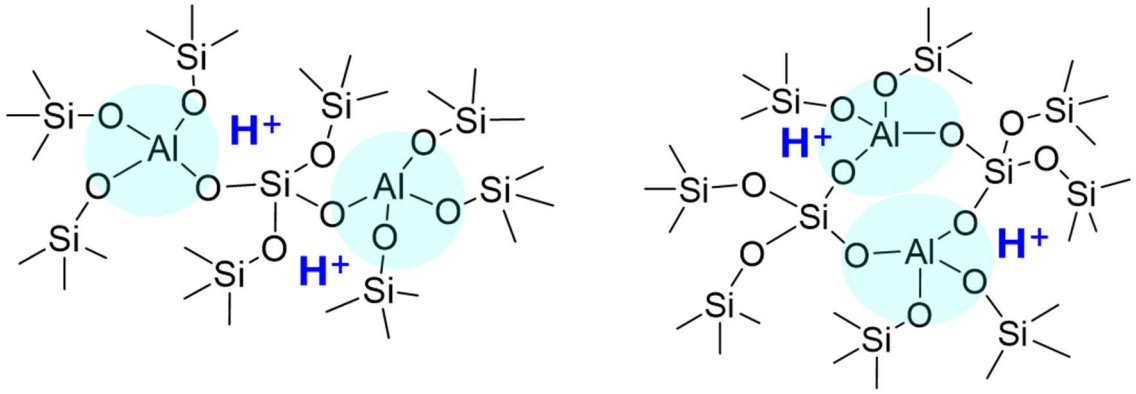

Figure 3 12 The model of Q^4(2Al) spices.

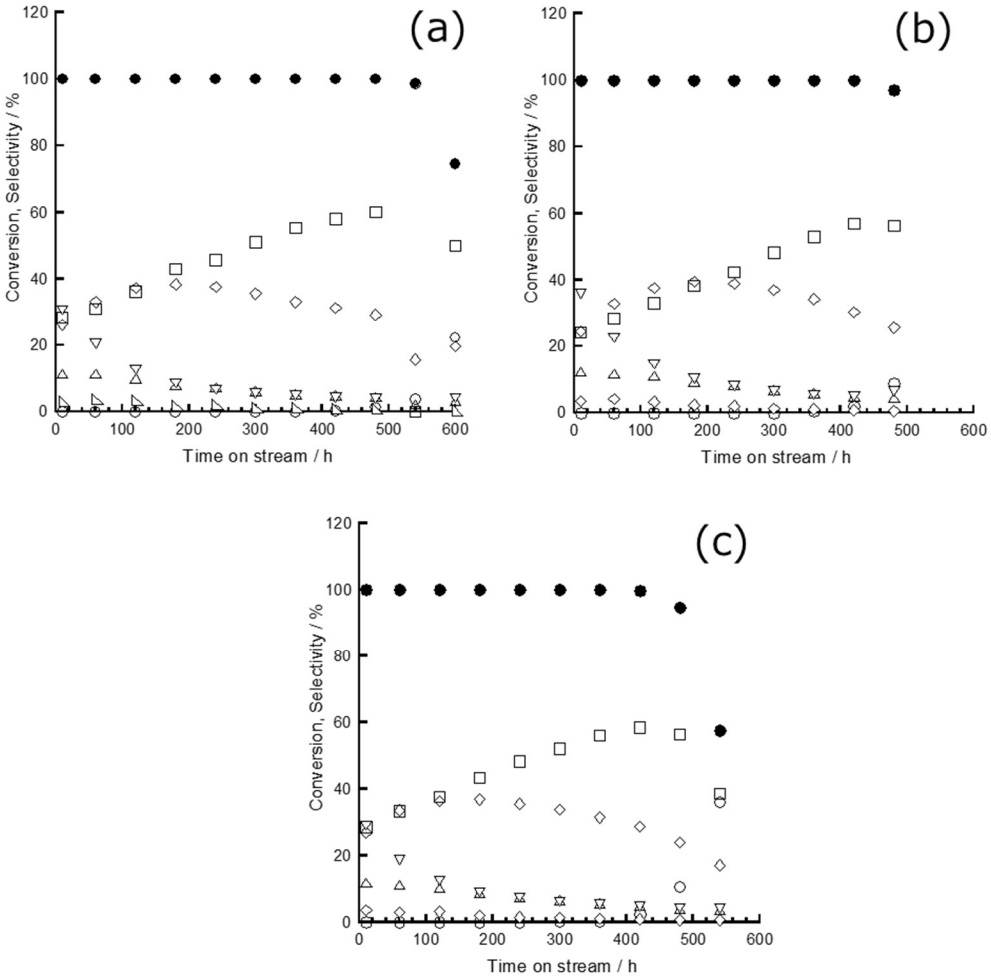

Figure3.12 Changes in the methanol conversion and the products' selectivities along with time on stream (TOS) at 623 K. (a): CHA-F-0.10, (b): CHA-F-0.25, (c): CHA-F-0.50.

Reaction conditions; $P_{(MEOH)}$, 5 kPa; W/F= 34 g h mol^{-1}; reaction temp.,623 K

● ; Conversion, ◇ : propene, ▽ : paraffin, □ : ethane, △ : C4s, ○: DME, ◇:over C5

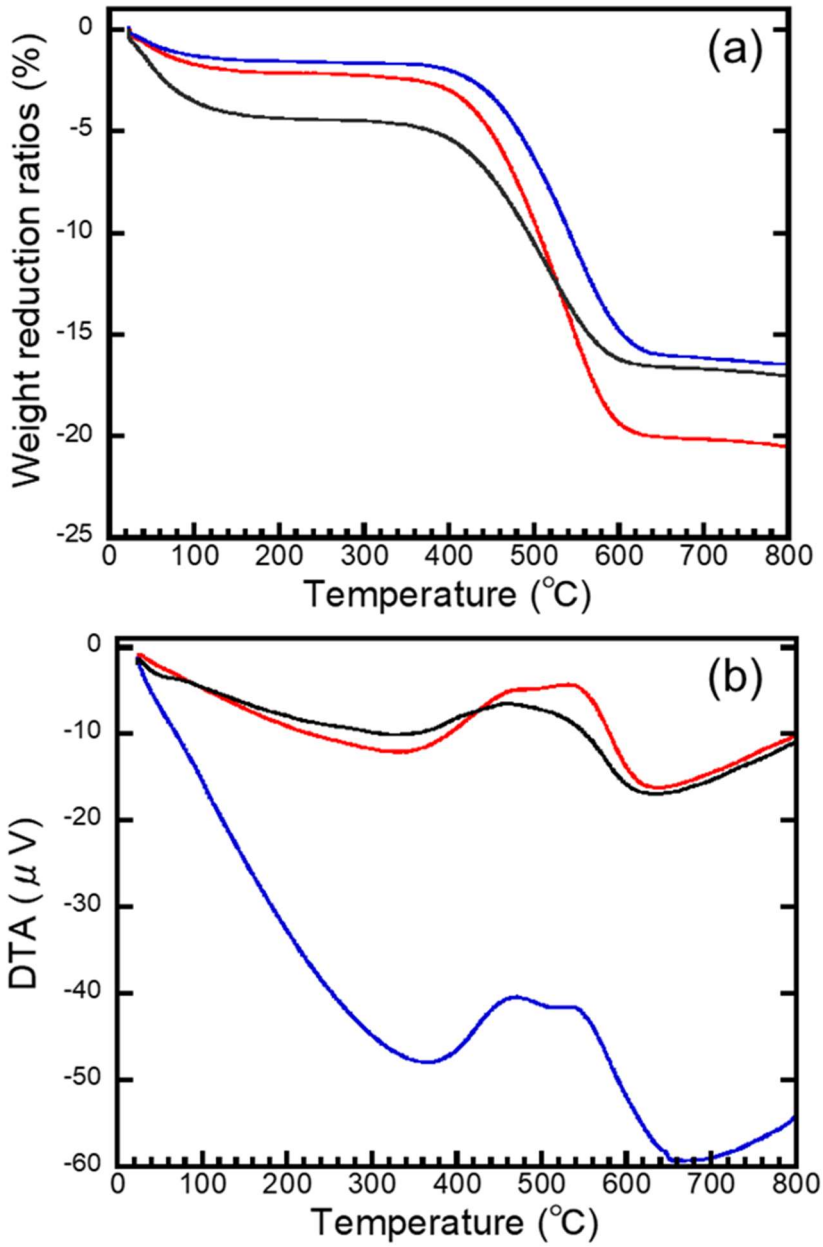

Figure 3.13 TG-DTA profiles of the CHA-F-0.1, CHA-F-0.25 and CHA-F-0.5 catalysts after the reaction. CHA-F-0.1 black line), CHA-F-0.25 (blue line), CHA-F-0.50 (red line)

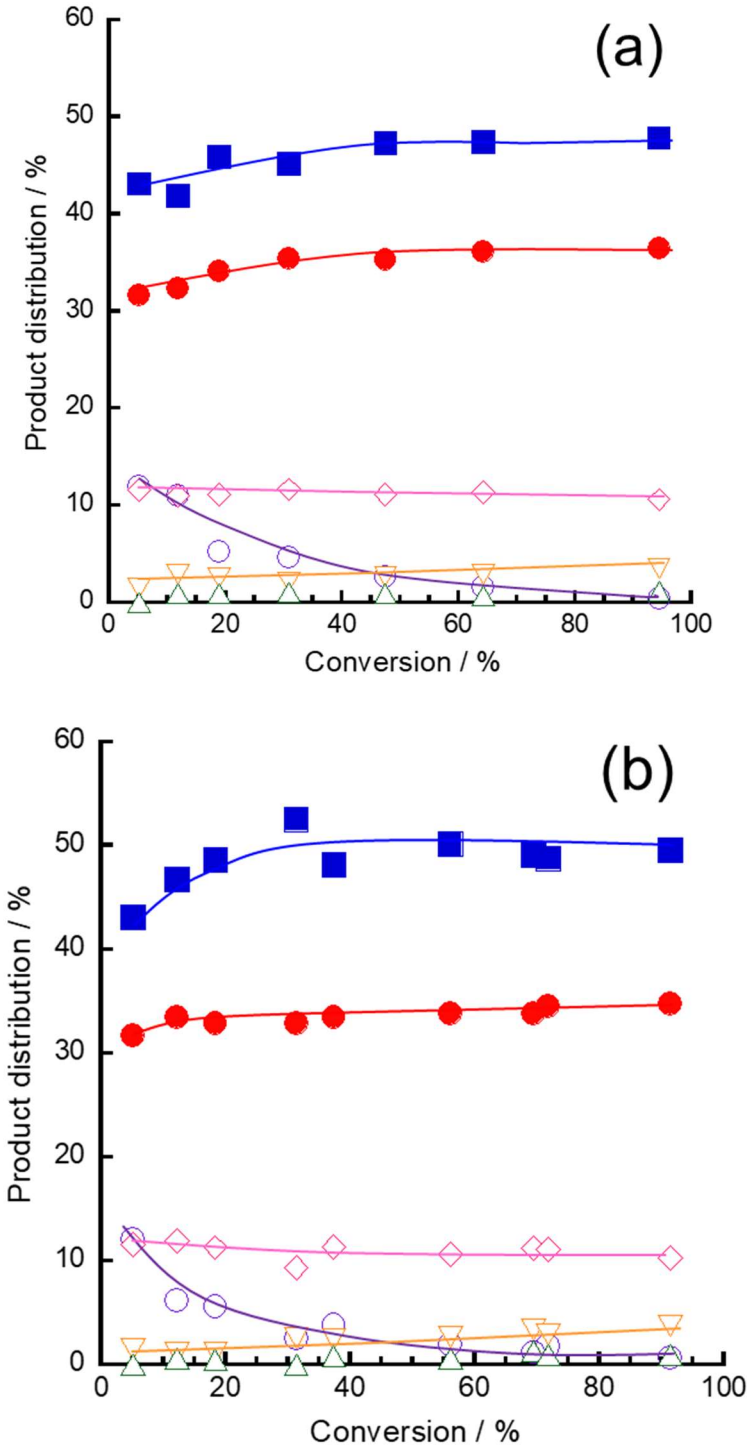

Figure 3.14 Relationship between the conversion and product distribution of CHA-F-0.1 (a) and CHA-F-1.0 (b). ■: propene, ▽: paraffin, ● : ethylene, △: over C5 :, ○: DME, ◇: C4s

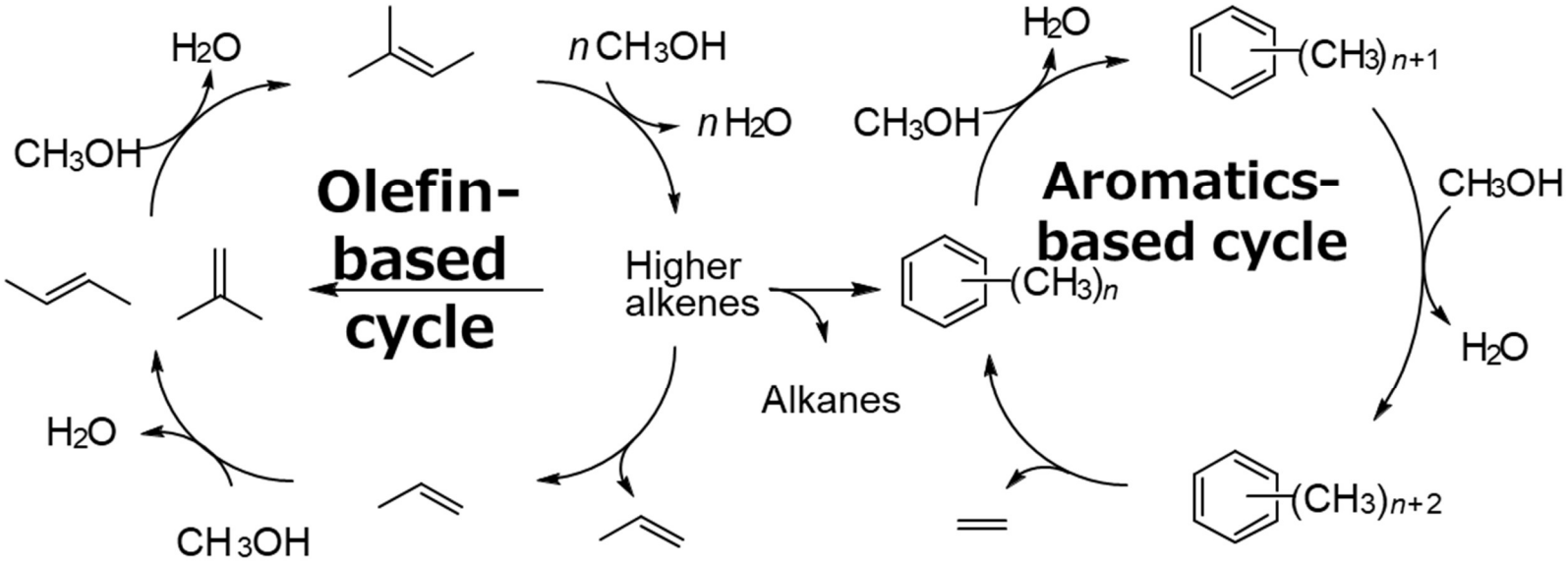

Figure 3.15 The reaction model of dual-cycle mechanism.

Table 3.1. Gel components of this synthesis method

Cab-O-Sil M5	FAU $Na_{0.26}(SiO_2)(AlO_2)_{0.26}$	$Al(OH)_3$	NaOH	Total Na^+	SDA	H_2O
1	0.0	0.10	0.2	0.200	0.2	30
0.965	0.035	0.075	0.2	0.225	0.2	10
0.93	0.070	0.050	0.2	0.250	0.2	10
0.895	0.105	0.025	0.2	0.275	0.2	10
0.874	0.126	0.010	0.2	0.290	0.2	10
0.86	0.14	0.0	0.2	0.300	0.2	10

Table 3.2 Chemical analyses and OSDA content of the as-synthesized Na-type products

	Yield / %	Si / Al[a]	Na / Al[b]	$TMAda^+$ / Al[c]	$TMAda^+$ per unit cell
CHA-F-0	95	9.0	0.22	0.71	2.4
CHA-F-0.1	95	10.6	0.14	0.72	2.2
CHA-F-0.25	95	10.9	0.18	0.73	2.2
CHA-F-0.5	88	11.3	0.19	0.81	2.4
CHA-F-0.75	75	13.7	0.24	0.70	1.5
CHA-F-1.0	63	13.5	0.21	0.72	1.8

Synthesis conditions: SiO_2 source, Fumed silica; Al source $Al(OH)_3$, FAU(Si/Al = 2.6); Seed 5 wt%; Temp. 150 ºC; Time 5 days

[a] Si/Al: Si/Al atomic ratio in the sample determined by ICP.

[b] Determined by AAS.

[c] Weight loss in the range 573−1073 K as measured by thermogravimetric analysis.

Table 3.3 Physicochemical Properties and Acid amount of the H-type products

	S_{BET} [a] / $m^2\ g^{-1}$	S_{EXT} [b] / $m^2\ g^{-1}$	V_{micro} [c] / $cm^3\ g^{-1}$	Acid amount [d] / mmol g^{-1}
CHA-F-0	730	73	0.28	0.59
CHA-F-0.1	794	30	0.34	0.58
CHA-F-0.25	700	16	0.28	0.59
CHA-F-0.5	726	14	0.30	0.54
CHA-F-0.75	826	19	0.36	0.61
CHA-F-1.0	737	24	0.34	0.56

[a] S_{BET}: BET specific surface area.

[b] S_{EXT}: External surface area estimated by the *t*-plot method.

[c] V_{micro}: Micropore volume estimated by the *t*-plot method.

[d] Acid amount: Estimated by the NH_3-TPD.

Table 3.4 Deconvolution of ^{29}Si MAS NMR spectra of the calcined Na-type products

	Si/Al ratio		Proportion of $Q^4(n\text{Al})$[b] and $Q^3(n\text{Al})$[c] / %					Q^4(2Al) /Q^4(1Al)
	ICP	NMR[a]	Q^4(3Al)	Q^4(2Al)	Q^3(0Al)	Q^4(1Al)	Q^4(0Al)	
CHA-F-0	9.0	10.2	< 0.1	5.5	1.2	28.1	65.2	0.19
CHA-F-0.1	10.6	11.4	< 0.1	3.1	2.2	29.9	64.7	0.10
CHA-F-0.25	10.9	11.8	< 0.1	4.5	5.1	24.8	65.6	0.19
CHA-F-0.5	11.3	11.0	< 0.1	7.3	5.0	21.5	66.2	0.34
CHA-F-0.75	13.7	14.0	< 0.1	5.8	5.5	16.8	71.8	0.34
CHA-F-1.0	13.5	13.0	< 0.1	7.0	9.0	16.7	67.3	0.42
FAU	2.8	2.5	14.9	47.0	< 0.1	44.5	8.5	1.06

[a] $Si/Al_{(NMR)}$: Si/Al atomic ratio in the sample determined by ^{29}Si MAS NMR spectra.

[b] $Q^4(n\text{Al})$: $\mathbf{Si}(OSi)_{4-n}(OAl)_n$.

[c] $Q^3(n\text{Al})$: $\mathbf{Si}(OSi)_{3-n}(OH)(OAl)_n$.

Chapter IV

Effects of Starting Materials on the Al distribution and Catalytic Performance of CHA-type Zeolite Synthesized without Organic Structure Directing Agents

4.1 Introduction

Zeolites of 8-membered ring (8-MR) channels have attracted attention due to high selectivities to ethene and propene in the methanol-to-olefins (MTO) reaction [1]. The aluminosilicate zeolite SSZ-13 and silicoaluminophosphate zeotype material SAPO-34 with the **CHA** topology are well-known as excellent catalysts for the MTO reaction; they exhibit high yields of light olefins with a long catalyst life [2–7]. In Chapter 3, the influence of starting materials on the Al atoms distribution in the **CHA**-type zeolite synthesized using N,N,N-trimethyladamantammonium hydroxide (TMAdaOH) as organic structure agent (OSDA) was investigated. It was suggested that the proportion of Q4(2Al), $Si(OSi)_2(OAl)_2$ species was increased as the proportion of **FAU** in the synthetic gel was increased.

It is well-know that SSZ-13, the **CHA**-type aluminosilicate zeolite, is directly synthesized using (TMAdaOH) as an OSDA [8]. Recently, imai and coworker report a method for directly crystallizing an amorphous aluminosilicate gel into the **CHA**-type aluminosilicate zeolite in the absence of any OSDAs. [9] The crystallization process of the **CHA** zeolite in the absence of OSDAs has been clarified. In the previous chapter, it was found that using **FAU**-type zeolite with high Al content (Si/Al=2.8) and large amount of Si $(OSi)_2(OAl)_2$ (Q^4 (2Al)) as a raw material produces **CHA** with many Q^4(2Al). This result indicates that the composition of starting **FAU**-type zeolite has influence on the Al distribution of final **CHA**-type zeolite products. In this chapter, **CHA**-type zeolites were synthesized using different starting materials (i.e., amorphous aluminosilicate and different FAU-type zeolites), without any OSDAs were used. The Al atoms distribution in the obtained **CHA**-type zeolites were compared. The effect of Al distribution on the hydrothermal stability and catalytic performance in MTO reaction were investigated.

4.2. Experimental

4.2.1. Synthesis of CHA-type zeolite

The starting materials used in this study were fumed silica (Cab-O-Sil M5), $NaAlO_2$ (Aldrich), NaOH pellet (Wako, 99.8%), KOH pellet (Wako, 99.8 %), and different **FAU**-type zeolites such as CBV-712 (Si/Al=6, zeolyst), CBV-720 (Si/Al=15, zeolyst), CBV-760 (Si/Al = 30), CBV-780 (Si/Al = 40). The molar compositions of the mother gels were 1 SiO_2 / 0.005 - 0.0833 Al_2O_3 / 0-1.2 NaOH / 0-1.2 KOH/ 100 H_2O. After adding the calcined SSZ-13 (Si/Al = 7.7) as seed crystals (20 wt% based on silica), the prepared mother gels were stirred at 353 K for 3 h followed by crystallized at 443 K in a rotating oven at 40 rpm for 2 days. The obtained as-synthesized Na-type products were filtered, dried at 373 K, calcined at 873 K in air. The ion-exchange was carried out with stirring at 353 K for 3 h using 2.5 M NH_4NO_3 aqueous solution twice to obtain the NH_4-type. After collecting the solid by filtration, the resultant products were calcined in air at 873 K for 3 h to obtain the H-type zeolites.

4.2.2. Characterization

Powder X-ray diffraction (XRD) patterns were obtained on a Rint-Ultima III (Rigaku) instrument using a CuKα X-ray source (40 kV, 20 mA). Nitrogen adsorption measurements to determine the BET surface area (S_{BET}), external surface area (S_{EXT}), and micropore volume (V_{micro}) were conducted at 77 K on a Belsorp-mini II (MicrotracBEL) instrument. Field-emission scanning electron microscopic (FE-SEM) images of the powder samples were obtained on an S-5200 microscope (Hitachi) operating at 1 kV. The Si / Al ratio of the samples was determined by using an inductively coupled plasma-atomic emission spectrometer (ICP-AES, Shimadzu ICPE-9000). To estimate the acidic

amount, ammonia desorption (NH_3-TPD) were recorded on Multitrack TPD equipment (MicrotracBEL). The high-resolution ^{27}Al MAS NMR spectra, ^{29}Si MAS NMR and ^{29}Si CP MAS NMR spectra were obtained on a JEOL ECA-600 spectrometer (14.1 T) equipped with an additional 1 kW power amplifier. The ^{27}Al and ^{29}Si chemical shifts were referenced to -0.54 at -34.12 ppm, $AlNH_4(SO_4)_2 \cdot 12H_2O$ and Polydimethylsiloxane (PDMS), respectively. The samples were spun at 15 kHz by using a 4 mm ZrO_2 rotor.

4.2.3. Hydrothermal treatment

About 300 mg of zeolite pellets (50/80 mesh) were packed into a quartz tubular flow microreactor (6 mm inner diameter) and heated under air stream at heating rate of 5 K min^{-1} from room temperature to 773 - 973 K. Then, hydrothermal treatment was carried out at 773 - 973 K for 1h with 20 vol% H_2O (P_{H2O} = 20.5 kPa, W/F =1.62, N_2 balance) to investigate hydrothermal stability of the zeolites. The stability was evaluated based on the relative crystallinity, which is defined as change in the sum of the intensities of the diffraction peaks assigned to the **CHA** structure.

4.2.4. MTO reaction

The MTO reaction over the H-type zeolites at 623 K under was carried out in a quartz tubular flow microreactor (6 mm inner diameter) loaded with 100 mg of zeolite pellets (50/80 mesh) without a binder. The pressure of methanol was set at 15 kPa with He as a carrier gas. W/F for methanol was set at 34 g-cat h mol^{-1}. The catalyst was activated in flowing He at 773 K for 2 h prior to the reaction, and then cooled to the desired reaction temperature. The MTO reaction gives ethylene (C2=), propene (C3=), butenes (C4=), paraffins (C1-C4), over-C5 hydrocarbons, and dimethyl ether (DME) as

products. The reaction products were analyzed by an online gas chromatograph (GC-2014, Shimadzu) equipped with HP-PLOT/Q capillary column and an FID detector. The selectivities of the products were calculated on the carbon number basis.

4.3. Results and discussion

4.3.1. Synthesis of CHA-type zeolite from amorphous alminaosilicate gel without OSDA

Frist, **CHA**-type zeolite was synthesized by amorphous silica, alumina under OSDA-Free condition in the same way [9]. Figure 4.1 showed Relationship with products and ratio of counter cation in synthetic gel. The peak of XRD was not observed in the region of K/Si ratio at 0.1 – 0.6 and Na/Si ratio at 0.1 - 0.6. In the region of Na/Si ratio at 0.6 -1.0, It was observed only **CHA** structure regardless of K/Si ratio, and **ANA**-type zeolite was produced by the condition of Na/Si over 1.2. It is known that in natural minerals, an analcime ($NaAlSi_2O_6 \cdot H_2O$) having an **ANA** structure is likely to be formed in a region with a large amount of sodium.[10] The region of K/Si ratio over 1.0 and Na/Si ratio 0.1 – 1.0, **CHA** structure was observed. In addition, Figure 4.1 shows the elemental composition and yield of **CHA**-type zeolite produced. Even in the synthesis method of Seed assist method using amorphous silica source and alumina source, **CHA** structure It was found that it is generated in the region where the amount of K is large for generation. The amount of Si contained in the produced **CHA**-type zeolite and the yield obtained by synthesis were found to increase as the amount of NaOH and KOH used in the synthesis gel decreased, irrespective of the type of counter cation.

4.3.2. Synthesis of CHA type zeolite from FAU−type zeolite without OSDA

Synthesis was carried out by changing the Si/Al ratio of **FAU**-type zeolite as a

raw material. Under this synthesis condition, formation of single phase **CHA** structure was confirmed when **FAU**-type zeolite that has Si/Al = 6 and 15 were used as raw material (Figure 4.2). Si/Al ratio of the products were 3.2 and 4.0 respectively by ICP analysis. When high silica **FAU**-type zeolite such as Si/Al = 30, 40 used starting material, the products of XRD peak was observed by **CHA** structure and amorphous silica. This result implied the silica of dissolved **FAU**-type zeolite remains without used for crystallization. Next, under the condition using **FAU**-type zeolite with Si/Al = 15 as a raw material, the relationship between the ratio of counter cation such as Na^+ and K^+ in the synthesis gel and the product was summarized in Figure 4.3. The region of K/Si ratio 0.1 - 0.6 and Na/Si ratio 0.1 - 0.6, the peak intensity of product was low. In addition, the products were observed by **CHA**-type structure in region of Na/Si ratio at 0.6 – 1.0, and Na/Si ratio over 1.2, **ANA** structure was observed. K/Si ratio over 0.6, **CHA**-type structure was produced regardless of Na/Si ratio in this conditions. To compered with using amorphous silica, alumina, the **CHA** structure was observed low Na/Si, K/Si ratio. The products of Si/Al ratio and yield using **FAU**-type zeolite as raw materials was same tendency with using amorphous silica and alumina. **CHA** using **FAU**-type zeolite as a raw material was produced even in a region where the amount of cations was smaller than that of **CHA** using amorphous silica alumina as a raw material. Furthermore, when **FAU**-type zeolite was used as a raw material, the **CHA** structure was formed in a single phase in a region of K/Si= 0.6, 0.8. This result suggested that when **FAU**-type zeolite is used as a raw material, nano parts are supplied, and when an amorphous silica source or alumina source is used as a raw material, nano parts are not supplied.

4.3.3. Effect of starting material on Al atom distribution

In the Chapter 3, it is known that under the condition that TMAdaOH is used as a structure directing agents, the Al atom distribution of the **FAU**-type zeolite used as a raw material influences the Al atom distribution of the **CHA**-type zeolite generated. Therefore, this chapter, to clarify the influence of raw material Si source on product under OSDA-Free condition. Figure 4.4 shows the XRD patterns of **CHA**-type zeolite synthesized using amorphous silica, alumina source and **FAU**-type zeolite as raw material under OSDA-Free conditions. In addition, SEM images of each sample are shown in Figure 4.5. As a result of comparing the particle shapes of both samples, the sample synthesized from the amorphous silica source and alumina source had a large particle size and layered structure, whereas the sample was synthesized as a raw material for **FAU**-type zeolite. Figure 4.6 showed that the result of ^{27}Al MAS NMR and ^{29}Si MAS NMR. The spectra of both sample only observed -58 ppm that was assigned by framework Al species. Both samples observed Q^4(0Al)、Q^4(1Al)、Q^4(2Al)、Q^3(0Al)、and Q^4(3Al) from ^{29}Si MAS NMR. Table 4.1 summarized deconvolution of ^{29}Si MAS NMR spectra. As a result, it was confirmed that the peak intensity of Q^4(1Al) was strong and the peak intensity of Q^4(2Al) was weaker as compared with the case of using an amorphous silica source, alumina source as a starting material when used as a **FAU**-type zeolite starting material all right. The **FAU**-type zeolite used as a raw material has Si/Al = 15, and contains a large amount of Q^4(1Al) in the framework. These results suggest that Si rich nano-parts are supplied at the time of zeolite formation when **FAU**-type zeolite of high silica is used as a raw material. Table 4.2 also shows the amounts of Na^+ and K^+ species contained when synthesized by each synthesis. This suggests that zeolite framework was formed with no counter cation because nano-parts were supplied. In addition, Figure 4.7

shows the ^{29}Si MAS NMR spectrum when a different amount of counter cation is contained in the framework from the raw material **FAU**-type zeolite. These results showed that even under OSDA-Free conditions, the source silica source has an influence on Al atom distribution of **CHA**-type zeolite produced. Especially when **FAU**-type zeolite of Q^4(1Al) rich was used as starting material in high silica, the produced **CHA** was also Q^4(1Al) rich.

4.3.4. Hydrothermal stability and MTO performance

A sample obtained by synthesis was subjected to a hydrothermal treatment to evaluate its stability. Figure 4.8 shows the XRD pattern before and after the hydrothermal stability test and Figure 4.9 shows the ^{29}Si MAS NMR spectrum. From these results, it was found that the more severe conditions of the hydrothermal treatment, the weaker the peak intensity of XRD and the peak intensities of Q^4(2Al) and Q^4(1Al) of ^{29}Si MAS NMR. When comparing the results of the hydrothermal stability test of each sample, it was found that the **CHA**-type zeolite using **FAU** as a raw material has higher hydrothermal stability. This is because the Al atom distribution in the framework is Q^4(1Al) rich. In addition, the result of MTO reaction on the sample synthesized by each raw material is shown in Figure 4.10. The catalyst life in both samples was about 3 h. Catalyst life time is known to be greatly affected by the amount of Al in the framework, **CHA**-type zeolite was synthesized by OSDA-Free conditions for a high Al content, it is considered to catalyst life was short. Comparing the product distribution of **CHA**-type zeolite synthesized by each synthesis method, no significant difference was found in either sample. The synthesized **CHA**-type zeolite contains 7 to 8 Al amount per unit cell. Synthesized sample differences in product distribution of Al distribution is not confirmed due to many Al species exist and are in

close proximity.

4.4. Conclusion

We investigated the influence of zeolite produced by **FAU**-type zeolite as raw material on Al atom distribution. In the OSDA-Free condition, synthesis of **CHA**-type zeolite was carried out using Q^4(1Al) rich **FAU**-type zeolite, amorphous silica source, alumina source. The sample synthesized using **FAU** was Q^4(1Al) rich from the ^{29}Si MAS NMR. As a result of the hydrothermal treatment, **CHA**-type zeolite synthesized using **FAU** has high hydrothermal stability. It was suggested that The formed **CHA**-type zeolite is hard to cause dealumination due to Q^4(1Al) rich.

References:

[1] Stocker M. *Micropor. Mesopor. Mater.*, **1999**, 29, 3.

[2] Stocker M. *Micropor. Mesopor. Mater.*, **2005**, 82, 257.

[3] Yuen L.T., Zones S.I., Harris T.V., Gallegos E.J., Auroux A., *Micropor. Mater.*, **1994**, 2, 105.

[4] Zhu Q., Kondo J.N., Tatsumi T., Inagaki S., Ohnuma R., Kubota Y., Shimodaira Y., Kobayashi H., Domen K., *J Phys. Chem. C*, **2007**, 111, 5409.

[5] Zhu Q., Kondo J.N., Ohnuma R., Kubota Y., Yamaguchi M., Tatsumi T., *Micropor. Mesopor. Mater.*, **2008**, 112, 153.

[6] Zhu Q., Kondo J.N, Inagaki S., Tatsumi T., *Top. Catal.*, **2009**, 52, 1272.

[7] Bleken F., Bjorgen M., Palumbo L., Bordiga S., Svelle S., Lillerud K.P., Olsbye U., *Top. Catal.*, **2009**, 52, 218.

[8] Bourgogne, M. et al., U. S. Patent 4,503,024 **1985**.

[9] Imai H., Hayashida N., Yokoi T., Tatsumi T., *Micropor. Mesopor. Mater.*, **2014,** 196, 341.

[10] Tominaga H., *ZEORAITONOKAGAKUTOOUYOU* (application and science of zeolite), KOUDANSYA-PUBLISHING, **1987**.

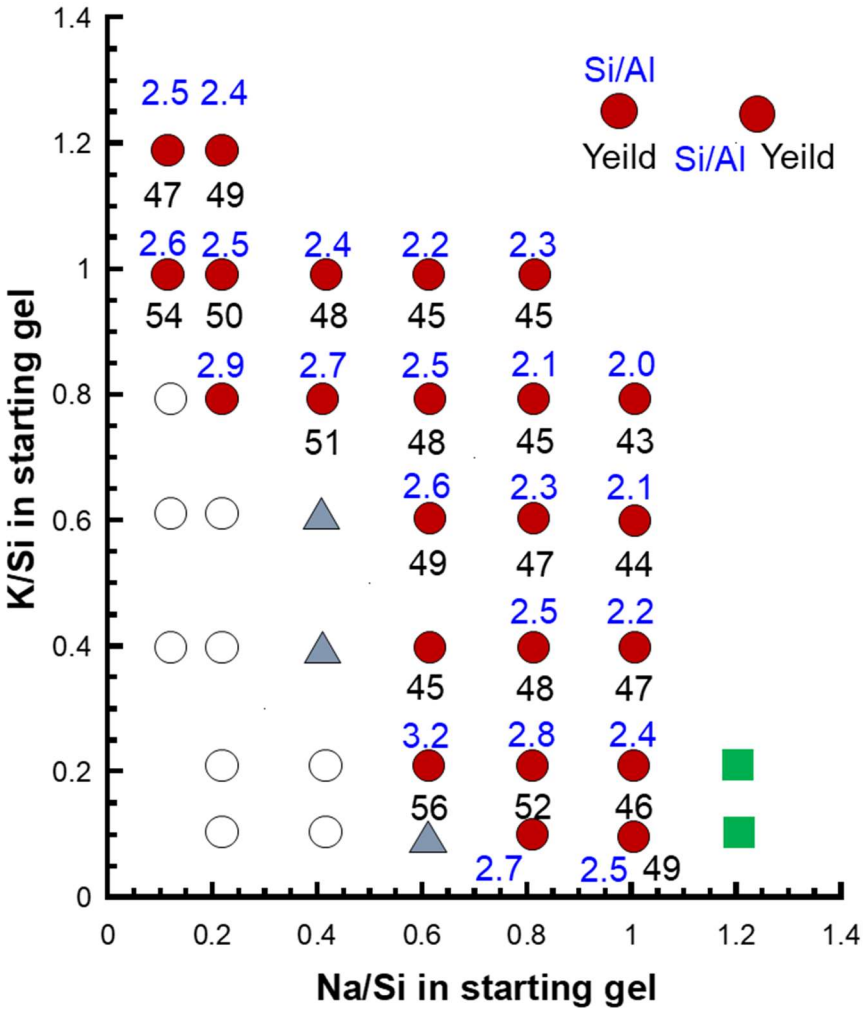

Figure 1 Relationship between the composition of the starting gel and the main phase of the product. Synthesis conditions: silica source, fumed silica; aluminum source, $NaAlO_2$; $SiO_2/Al_2O_3 = 30$; $H_2O/SiO_2 = 100$; seed, 20 wt.%; temp., 170 °C; time, 40 h. The Si/Al ratio of the products is given above the main-product symbol. The phase of by-products is described below the symbol.

● : CHA, ○ : amorphous, ▲ : amorphous+CHA, ■ : ANA

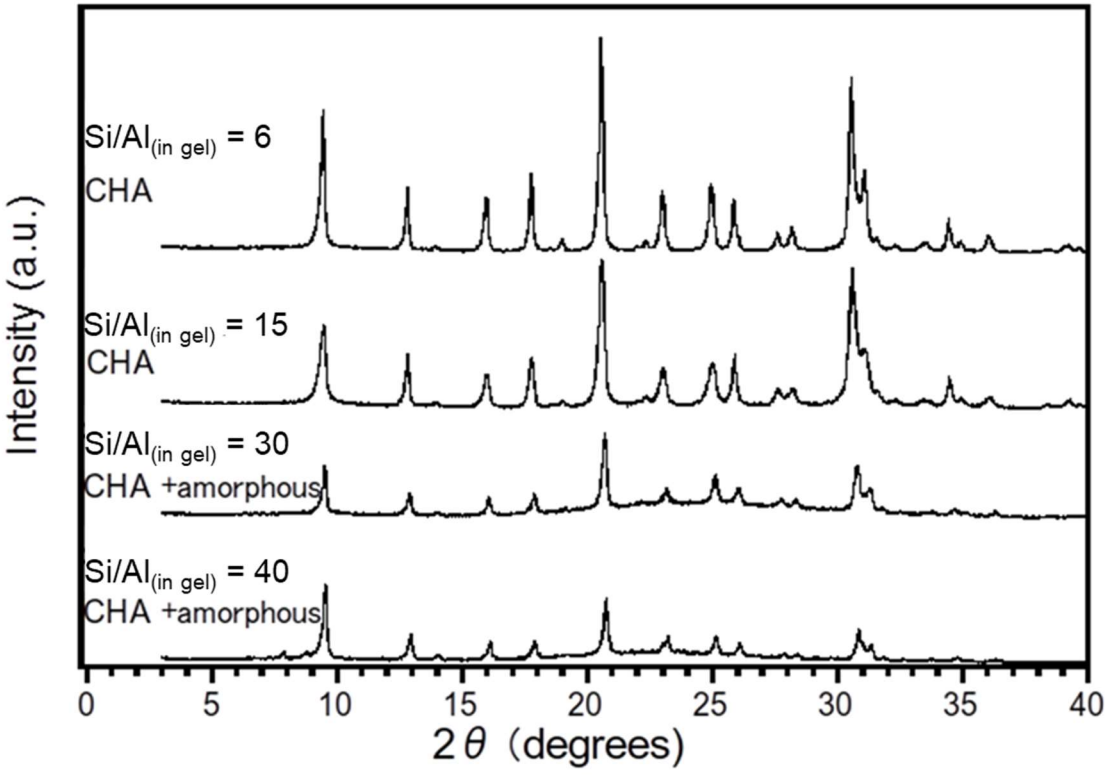

Figure 4.2 XRD patterns of **CHA**-type zeolites Using **FAU**-type zeolite with different Si/Al ratio as raw material.

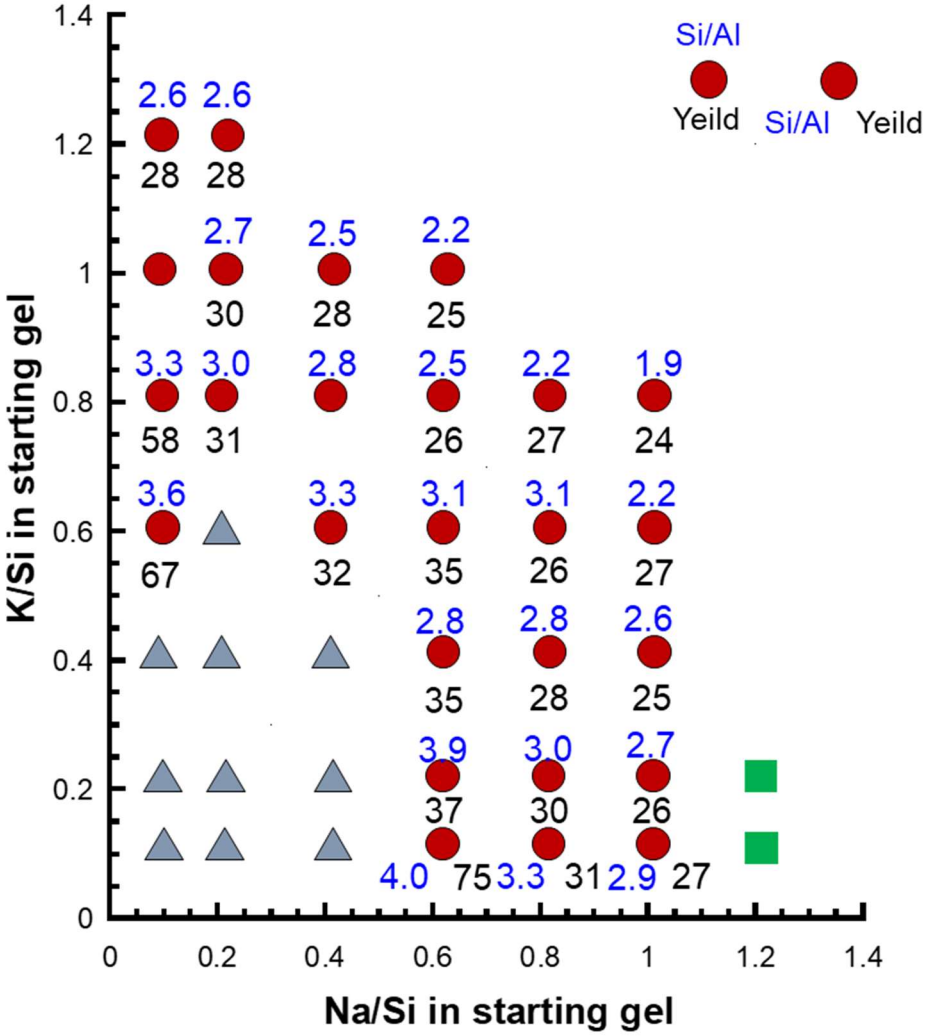

Figure 4.3 Relationship between the composition of the starting gel and the main phase of the product. Synthesis conditions: silica, aluminum source, **FAU**-type zeolite (CBV-720); SiO_2/Al_2O_3 = 30; H_2O/SiO_2 = 100; seed, 20 wt.%; temp., 170 °C; time, 40 h. The Si/Al ratio of the products is given above the main-product symbol. The phase of by-products is described below the symbol.

● : CHA, ▲ : amorphous + CHA, ■ : ANA

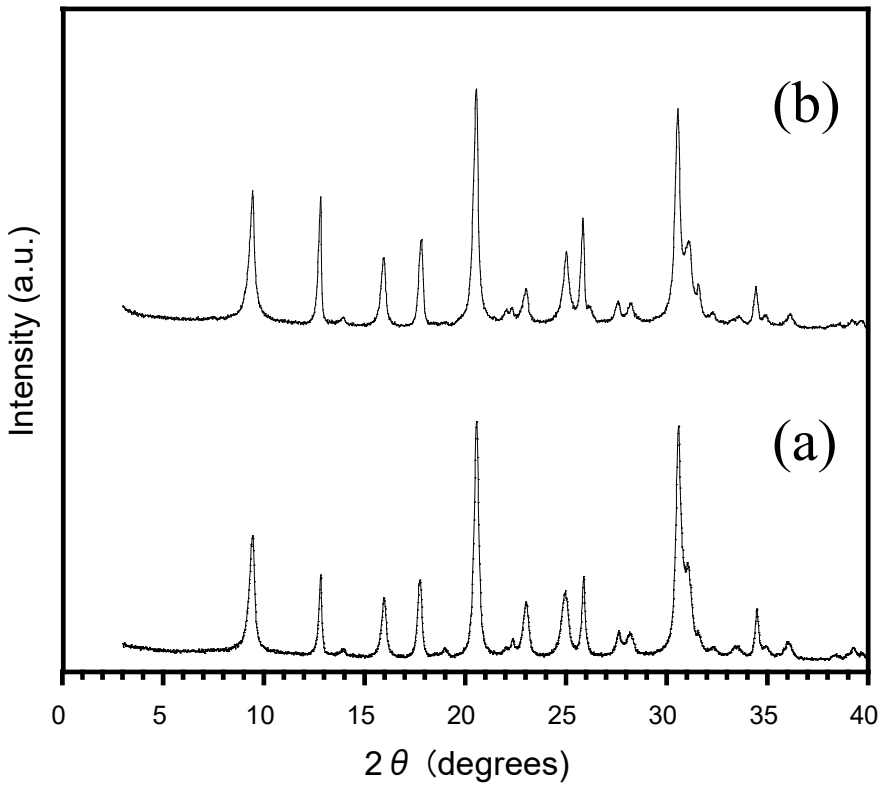

Figure 4.4 XRD patterns of **CHA**-type zeolites under OSDA-Free condition.
(a) Using **FAU**-type zeolite (CBV-720) and (b) Using amorphous silica, alumina

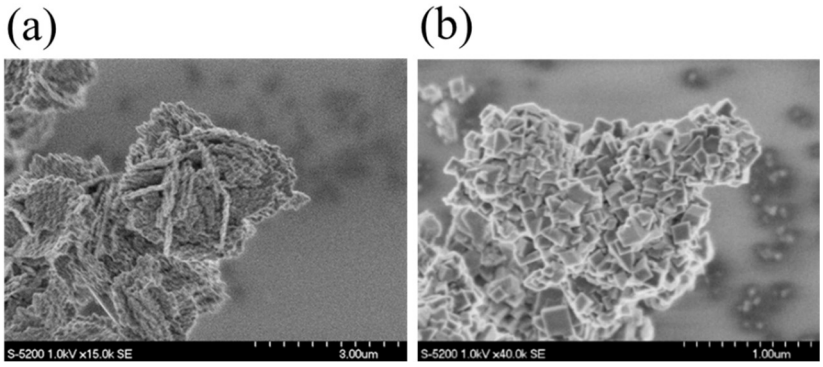

Figure 4.5 SEM image of **CHA**-type zeolite under OSDA-Free condition.
(a) Using amorphous silica, alumina and (b) Using **FAU**-type zeolite (CBV-720)

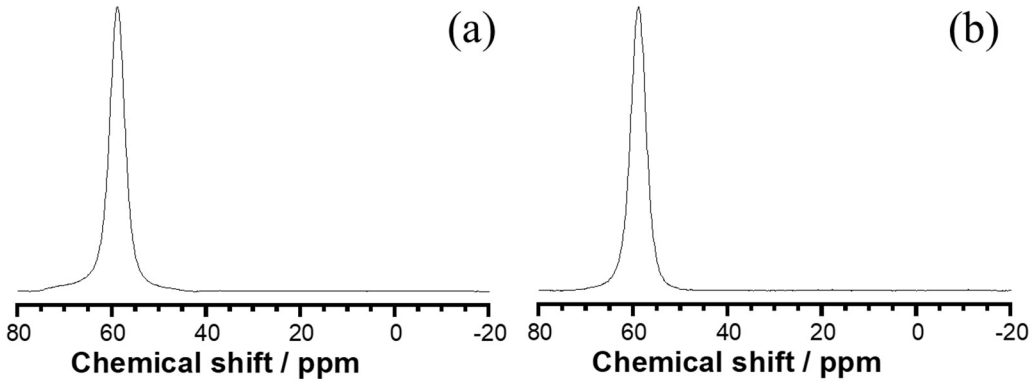

Figure 4.6 ^{27}Al MAS NMR spectra of **CHA**-type zeolite under OSDA-Free condition. (a) Using amorphous silica, alumina and (b) Using **FAU**-type zeolite (CBV-720)

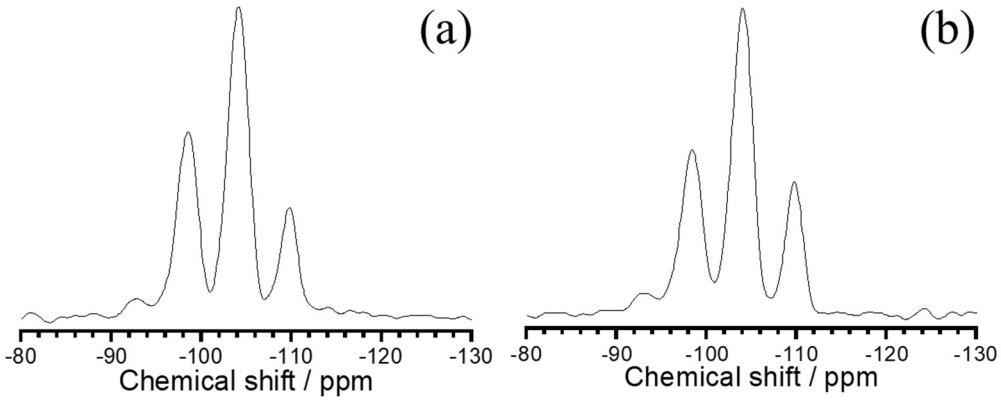

Figure 4.7 ^{29}Si MAS NMR spectra of **CHA**-type zeolite under OSDA-Free condition. (a) Using amorphous silica, alumina and (b) Using **FAU**-type zeolite (CBV-720)

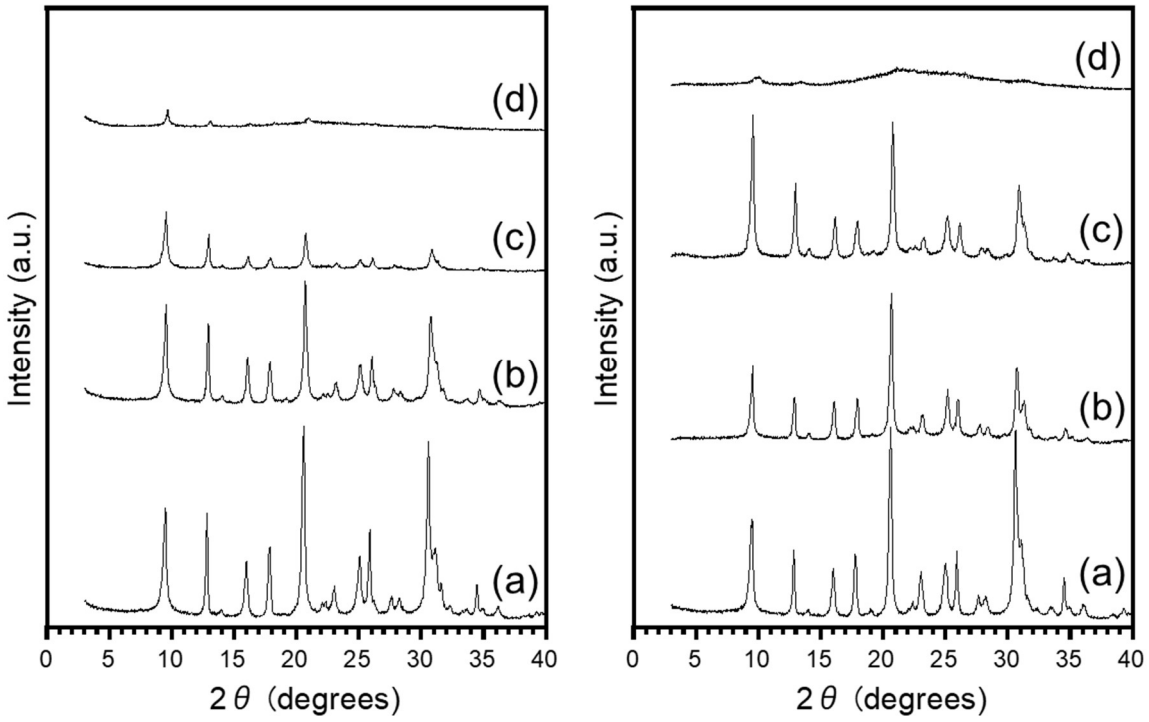

Figure 4.8 XRD patterns of **CHA**-type zeolite under OSDA-Free condition after hydrothermal treatment using amorphous silica, alumina (left), using **FAU**-type zeolite (CBV-720) (right), (a) as-made, (b) 773 K, (c) 873K and (d) 973K

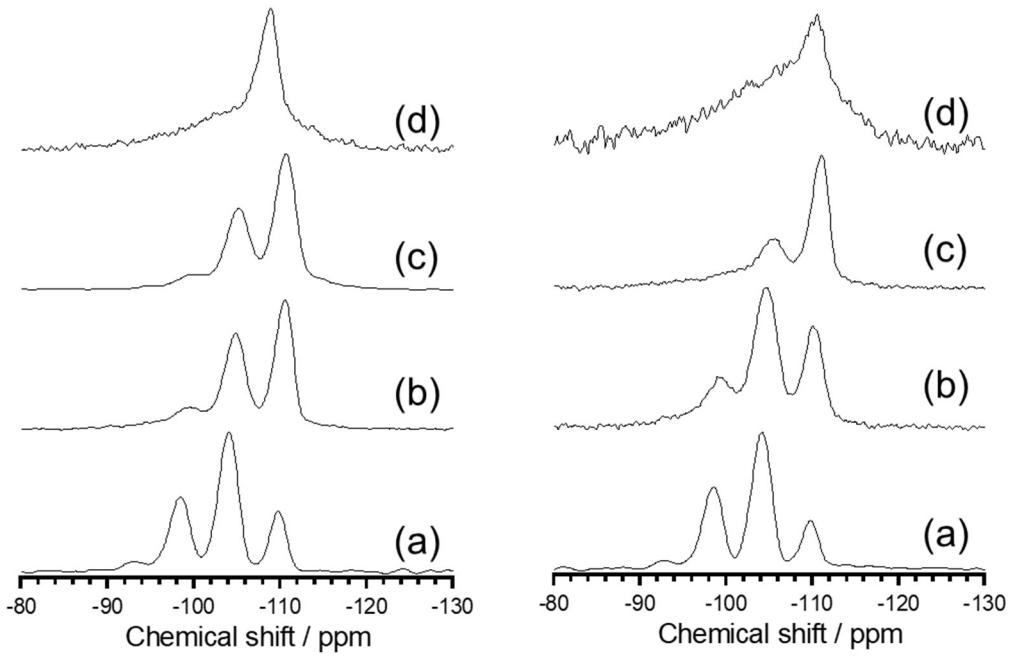

Figure 4.9 ^{29}Si MAS NMR spectra of **CHA**-type zeolite under OSDA-Free condition after hydrothermal treatment using amorphous silica, alumina (left) and using **FAU**-type zeolite (CBV-720) (right). (a) as-made, (b) 773 K, (c) 873K and (d) 973K

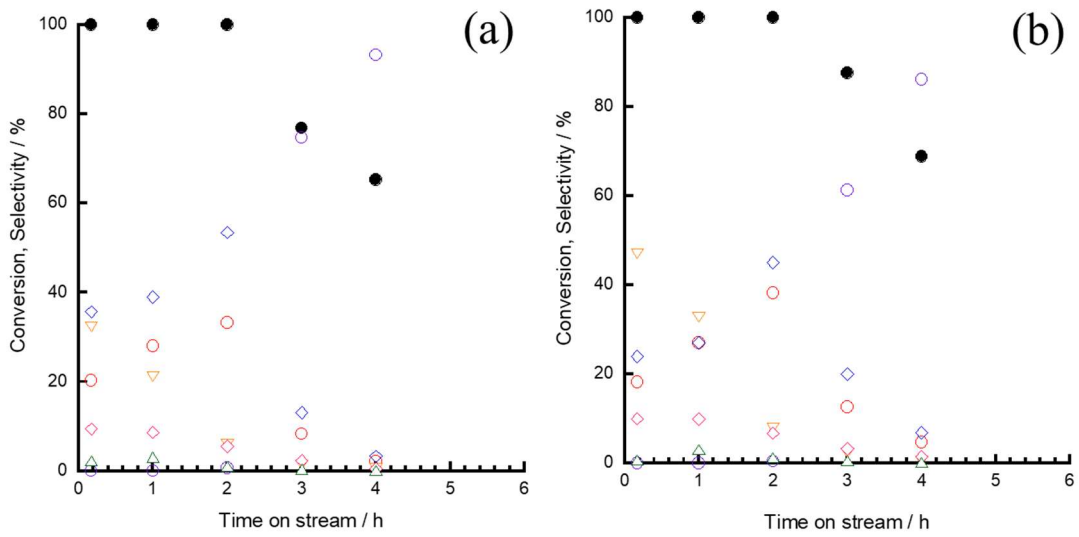

Figure 4.10 MTO reaction of **CHA**-type zeolite under OSDA-Free condition after hydrothermal treatment (a) using amorphous silica, alumina, (b) using **FAU**-type zeolite (CBV-720).

Reaction conditions; P(MeOH), 5 kPa; W/F= 34 g h mol-1; reaction temp.,623 K

● ; Conversion, ◇: propene, ▽: paraffin, ○: ethane, ◇ : C4s, ○: DME, △:over C5

Table 4.1 Physicochemical Properties of the H-type products

Sample	Si/Al (ICP)	Yield (%)	S_{BET} [a] / $m^2 g^{-1}$	S_{EXT} [b] / $m^2 g^{-1}$	V_{micro} [c] / $cm^3 g^{-1}$
CHA-FAU	3.6	65	598	60	0.26
CHA-Am	3.8	97	623	41	0.26

Table 4.2 Deconvolution of ^{29}Si MAS NMR spectra of the calcined Na-type products.

Sample	Proportion of $Q^4(nAl)^a$ and $Q^3(nAl)^b$ / %			
	$Q^4(3Al)$	$Q^4(2Al)$	$Q^4(1Al)$	$Q^4(0Al)$
CHA-TF-FAU	2.8	25.6	52	19.0
CHA-TF-Am.	2.3	30.9	48.4	18.6

Chapter V

General Conclusion

In this research, I aimed to develop a **CHA**-type zeolite catalyst with high hydrothermal stability and catalytic performance in (methanol-to-olefins) MTO reaction. I studied the effect of organic structure directing agent (OSDA) and starting materials on the Al atoms distribution in **CHA**-type zeolite. The hydrothermal stability and MTO performance of the obtained **CHA**-type zeolite were investigated.

In Chapter I, firstly, I showed the general introduction on the zeolite catalyst and the application in the chemical industry. Further, I introduced the previous work regarding the control of the Al atoms distribution in zeolite framework especially for **MFI**-type zeolite. In particular, the different synthesis method for **CHA**-type zeolite with small size was summarized.

In Chapter II, I performed the synthesis of **CHA**-type zeolite by using different OSDAs. The amount of Al and the particle shape of **CHA** obtained are greatly different depending on the type of OSDA. In addition, when [K, Na] and [M3HQui, Na] was used as OSDA, the obtained **CHA**-type zeolite had high hydrothermal stability, long catalytic lifetime, and high propylene selectivity in MTO reaction. This result suggested that dense and sparse Al atoms in the resulting **CHA**-type zeolite particles are present.

In Chapter III, I focused on changing the starting materials (Si and Al source) with TMAdaOH as OSDA in the synthesis of **CHA**-type zeolite. When the synthesis was carried out by changing the proportion of **FAU**-type zeolite in the raw material, the Al amount, particle morphology, and texture properties were similar. However, the Al atom distribution in the zeolite was very different based on the ^{29}Si MAS NMR results. The

proportion of Q^4(2Al) in **CHA** framework was increased with increasing **FAU** amount as raw material. The obtained **CHA**-type zeolite with high Q4(2Al) had low hydrothermal stability, produced more ethylene and deposited heavy coke in MTO reaction. This results implied that the sample of including large amount of Q4(2Al) in the framework was unstable and it was easy to generate of the aromatics, and promoted the produced of ethylene.

In Chapter IV, I studied the synthesis of **CHA**-type zeolite without using any OSDAs. When amorphous aluminosilicate (or **FAU**) was used as the starting material, the Al amount, and texture properties were similar, but particle morphology was little different. Compared to the amorphous aluminosilicate was used as the starting material, the **FAU** (Si/Al=15) as the starting material produced the **CHA**-type zeolite with more Q^4(1Al) species from ^{29}Si MAS NMR. This results suggested that high silica **FAU** (Si/Al = 15) was provided the nano parts of Si rich to **CHA**-type zeolite. As a result of hydrothermal treatment, **CHA**-type zeolite synthesized using **FAU**-type zeolite with many Q^4(1Al) species showed higher hydrothermal stability.

In this dissertation, I succeeded in controlling the Al atom distribution in the **CHA**-type zeolite. The Al atom distribution was estimated by ^{29}Si MAS NMR. The obtained **CHA**-type zeolite with more Q^4(1Al) showed high hydrothermal stability and high propylene selectivity in MTO reaction. Furthermore, for the first time, we clarified that Al atom distribution of zeolite used as starting material had influence on the Al atom distribution in the final zeolite product.

Finally, I considered the further progress for zeolite synthesis methods. As a new approach to zeolite synthesis, the synthesis of zeolite using zeolite having various structures as a raw material can be mentioned. In this synthesis method, it is considered that the characteristic of the raw material zeolite also appears in the product. For example, **BEA**-zeolite is an industrially important zeolite, and it is often reported that Al atoms are introduced into a specific T site. Zeolite known of Al atom position by performing the synthesis raw material, considered to perform a more precise control of the Al atoms distribution than ever. In addition, besides Al atomic distribution characteristics of the material is considered to affect the product. We believe that by synthesizing zeolite using sodalite with high hydrothermal durability as a raw material, products with relatively high hydrothermal durability can be obtained.

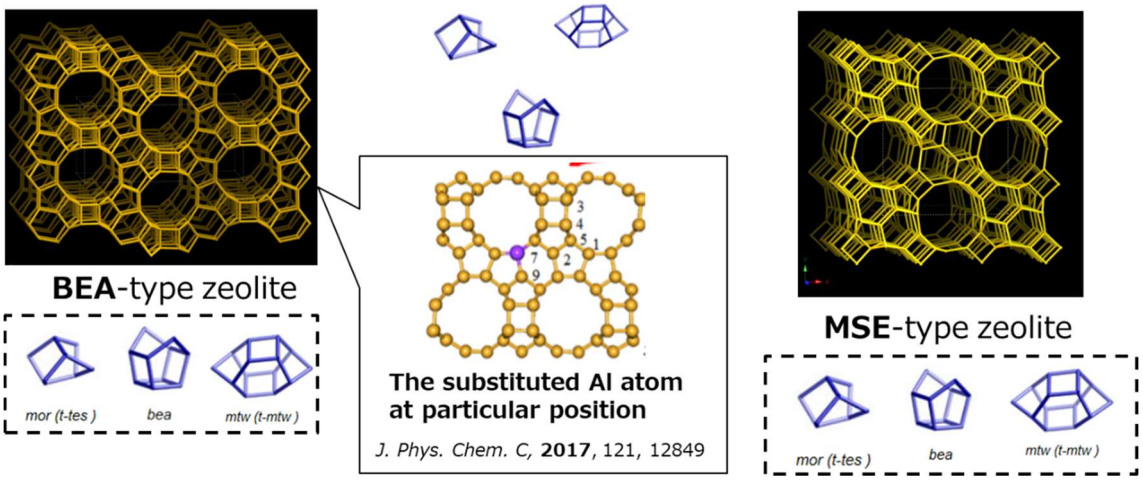

Figure 5.1 proposal of future work